ISSN 1016-197X

Nuclear Science and Applications

Volume 27 Number 1 & 2 June, December 2018

The Journal of
BANGLADESH ATOMIC ENERGY COMMISSION

ISSN 1016-197X Volume 27 Number 1 & 2 June, December 2018

Nuclear Science and Applications

The Journal of
BANGLADESH ATOMIC ENERGY COMMISSION

CONTENTS

NUCLEAR SCIENCE AND APPLICATIONS VOLUME 27 NUMBER 1 & 2 June, December 2018

Heavy Mineral Distribution and Geochemical Studies of Coastal Sediments at Sonadia Island, Bangladesh

M. Z. Kabir*, F. Deeba, M. G. Rasul, R. K. Majumder, M. I. Khalil and M. S. Islam

Institute of Nuclear Minerals, Atomic Energy Research Establishment, Dhaka-1349, Bangladesh

Abstract

This work attempts to understand the heavy minerals distribution, mineralogical composition and trace elements distribution in beach sands of Sonadia Island, Cox's Bazar district, Bangladesh. Total 14 beach sand samples were collected from the study area to determine the heavy mineral percentage, mineralogical composition and elemental concentrations. The separated minerals were examined by a polarizing petro graphic microscope. About 12.8 – 84.96% heavy minerals concentrations were found in the analysed samples by heavy liquid separation technique. Result of mineralogical composition suggests that garnet is the dominant mineral component followed by ilmenite, magnetite, rutile and zircon. Elemental concentration using XRF techniques reveals the average concentrations of Zr (198.75 ppm), Sr (82.76 ppm), Rb (93.62 ppm), Pb (9.03 ppm), Zn (38.75 ppm), Mn (390.73 ppm), Fe (15127 ppm), Th (3.78 ppm), Cu (18.08 ppm), Co (70.84 ppm), Ti (1598 ppm), Ba (280.47 ppm), Cs (91.62 ppm) and Ni (16.03 ppm). The radioactivity of the study area was found to be 24 and 170 cps. The source of the heavy minerals observed in the Sonadia Island is possibly from the Miocene sedimentary rocks exposed along the Cox's Bazar beach, which have been distributed along the beach by the long shore current, waves and winds.

***Keywords**:* Heavy minerals, heavy liquid separation, radioactivity, XRF, placer deposits, Sonadia Island

1. Introduction

The heavy mineral deposits along the coastal belt of Bangladesh constitute potential resources for Bangladesh. The fore dune deposits also contain noticeable amount of heavy minerals, which are being accumulated within the intertidal zone. This part is very dynamic and exposed subject to wave, current and wind actions. Mineral sands on those deposits contain some important metallic minerals mainly ilmenite, magnetite, rutile, zircon, garnet, monazite, kyanite and leucoxene [1]. The heavy mineral concentration along the recent fore dune deposit of Bangladesh coast ranges from 13% to 70%, which is quite significant [2]. Presence of radioactivity in Cox's Bazar beach of Bangladesh was first reported by Schmidth and Asad [3]. Placer deposits of Bangladesh coast contain several heavy minerals, in which monazite is radioactive mineral because of thorium in its composition [4]. Radioactivity is also observed in the separated zircon assemblages [5].

The islands of Bangladesh are scattered along the Bay of Bengal and the river mouth of the Padma. A huge amount of sediments are also thought to be carried by under currents into the deeper Bay of Bengal and the Indian Ocean. The bottom topography of the Bay of Bengal plays a dominant role in the dynamic processes in the North Bay and Bangladesh coast which results in frequent geomorphological changes in the adjacent coast and islands [6-7].

Sonadia is a small offshore island of about 9 km^2 and is located in the Bay of Bengal on the West side of Cox's Bazar under Kutubjum union of Moheshkhali Island. Though Moheshkhali Island is little far from the active delta formation region, it still receives a lot of sediment and undergoes coastal process which helps re-shape the morphology of the island's coast, especially the south and south-eastern part including Sonadia Island [8]. An intertidal beach and sandy ridge extends along the length of the western side of the Island's length from north-west to south-east. Changes are apparent in the south-eastern coastline of Sonadia Island, which thus gets the characteristics of a sandbar [9]. An intertidal sandy beach and sandy ridge extends for approximately 12.5 km along the length of the western side of Sonadia Island, from north-west to south-east [10]. The Sand bars and sandy shoals occur along the Ghotivanga coastline and extend along the length of the western beach of Sonadia Island.

Consisting of gently sloping low-lying coast unprotected from the sea, Sonadia Island hasformed as a barrier island just south-west of Moheshkhali Island. Natural sandy breakwaters face parallel to the flat coastlines of Moheshkhali. To the east a smallchannel separates the two islands while to the south-east shallow bays separate it by 3.5 km from the mainlandof Cox's Bazar.

The dunes run along the entire coast and are also fringed several hundred meters inward. Wind and waves are the major forces determining the features of the dunes. The western side of the island is sandy and different kinds of shells are found on the beach.

Sonadia Island constitutes a complex and unique geological system on the eastern cliff coast of Bangladesh (Fig.1). Holocene evolution of the island is very different and rather complex than those of the other estuarine or deltaic islands of Bangladesh. Sonadia Island is neither deltaic Bay mouth bar nor estuarine mouth bar but sub maridional bar to the cliff coast and situated within the shallow and wide inner shelf. The present shore face of the area is characterized by the presence of numerous long shore bars along the west coast and barriers are found along the northern coast of Sonadia Island. Geomorphologic study reveals that the Island is largely initiated due to the combined erosional and depositional processes on an open to semi-protected depositional basin under the transgressive shore face [11].

Corresponding author: zafkab_geoaec@yahoo.com

Many investigations have been carried out on different physical and chemical aspects like mineralogical composition of the beach sands [12] and mechanism of heavy mineral deposition in the beach of Cox's Bazar [13], but a few studies have been conducted on Sonadia Island.

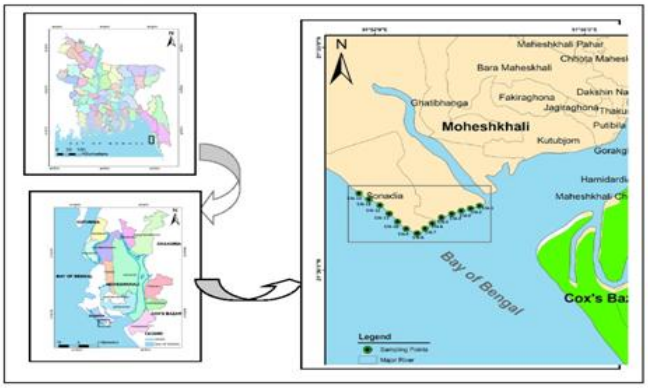

Fig. 1 Location map of the study area

The present study was done with a view to understand the heavy mineral distribution, mineralogical composition and trace element distribution within the beach sediment of Sonadia Island. Several hand auger drilling were made in order to observe the vertical extent of the heavy minerals in the island. During auger drilling, sand samples were taken in order to make laboratory investigation. In the laboratory, physical separation and microscopic techniques were employed to characterize the heavy minerals. A portable Radiation Survey Meter was used to measure radioactivity of the study area. Global Positioning System (GPS) was used to locate the position of sampling points.

2. Materials and Method

The present work incorporates various methods, such as field investigation, heavy mineral separation and mineralogical analysis by microscope and elemental analysis through portable XRF analyzer.

2.1 Field investigation

A geological fieldwork has been carried out at Sonadia Island of Moheshkhali Upazilla. Sandy beach and ridge extends along the length of Sonadia Island from north-west to south-east. The dunes run along the entire coast and are also fringed several hundred meters inward. The average height of the dunes was 1 m while average length and width was 60 m and 38 m respectively. Samples were collected from the dune sand where heavy minerals were relatively concentrated. In the field, Global Positioning System (GARMIN handheld Land GPS) was used to locate the Latitude-Longitude of the survey area. 14 representative samples were collected using hand auger for subsequent laboratory study. Radioactivity counts in cps (counts per second) were recorded by a portable Gamma Ray Spectrometer (Scintrex GRS-500). About 5~10 kg of beach sand samples were taken at each location for subsequent laboratory investigation (Fig. 2). Sampling location, depth, radioactivity at different locations of the collected samples was shown in Table 1.

2.2 Laboratory investigation

Laboratory investigations were carried out through sample treatment for further mineralogical analysis, heavy-liquid separation for separating heavy minerals from raw sand, microscopic study to get mineralogical composition and elemental analysis of the samples.

Table 1: Sampling description at Sonadia Island

Sample code	Longitude	Latitude	Depth (cm)	Radioactivity (cps)
SN01	91.900	21.524	90	40
SN02	91.895	21.523	90	34
SN03	91.893	21.522	152	50
SN04	91.890	21.521	90	80
SN05	91.888	21.520	152	170
SN06	91.885	21.517	60	90
SN07	91.883	21.516	60	60
SN08	91.880	21.514	30	50
SN09	91.877	21.515	60	90
SN10	91.874	21.518	30	90
SN11	91.871	21.521	122	100
SN12	91.868	21.524	60	100
SN13	91.865	21.528	60	120
SN14	91.861	21.529	30	100

2.3 Heavy Mineral Separation

Heavy mineral separation was done to know the percentage of heavy fraction in the raw sand. For the study Bromoform ($CHBr_3$) was used as density separator to separate the heavy from light minerals. The specific gravity of Bromoform is 2.9 at 20^0 C. The minerals that have specific gravity higher than the Bromoform are called heavy minerals. For this purpose 50 gm of raw sand sample was poured with stirring into 100-150 ml Bromoform contained in a wide-mouthed separating funnel. The funnel was fitted with a stopcock, the bore of which is of greater diameter than the inner diameter. The mineral floating on the Bromoform was stirred and the funnel then left until all the heavy minerals had settled. The heavy minerals with some Bromoform were then run from the bottom of the separating funnel into a filter funnel containing a filter paper. The heavy mineral in the filter paper was washed, free from Bromoform using acetone, dried, weighed and finally calculated as a percentage of the weight taken.

2.4 Microscopic study

For identification and counting the percentages of heavy minerals by grain count method, 42 (forty two) grain slides were prepared. For the preparation of slides, the grains were mounted on glass slide using Canada balsam. The glass slide was heated carefully in a hot plate to get required viscosity by avoiding of producing bubbles. Finally the slide was then kept in room temperature for few hours,

dried and covered by cover slip. Accessory balsam was washed with xylene (C_8H_{10}) and the grain slide was then ready for optical study. For the study, MEIJI ML 9300 polarizing petrographic microscope was used. For counting the grains under microscope, a magnification was selected such that the numbers of particles in the field of view are in the range of 50-100 grains (Fig. 3). At least 10 separate views were counted on each slide to give a total count per slide of 1000-3000 grains.

Fig. 2 Sample collection activities in the field

The weight percentage of individual mineral was calculated according to the following equation [14].

$$\text{wt\%} = \frac{100(bXc)}{\Sigma(\text{bxc})} \text{x} \frac{a}{100}$$

Where *a*, *b* and *c* represents the weight percentage of individual size fraction, number of grains of a particular mineral of interest and specific gravity of a particular mineral of interest respectively.

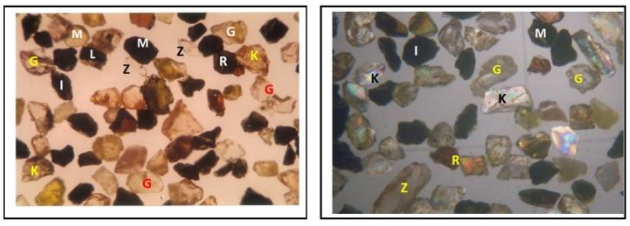

Fig. 3 Photomicrographs of heavy minerals (Ilmenite, Magnetite, Garnet, Zircon, Rutile, Leucoxene, Monazite and Kyanite)

2.5 Elemental analysis of the sample

Elemental analysis of collected samples was performed using a portable handheld XRF analyzer (NITON XL3) for detecting qualitative and quantitative elemental percentage presents in the samples. The analyzer is a single unit, high performance portable x-ray fluorescence (XRF) elemental analyzer.

For elemental analysis, 10 (ten) samples each of 50 gm were dried for 4-6 hours at 105°C in the laboratory drying oven. After then the samples were kept for air dry for overnight at room temperature in a shallow pan. Samples were then crushed into fine powder with an agate mortar and pestle. Then <0.075 mm size was taken using sieve shaker to avoid variations in particle size. The powdered sample was then placed in an XRF sample cup. A circle of polypropylene film was placed on the top of the sample cup. This film on the end of the cup with the indented ring was secured with the collar. The cup was filled with at least 10 gm of the powdered sample and confirmed that no voids or uneven layers were found. A filter paper was placed on the sample disk and a polyester fiber stuffing was put to prevent sample movement. The data were collected using different analytical mode to reveal the percentage of the elements of the samples.

3. Result and Discussion

The heavy minerals weight percentages of various locations for the study area are given in Table 2. The maximum and minimum amount of heavy minerals of the study area by Bromoform separation technique was measured as 84.96% in sample SN05 and 12.8% in sample SN04.

Table 2: Heavy mineral concentration in raw sand measured by heavy liquid separation of the study area

Sampling point	Heavy (%)	Light (%)	Loss (%)
SN 01	20.62	79.20	0.18
SN 02	29.36	70.60	0.04
SN 03	17.00	82.92	0.08
SN 05	84.96	14.90	0.14
SN 04	12.80	87.08	0.12
SN 06	77.20	22.68	0.12
SN 07	14.84	85.04	0.12
SN 08	16.18	83.66	0.16
SN 09	20.04	79.86	0.10
SN 10	34.20	65.76	0.04
SN 11	21.92	78.04	0.04
SN 12	32.62	67.33	0.05
SN 13	62.46	37.50	0.04
SN 14	56.00	43.97	0.03
Average	35.73	64.19	0.08

The heavy mineral assemblage of the study region is governed by the distribution of different types of minerals. The area is characterized by the presence of garnet (33.24% - 62.43%), ilmenite and magnetite together (21.39% - 56.27%), rutile (0.5% - 3.74%), zircon (0.11% - 3.16%), monazite (0.0% - 0.83%), leucoxene (0.57% - 1.81%) and kyanite (0.57% -1.81%). The minerals of the study area like garnet and kyanite may be assigned to the contribution of different high grade metamorphic rocks. Ilmenite, magnetite, zircon and rutile might have been derived from igneous rocks of acidic and basic composition. Table 3 shows the mineralogical percentage of the study area.

The concentrations of different elements measured in the samples by XRF are shown in Table 4. Zirconium (Zr), Strontium (Sr), Rubidium (Rb), Lead (Pb), Zinc (Zn), Manganese (Mn), Iron (Fe), Thorium (Th), Copper (Cu),

Cobalt (Co), Titanium (Ti), Barium (Ba), Cesium (Cs), Nickel (Ni) were determined in the samples, where each element's concentration was compared with world average value of that metal. The significance of trace elements in marine sediment is increasingly becoming an issue of global concern and needs proper assessment [15-16].

Table 3: Mineralogical abundance at Sonadia Island

Mineralogical abundance (%) in heavy fraction									
Sample ID	Ilm & Mag	Gar	Rut	Zir	Mnz	Leu	Kya	Qtz	Others
SN01	21.39	45.32	2.5	0.11	0	1.77	1.77	3.19	19.53
SN02	24.32	56.01	1.82	0.4	0	1.81	1.81	1.94	8.52
SN03	22.9	56.92	1.09	0.11	0	1.31	1.31	4.35	8.09
SN04	21.94	52.06	1.28	0.23	0	1.71	1.71	1.87	14.74
SN05	56.27	33.24	2.03	2.54	0.83	1.32	1.32	0.79	2.43
SN06	54.06	36.53	1.66	1.65	0.09	1.04	1.04	0.79	2.68
SN07	40.59	45.75	2.88	0.32	0	1.36	1.36	0.72	4.9
SN08	24.93	62.43	1.76	0.43	0.23	1.75	1.75	0.61	3.32
SN09	36.13	48.89	3.74	2.22	0	0.57	0.57	0.57	4.22
SN10	29.7	54.69	3.03	1.07	0	1.11	1.11	1.71	5.25
SN11	25.88	57.81	2.05	1.19	0.25	1.22	1.22	3.11	3.37
SN12	30.14	57.37	0.5	0.67	0.12	0.85	0.85	1.25	5.51
SN13	37.12	46.12	1.06	3.16	0.34	0.9	0.9	2.04	4.89
SN14	27.91	56.3	1.29	1.28	0	1.77	1.77	5.27	3.56
Average	32.38	50.67	1.91	1.10	0.13	1.32	3.98	2.02	6.50

Ilm=Ilmenite, Mag=Magnetite, Gar=Garnet, Rut=Rutile, Mnz=Monazite, Leu=Leucoxene, Kya=Kyanite, Qtz=Quartz

The concentration ranges 119-366 ppm for Zr and its average is 198 ppm. The concentration of Sr and Rb are 72-104 ppm and 81-106 ppm with an average value of 82 ppm and 93 ppm respectively. Mn, Ti and Th concentration are found as 309-478 ppm, 1221-1928 ppm and 1.01-9.25 ppm respectively and their average values are 390 ppm, 1598 ppm and 3.78 ppm. Iron is the most abundant metal, and is believed to be tenth most abundant element in the universe. The range of Fe concentration is found 12757-17638 ppm with an average of 15127 ppm. The iron concentration is much higher than average continental crust values [17]. The range of Cu concentration varies from 14.61-21.95 ppm. The average concentration of Cu is 18.08 ppm. The Cu concentration is lower than the average continental crustal value. Pb concentration varies from 7.8-12.15 ppm with an average concentration of 9.03 ppm. The Pb concentration is lower comparing with the coastal sediments and some other marginal marine areas. The concentration of Pb is low due to the dilution of monsoonal rainfall.

The average concentration of Ba and Cs are 280 and 91 ppm. The Ba concentration is lower than average continental crustal value whereas Cs is higher than it. Maximum Zn concentration of the study area is found 70.85 ppm with an average concentration of 38.75 ppm. It is higher than the average continental crustal values. The highest concentration of Zinc is mainly due to input of organic wastes in aquatic environment. Zinc can enter the aquatic environment from a number of sources including industrial discharge, sewage effluent and runoff [18]. The Ni concentration in the study area varies from 2.5 to 30.16 ppm with an average of 16.03 ppm. It is low compared to other coastal sediments. Cobalt is relatively scarce in the earth's crust. The Co concentration varies 99.40 - 49.71 ppm with an average of 70.84 ppm. The Co concentration is higher than the average continental crustal value. The presence of Co in the sediments of the study area is associated with lithogenic origin with little contribution from external sources.

Table 4: Concentration of different elements

Concentration of elements in samples (in ppm)											
Element	SN01	SN02	SN03	SN04	SN05	SN06	SN07	SN08	SN-09	SN10	Average crustal values
Zr	366.23	257.80	127.47	156.65	178.07	195.72	119.43	141.49	276.55	168.08	237
Sr	76.08	82.21	84.94	74.72	82.52	77.25	104.17	93.91	79.29	72.48	316
Rb	103.94	106.45	81.40	96.01	97.21	86.63	96.38	92.45	88.24	87.46	110
Mn	325.72	357.22	437.48	410.15	411.40	345.61	478.45	414.40	417.25	309.60	78
Ti	1928.3	1445.9	1226.7	1779.7	1660.3	1749.0	1221.4	1461.7	1904.1	1604.7	-
Th	9.25	7.99	1.02	4.30	4.41	1.01	3.23	1.141	3.65	1.83	10.3
Fe	15103.3	12757.0	14616.5	17638.7	15682.8	16597.9	13242.1	15261.7	16560.5	13810.2	-
Cu	19.47	18.076	19.12	21.95	17.61	18.07	16.19	14.61	18.84	16.91	28
Pb	8.18	7.86	9.20	8.58	9.36	7.97	12.15	9.14	8.48	9.40	17
Ba	400	488.01	393.33	0.038	0.041	0.039	400	410	373.33	340	668
Cs	79.37	87.91	90.91	97.31	94.77	97.50	91.99	88.10	96.79	91.58	5.8
Zn	70.85	59.18	29.90	33.94	32.60	36.26	25.23	32.57	35.88	31.12	67
Ni	11.01	2.52	16.92	19.42	27.04	30.16	16.93	8.88	16.44	11.01	47
Co	81.97	49.71	66.87	99.40	72.02	69.73	73.55	78.54	65.62	50.96	17.3

4. Conclusion

As there is no report of presence of significant amount of heavy minerals for being a deposit on Sonadia Island, it can be assumed that the erosion of Moheskhali and Cox's Bazar deposit, through Moheshkhali channel played a role of deposition of heavy minerals on this Island. Ocean current dynamics of the Bay of Bengal is another major factor to know the environment of deposition of these heavy minerals. The source of the heavy minerals observed in the Sonadia Island is possibly from the Miocene sedimentary rocks exposed along the Cox's Bazar beach, which have been distributed along the beach by the long shore current, waves and winds.

Mineralogical composition of heavy mineral concentrates indicates that garnet is the dominant mineral component followed by ilmenite, magnetite, rutile and zircon in heavy mineral composite. The radioactivity of the study area varies from 24 to 170 cps. The minerals like garnet, kyanite may be assigned to the contribution of different high grade metamorphic rocks. The opaque minerals mainly ilmenite and magnetite, rutile and zircon have been derived from igneous rocks of acidic and basic composition.

The concentrations of Zr, Sr, Rb, Pb, Zn, Mn, Fe, Th, Cu, Co, Ti, Ba, Cs, Ni that were studied can be treated as the baseline data of the area where detailed mineralogical and geochemical investigation in trace element level is needed. Extensive field work as well as laboratory works is required on Sonadia Island to identify the presence of any subsurface heavy mineral deposition cycle and their mineralogical percentages.

Acknowledgement

The first author would like to express the sincere gratitude to the Ministry of Science Technology (MOST), Government of the People's Republic of Bangladesh for providing fund for this Research Project for the financial year 2015-2016.

References

1. F. Deeba, M. Z. Kabir, M. M. Zaman, M. Rajib and S. M. Rana, Difference in Grain Size Distribution Among Heavy Minerals of Cox's Bazar, Barchara, Patuartek and Teknaf Fore Dune Deposit, Proceed. of Int. Confer. on Geosci. for Glob. Dev., 26-31 October, 2009, Dhaka, Bangladesh, 24-27 (2009).
2. M. Rajib, M. Z. M. Kabir, F. Deeba, M. M. Zaman and S. M. Rana, Distribution of five major heavy minerals along the recent beach areas of Bangladesh, The J. of NOAMI, **24(1)**, 1-9 (2007).
3. R. G. Schmidth, and S. A. Asad, A reconnaissance survey of radioactive beach sand at Cox's Bazar, Inter. Geol. Report, The Geological Survey of Pakistan, East Pakistan, **3,** 1-15 (1963).
4. M. M. Zaman, M. Z. Kabir, F. Deeba, M. Rajib and S. M. Rana, Finding a new heavy mineral deposit and its mineralogical composition at Sonarpara, Cox's Bazar, The J. of NOAMI, **26(1)**, 17-30 (2009).
5. M. M. Zaman, M. Rajib, M. Z. Kabir, F. Deeba, S. M. Rana, S. M. Hossain, S. A. Latif and G. Rasul, Presence of uranium and thorium in zircon assemblages separated from beach sands of Cox's Bazar, Bangladesh, J. of Sci. Tech. Environ. Informatics. **03 (01)**, 161-169 (2016).
6. M. H. Siddiqui, Land Accretion and Erosion in the Coastal Area, Proceed. of the Nat. Workshop on Bangladesh Coast. Area Res. Dev. and Manage., Dhaka, 3-4 October, 1988.
7. D. K. Barua, The Coastline of Bangladesh-An Overview of Process and Forms, Proceed. of 7th Sympo. on Coastal and Ocean Management, ASCE, Long Beach, CA, 8-12 July, 2285-2301 (1991).
8. M. S. Islam and A. Hoque, Application of Remote Sensing Technique to Study the Landuse Changes of Moheshkhali Island in Bangladesh, J. of Remote Sensing and Environ, **3**, 69-85 (1999).
9. M. E. Hoque, S. R. Chowdhury, M. M. Uddin, M. S. Alam and M. M. Monwar, Grain Size Analysis of a Growing Sand Bar at Sonadia Island, Bangladesh, J. of Soil Sci., **3**, 71-80 (2013).
10. L. A. Molony, Sonadia Island ECA Conservation Management Plan Coastal and Wetland Biodiversity Management Project BGD/99/G31, **5** (2006).
11. A. B. K. Majlis, M. A. Islam, M. H. Khasru and M. K. Ahsan, Protected to Open Basin Depositional System: An Appraisal for Moheshkhali-Kutubdia Coastal Plain (Abstract), Bangladesh Coast: Geology, Hazards and Res., 29-30 May, Dhaka Bangladesh, **3** (2011).
12. M. A. B. Biswas, Some information about mineralogical composition of the beach sands of Cox's Bazar, Bangladesh, Geology and Prospecting, Moscow, 7, 32-38 (1977).
13. M. A. B. Biswas, Mechanism of heavy mineral concentration in the beach sands of Cox's Bazar, Nucl. Sci and appl. **B (12-13)**, 74-83 (1981).
14. E. H. Macdonald, Manual of beach mining practice-Exploration and Evaluation: 2nd edition, Department of Foreign Affairs, Canberra, Australia (1972).
15. A. A. Adeniyi and J. A. Afolabi, Determination of total petroleum hydrocarbons and heavy metals in soils within the vicinity of facilities handling refined petroleum products in Lagos metropolis, Environ. Int., **28 (1-2)**, 79–82 (2002).
16. H. S. Lim, J. S. Lee, H. T. Chon and M. Sager, Heavy metal contamination and health risk assessment in the vicinity of the abandoned Songcheon Au-Ag mine in Korea, J. of Geochem. Expl., **96 (2-3)**, 223–230 (2008).
17. H. Wedepohl, The composition of the continental crust, Geochemica et Cosmochimica Acta, **59**, 1217-1239 (1995).
18. A. B. A. Boxall, S. D. Comber, A. U. Conrad, J. Howcroft and N. Zaman, Inputs, monitoring and fate modeling of antifouling biocides in UK estuaries, Marine Pollu. Bul., **40**, 898-905 (2000).

25 to 1044 MeV Protons Scattering from ^{40}Ca

M. S. Uddin[1, 3*], A. U. Huda[1], D. R. Sarker[1] and M. A. Rahman[2]

[1]*Department of Physics, Jagannath University, Dhaka -1100*
[2]*Department of Physics, University of Dhaka, Dhaka – 1000*
[3]*German University Bangladesh, Gazipur -1702*

Abstract

The experimental data for the angular distribution of 25 - 1044 MeV protons elastically scattered from ^{40}Ca have been analyzed in terms of the three parameters formalism of Strong Absorption Model (SAM) of Frahn and Venter. The best fit parameters T, Δ, and μ are obtained. The inelastic scattering of protons from ^{40}Ca leading to the 2^+ and 3^- states are studied to check the validity of the derived elastic scattering parameters. The quadruple and octupole deformation parameters β_2 and β_3 are extracted from the analyses. The deformation parameters are in good agreement with other works.

Keywords: Nuclear reactions and scattering, strong absorption model, elastic and inelastic proton scattering

1. Introduction

Proton-nucleus scattering has been the subject of a number of studies mostly using the optical model. The strong absorption model (SAM) was introduced by Frahn and Venter [1, 2] as an alternate to the optical model, where the projectiles are strongly absorbed by the target nucleus. In these cases the elastic scattering is describable without any knowledge of the absorption mechanism. The nuclear projectiles n, p, ^{3,4}He and heavy ion are strongly absorbed by the target nucleus. The diffraction model or the so-called strong absorption model starts with the direct parameterization of the scattering function η_ℓ [3, 4] avoiding the usual potential concept. Different non-elastic processes are accounted for by making η_ℓ complex. The SAM is particularly suitable to a situation dominated by strong absorption of incident particles at the nuclear surface.

In the present work we study the elastic scattering of protons from ^{40}Ca at 25 – 1044 MeV energies. Angular distribution data for the inelastic scattering of protons leading to 2^+ and 3^- states were then studied using the best fit SAM elastic scattering parameters and the corresponding deformation parameters are extracted.

2. Materials and Method

The strong absorption model (SAM) is used for the theoretical calculation of the differential cross section. The model starts with an explicit functional form for the scattering function η_ℓ as given by

$$\eta_\ell \exp\left(2i\sigma_\ell\right) = g(\ell) + i\mu \frac{dg(\ell)}{d\ell} \quad (1)$$

Where, σ_ℓ is the coulomb phase shift for the ℓ-th partial wave and g (ℓ) is a continuous monotonic function of the angular momentum. We consider the Woods - Saxon form of g (ℓ), namely

$$g(\ell) = \left[1 + \exp\left(T - \ell\right)/\Delta\right]^{-1} \quad (2)$$

Here, T is the critical or cut-off angular momentum that is just grazing the nuclear surface and Δ is the rounding parameter. The parameter μ more accurately $\mu/4\Delta$ is a measure of real nuclear phase shift. A closed form expression for the elastic cross- section is then arrived at refs. [5, 6] in terms of three adjustable parameters, namely T, Δ and μ.The parameters T and Δ are related respectively to the interaction radius R and the surface diffuseness d through the relations

$$T = kR\left[1 - \frac{2n}{kR}\right]^{1/2} \quad (3)$$

$$\text{And} \quad \Delta = kd\left[1 - \frac{n}{kR}\right]\left[1 - \frac{2n}{kR}\right]^{1/2} \quad (4)$$

Where, n and k are respectively the Coulomb parameter and wave number.

The formalism developed for elastic scattering can be readily extended, under the condition for strong absorption, to describe inelastic scattering to collective states in nuclei. The inelastic scattering amplitude can be expressed in terms of the first derivative of scattering matrix η_ℓ used to describe the elastic scattering process.

It is clear from relations (1) and (2) that the real part of the scattering function η_ℓ varies smoothly with ℓ from small values at low ℓ's to unity at high ℓ's with a rapid transition around the critical values, while the imaginary part of η_ℓ is clearly surface peaked. A partial wave expression is made for the amplitude for elastic scattering and a closed form expression is obtained for the cross – section under suitable approximations.

3. Results and Discussion

3.1 Elastic SCATTERING

Results of the present analysis of elastic scattering are

Corresponding author: msuraju1971@yahoo.com

presented in Table 1 and the experimental data along with the theoretical calculated angular distributions are shown in Figs. 1-2. The data are taken from refs. [7-17]. A reasonably good description of the elastic scattering is possible in terms of the simple model. The observed oscillations in higher mass nuclei are also nicely matched over the entire angular range. The fit is generally poor at lower projectile energies. The quality of fit improves as we go higher up in energy. This is understandable, since the SAM conditions are strictly not satisfied in such light nucleus, more so at lower energies. The cut-off angular momentum T increases smoothly with an increase in beam energy, as expected. It is observed that rounding parameter Δ lies between 0.50- 5.10. The rounding parameter Δ increases with the increase in projectile energy. The parameter Δ controls the overall slope of the angular distribution and gives the periods of the diffraction of oscillation. The value of T and Δ are presented in Table 1. The value of nuclear phase shift μ or more accurately $\mu/4\Delta$ lies in the domain $0.07 \leq \mu/4\Delta \leq 0.40$ shown in Table 1.

Table 1: SAM parameters and derived parameters for elastic scattering of protons

Serial No.	Target nucleus	Beam energy (MeV)	SAM parameters				Derived parameters						
			T	Δ	μ	μ/4Δ	R (fm)	d (fm)	θ_c (deg)	σ_R (mb)	r_o (fm)	$\frac{\sigma_R}{\pi R^2}$	n.v*
1	^{40}Ca	25	5.84	0.50	0.80	0.40	6.10	0.58	12.30	762.20	1.38	6.52	1
2	^{40}Ca	40	6.96	0.61	0.85	0.34	5.54	0.61	8.18	856.08	1.25	8.88	1.36
3	^{40}Ca	65	7.84	0.80	1.23	0.38	4.79	0.56	5.70	755.75	1.08	10.48	1.60
4	^{40}Ca	156	11.00	1.60	1.10	0.17	4.22	0.60	2.63	716.10	0.96	12.80	1.96
5	^{40}Ca	181	12.10	1.72	0.90	0.13	4.30	0.60	2.21	746.69	0.97	12.86	1.97
6	^{40}Ca	200	12.80	2.10	0.92	0.10	4.30	0.60	1.99	795.00	0.97	13.68	2.10
7	^{40}Ca	300	15.10	2.75	1.05	0.09	4.13	0.64	1.38	768.20	0.94	14.32	2.20
8	^{40}Ca	400	17.60	3.00	1.03	0.08	4.10	0.60	1.03	764.20	0.93	14.47	2.22
9	^{40}Ca	500	20.20	3.15	0.93	0.07	3.89	0.64	0.71	753.90	0.88	15.85	2.43
10	^{40}Ca	613	20.50	3.10	0.98	0.08	3.70	0.59	0.56	749.51	0.88	17.42	2.67
11	^{40}Ca	800	28.20	4.15	1.20	0.07	4.60	0.59	0.42	934.11	1.06	14.05	2.15
12	^{40}Ca	1044	33.20	5.10	2.25	0.11	5.89	0.64	0.34	950.90	1.09	8.72	1.34

Here, n.v* refers to the normalized value of $\frac{\sigma_R}{\pi R^2}$

The best fit SAM parameters are then used to determine the interaction radius R, the surface diffuseness d and the reaction cross-section σ_R. These are also shown in Table 1. It is evident from our studies that the value of R decreases as the beam energy increases for the same target nuclei shown in Fig. 3. The interaction radius R is sensibly constant as evidenced by the least squares fit given by

$$R = 5.03 - 0.0019E \text{ (fm)}$$

We see from the present study that the surface diffuseness d is approximately the same for different nuclei at all the energies shown in Fig. 4.

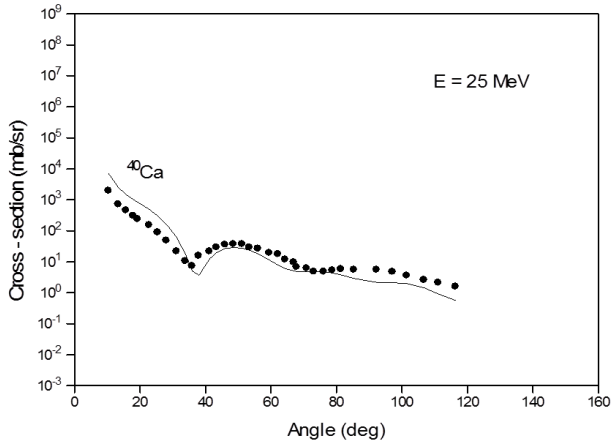

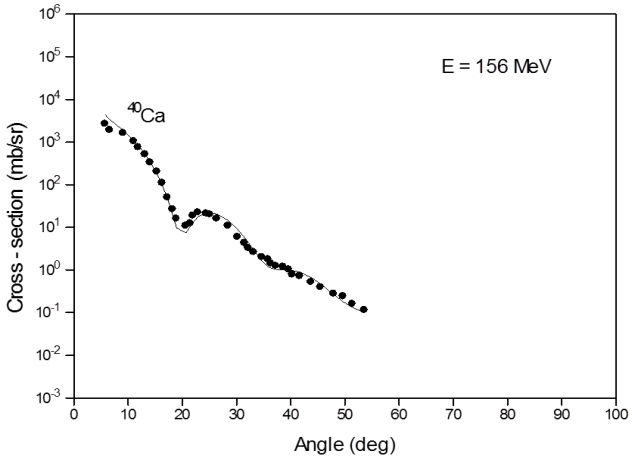

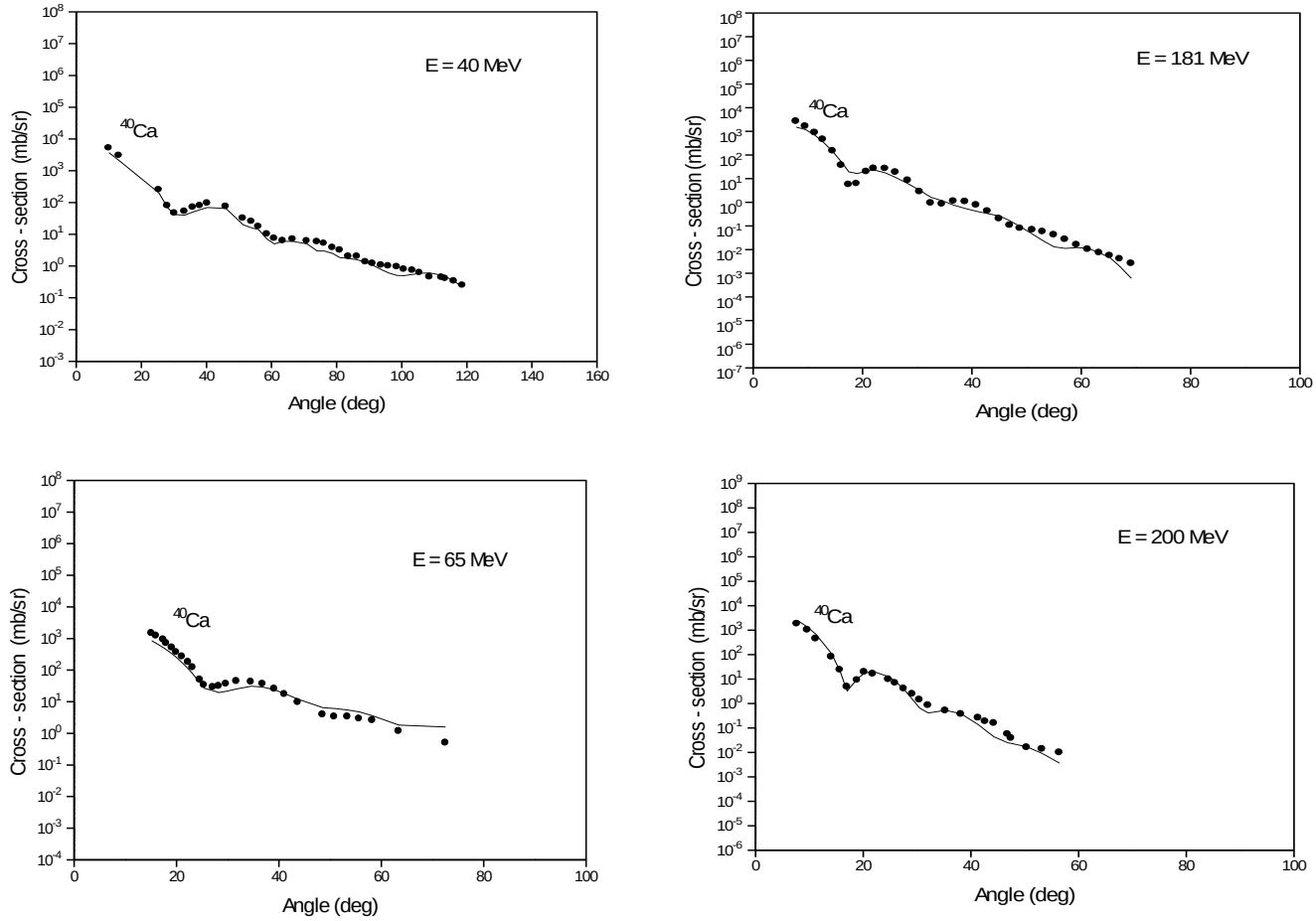

Fig. 1 SAM analysis of elastic scattering of protons

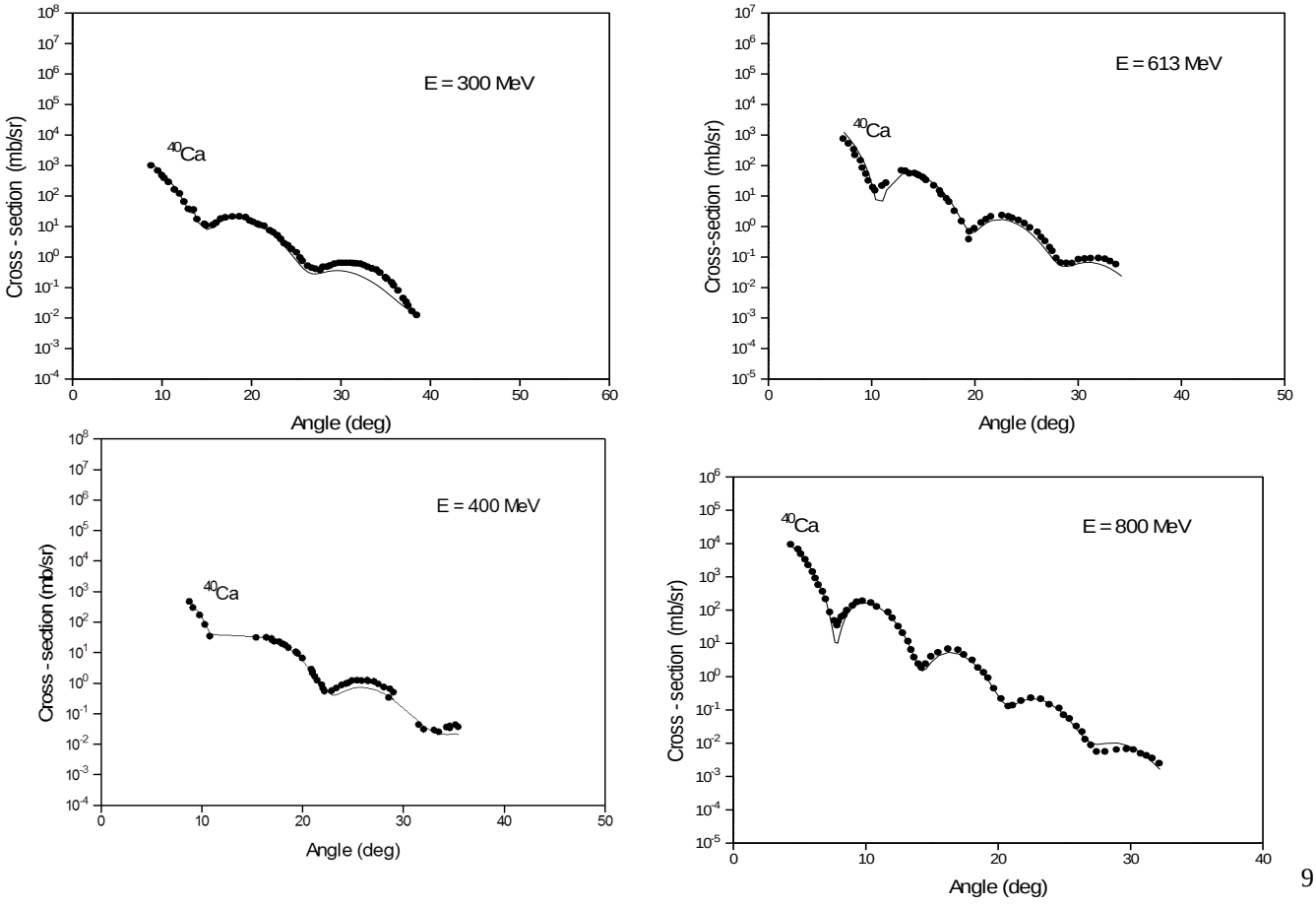

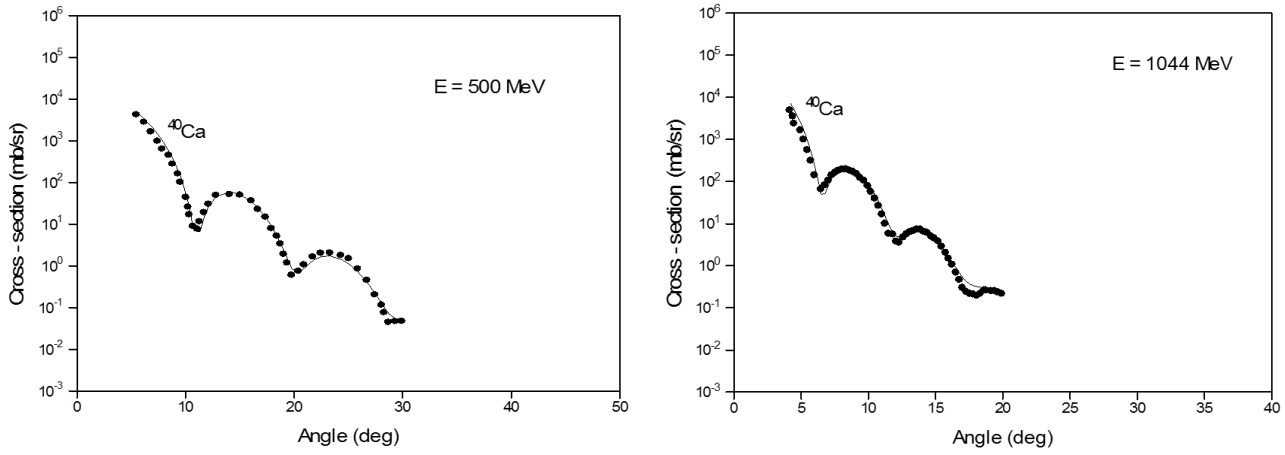

Fig. 2 SAM analysis of elastic scattering of protons

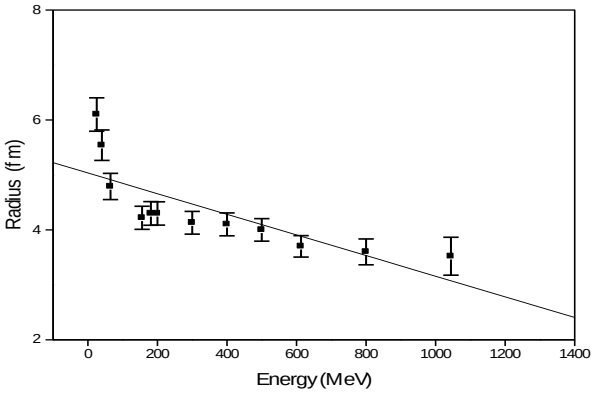

Fig. 3 Dependence of Radius (R) on proton energies

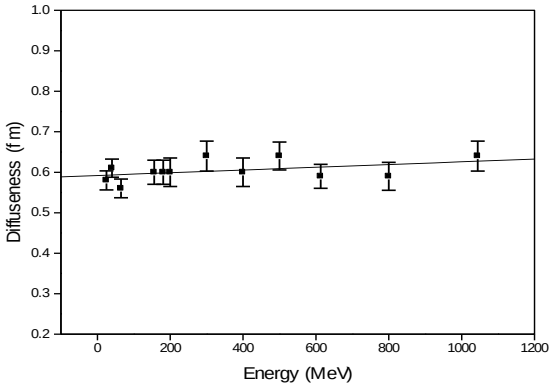

Fig. 4 Dependence of diffuseness (d) on Proton energies

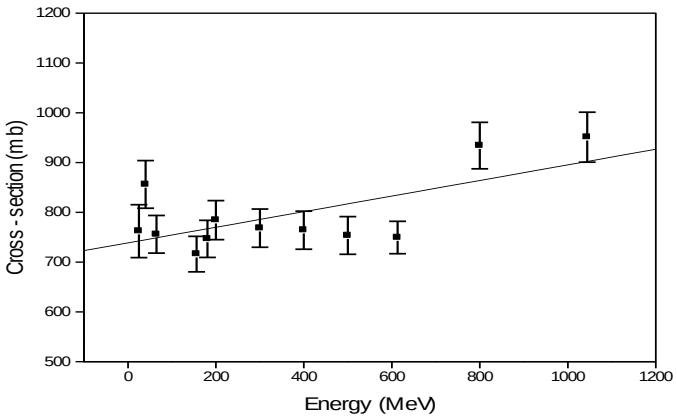

Fig. 5 Dependence of Cross section (σ_R) on proton energies

The energy dependence of reaction cross-section σ_R is shown in Fig.5. The least square fit given by

$$\sigma_R = 738.69 + 0.150E \text{ (mb)}$$

3.2 Inelastic scattering

The best fit parameters T, Δ and μ have been used to study the inelastic scattering of protons. The angular distribution data for the inelastic scattering of protons leading to a few collective states such as 2^+ and 3^- in ^{40}Ca have been analyzed in terms of the SAM formalism given by Potgieter and Frahn [16]. Fits to the inelastic angular distributions are shown in Figs. 6-7. The overall trend of the angular distributions is reproduced by the theory. Results of the inelastic scattering analyses are presented in Table 2. Also included the various obtained data in the previous studies. The β_2 and β_3 values from the various measurements are summarized respectively by Raman et al. [14] and Spear [15]. The present values are in good agreement with the previous values. It has been pointed out by Satchler [18] that the real test of the parameters obtained from the elastic scattering lies in their ability in reproducing the non-elastic data.

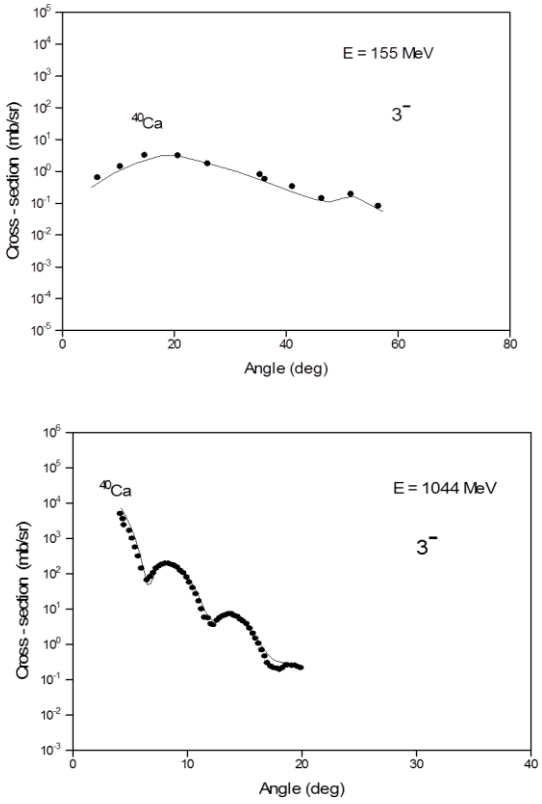

Fig. 6 SAM fit to the inelastic scattering of proton leading to the 3^- state

The β_2 and β_3 values from the various measurements are summarized respectively by Raman et al. [14] and Spear [15]. The present values are in good agreement with the previous values. It has been pointed out by Satchler [18] that the real test of the parameters obtained from the elastic scattering lies in their ability in reproducing the non-elastic data.

Table 2: Deformation parameters from inelastic scattering of protons leading to 2^+ and 3^- states in nuclei

Nucleus	E_p (MeV)	E_x (MeV)	J^π	Deformation parameters β_L		
				a	b	C
^{40}Ca	500	3.904	2^+	0.447	0.49 – 0.50	
^{40}Ca	155	3.737	3^-	0.36		0.33 –0.36
^{40}Ca	1044	3.737	3^-	0.34		0.33 –0.36

a. Present work (SAM analyses), b. Previous work [14] c. Previous work [15]

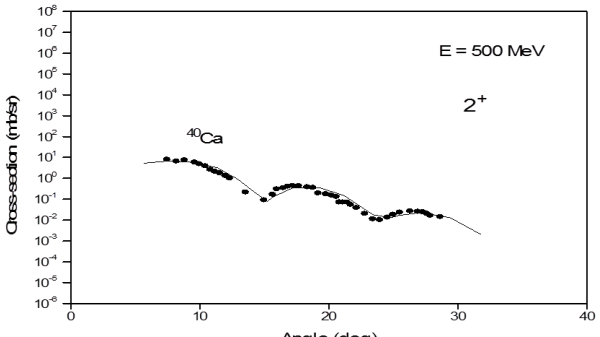

Fig. 7 SAM fit to the inelastic scattering of proton leading to the 2+ state

4. Conclusion

The three parameters (T, Δ, and μ) SAM formalism of Frahn and Venter [1, 2] can reasonably well account for the elastic scattering of protons. The angular distributions of the elastic scattering of protons from ^{40}Ca at 25 - 1044 MeV energies have been analyzed with SAM formalism and the best fit parameters T, Δ, and μ have been obtained. The quality of agreement between experiment and theory is much better for both the elastic and inelastic scattering using SAM formalism of Frahn and Venter. It is observed that the fittings of theoretical angular distribution are poor at low beam energies and smaller angels while at large energies the fittings become fairly improved. The values $\frac{\sigma_R}{\pi R^2}$ lie in the limit 0.4 ~ 1.0 and can be considered to be roughly the same, justifying the validity of the SAM parameters obtained from elastic scattering analyses. Another validation comes from the reasonable reproduction of the inelastic angular distribution and from quadrupole (β_2) and octupole (β_3) parameters values. The SAM is thus a successful model; the parameters are all unique and physically meaningful. The beauty of the model lies in its simplicity.

References

1. W. E. Frahn and R. H. Venter, Strong absorption model for elastic nuclear scattering part–I, Ann. Phys., (N.Y.), **24**, 243 (1963).
2. W. E. Frahn and R. H. Venter, Strong absorption model for elastic nuclear scattering and polarization of spin-12 particles, Ann. Phys., (N.Y.), **27**, 385 (1964).
3. K. R. Greider and Glassgold, Diffraction theory for very-high-energy scattering, Ann. Phys., **10**, 100 (1960).
4. J. A. McIntyre, K.W Wang and L. C. Beeker, Analysis of alpha-particle elastic scattering experiments, Phys. Rev., **A117,** 1337 (1960).
5. R. H. Venter, Strong absorption model for elastic nuclear scattering part –II, Ann. Phys., **25**, 405 (1963).
6. W. E. Frahn and B. Wiechers, Analysis of ^{3}He-nucleus scattering and polarization, Nucl. Phys., **74**, 65 (1965).
7. W. E. Frahn, Fundamentals in Nucl. Theory (IAEA), Vienna, **I** (1967).
8. L. F. Hansen, J. L. Kammerdiener and M. S. Weiss, Analysis of the scattering of 24-MeV ^{3}He particles from the even isotopes of zinc, Phys. Rev., **C4,** 1189 (1971).
9. N. Wills. I. Brissaud, Y. L. E. Bornec, B. Tatischeff and G. Duhames, Analysis of the (^{3}He, t) reaction on some 1p shell nuclei, Nucl. Phys., **A204**, 454 (1973).
10. M. Hyakutake, I. Kumabe, M. Fukuda, T. Komatuzaki, I. Yamagata, M. Inoue and H. Ogata, Elastic scattering of 119MeV He^{3} particles and ^{15}N energy and mass number dependence of optical potential parameters, Nucl. Phys., A333, 1 (1980).
11. N. Matsuoka, K. Hatanaka, M. Fujiwara. Y. Fujita. T. Saito, K. Hosono, A. Shimizu and M. Kondo, DWBA analysis of (^{3}He, d) reactions at 90Mev and contributions from the nuclear interior, Nucl. Phys., **A373**, 377 (1982).
12. P. M. Lewis, A. K. Basak, J. D. Brown, P. V. Drumm, O. Karban, E.C. Pollacco and S. Roman, The elastic and inelastic scattering of 33Mev polarized ^{3}He from oxygen and iron isotope, Nucl. Phys., **A395,** 204 (1983).
13. S. Raman, C. H. Malarkey, W. T. Milner, C. W. J. Nestor and P. H. Steslon, Atomic data and nuclear data tables, **36**, 1 (1987).
14. M. A. Rahman, H. M. S. Gupta and M. Rahman, Strong absorption model for pion nucleus scattering around (3, 3) resonance, Phys. Rev., **C44**, 2484 (1991).
15. R. H. Spear, Atomic data and nuclear data tables, **42**, 55 (1989).
16. J. M. Potgietr and W. E. Frahn, Strong absorption model for inelastic nuclear scattering, Nucl. Phys., **80**, 434 (1967).
17. D. R. Sarker, H. Kabir, M. A Rahman and H. M. S. Gupta, Generalized diffraction model study of intermediate energy proton-nucleus scattering, Int. J. Mod. Phys., **E13(2),** 505 (2004).
18. G. R. Satchler, Proc. Int. Conf. Reactions between complex Nuclei, Nashville Tennessee (North-Holland Publishing Co., Amsterdam, 1974).

Studies on Pesticide Residues in Soils of Some Selected Spots of Coastal Region of Bangladesh

M. A. Uddin, M. H. Rahman[1] , M. Nesha*, M. A. Z. Choudhury, Z. Fardous and M. A. Rahman

Institute of Food and Radiation Biology, Atomic Energy Research Establishment
Ganakbari, Savar, G.P.O Box-3787, Dhaka-1000
[1]*Department of Environmental Science, Jahangirnagar University, Savar, Dhaka*

Abstract

A study was conducted to determine the presence of insecticide residues including organophosphorous, carbamate and organochlorine in soil samples from vegetables and paddy fields in the coastal district Feni of Bangladesh. Samples collection and preparation were carried out using standard procedures. The concentrations of all the pesticides in the samples were determined using High Performance Liquid Chromatography (HPLC) technique. The result revealed that some samples out of 21 samples were found to be contaminated with organophosphorus (OP) pesticide namely diazinon; carbamate pesticide namely carbofuran and carbaryl ranging from 0.01-0.235 μg/kg and 0.381-3.21 μg/kg respectively. On the other hand, no organochlorine pesticide residue was detected in the soil samples. However, the contamination level of organophosphorous and carbamate was relatively low compared to the IAEA/FAO/Codex Alimentarious Guideline value.

Keywords: Pesticide**,** residue, organophosphorus, carbamate, organochlorine, HPLC

1. Introduction

Bangladesh is a tropical country. Because of the prevailing high temperature and humidity, rapid multiplication of pests occurs in the country and those harmful insects cause intense loss of food production [1, 2]. Every year more than 45% of food production is lost due to pest infestation which leads serious economic loss and hence pests are considered as the major challenge in agriculture. To combat pests, the use of a wide variety of pesticides on agricultural practices in the tropics has increased.

Although the use of pesticides in Bangladesh is relatively low (300g active ingredient/hectare) in comparison to other countries of the world and even much lower than India (380g active ingredient/hectare), consumption of pesticides has now increased and been an inherent part of agriculture in recent years with the introduction of high yielding varieties of crop to control pest and diseases [3-5]. About 33,371 tons formulated products were used in 2016 compared to 18,090 tons in 2003 and 25,479 tons in 2005 [6, 7]. Chemical fertilizers and pesticides have contributed significantly to improve yields of crops, increasing the production of food grains from 9.7 million mt in 1961 to about 20 million mt in 1993 [8]. Because of widespread use of these agrochemicals to increase crop yield and reduce postharvest losses, they are detected in various environmental matrices (soil, water and air) as well as they leave residues in food and thereby produce adverse effects when concentration exceeds the maximum residue limit (MRL). The increased use of these chemicals may show negative effects on the quality of soils and drinking water sources. When entering into the soil, pesticides may be taken up by plants roots and have the potential to cause toxicity to plants, their products and contaminate the food chain. Through leaching and surface runoffs, pesticide residues in soil and the environment may pollute groundwater and surface water, thereby increasing the risk of environmental contamination. Increased accumulation of pesticide residues in the food chain and drinking water have been reported to pose serious human health hazards [9, 10]. Human health hazards vary with the type of the pesticides and also with the extent of exposure. Moderate human health hazards from the misapplication of pesticides include mild headaches, flu, skin rashes, blurred vision and other neurological disorders while rare, but severe human health hazards include paralysis, blindness and even death [11]. International development research centre, Ottawa, has claimed that every year about 10,000 people die and 4,00,000 people suffer from various effects of pesticide poisoning in developing countries [12]. There is a great concern over growing incidence of cancer due to their excessive use [13]. Pesticide residue pollution to the local environment (air, soil and surface water) also affects the lives of birds, wildlife, domestic animals and fish [14]. For the above reasons, use of pesticides has to be controlled to avoid contamination of food supplies and ecological imbalance, but present measures in Bangladesh are inadequate and farmers rarely implement standards [15].

The introduction of organophosphate (OP) and carbamates insecticides were in the 1960s and in 1970s respectively contributed greatly in pest control and agricultural output. Organophosphorous insecticides are the most commonly used and detected pesticides in water streams around the world [16]. In terms of formulated product of carbamates, Bangladesh shared the highest portion (64%) followed by organophosphates [17]. Again, among the pesticides used in agriculture, organochlorine pesticides (OCs) are very toxic and persistent in the environment, which tend to accumulate in living organisms. Although most of them have been banned or restricted after the 1960s in most of the technologically advanced countries, they are still detected in natural ecosystems [18]. Though the organochlorine pesticide DDT was banned in late 1993 in Bangladesh,

Corresponding author: meher.bmb@gmail.com

DDT along with its metabolite DDE were found in soil of Narshingdi area [19, 20]. Due to long persistence nature of DDT that may pose a big threat to human, it is a necessity to monitor foods, water, soils and other environmental samples for their presence.

Literature suggests that information regarding the significance of persistence of pesticide residues in soil is very little in Bangladesh and no information is available on levels of pesticide residues in soils of coastal Feni district. So, an attempt was undertaken to assess the types of pesticide residues (i.e. organophosphorous, carbamate and organochlorine) used and their concentration levels in some selected soils extensively used for vegetables and rice cultivation of coastal Feni district of Bangladesh.

2. Materials and Method

2.1 Sampling

Soil samples were collected from Sonagazi upazila, Feni, near the coastal area and were processed for subsequent experiments and necessary analysis. After collecting, the samples were taken to the Agrochemical and Environmental Research Division (AERD), Institute of Food and Radiation Biology (IFRB), Atomic Energy Research Establishment (AERE), Ganakbari, Savar, Dhaka as early as possible and preserved in deep fridge for avoiding loss of the residues.

2.2 Equipments

HPLC: High Performance Liquid Chromatography (Shimadzu, LC-10 ADvp) equipped with a SPD-M 10 Avp, PDA detector; C_{18} Reverse Phase Alltech analytical column (250 × 4.6 mm), Rotary vacuum evaporator (Type -350, USA).

2.3 Extraction

The soil samples were dried at room temperature in a fume cupboard and then made fine powder form by using morter-pastle. To analyze the residues, 50 g of each sample were extracted with 100 ml mixed solution of Hexane and Acetone (1:1) by using electronic shaker. The extract was treated with 5 g anhydrous sodium sulphate to remove traces of water.

2.4 Clean-up

The extract was subjected to clean-up using florisil column chromatography [21]. The top 1.5 cm of the florisil column was packed with anhydrous sodium sulphate. Elution was done with 2% diethyl ether in hexane (5 ml/min). The eluate was concentrated in a rotary vacuum evaporator and transferred to glass-stoppered test tubes. Solvents were completely removed under mild nitrogen flow. The evaporated sample was dissolved in hexane and made to volume in a volumetric flask for subsequent liquid chromatography.

2.5 Analysis

Injections of the aliquots were done by micro syringe into HPLC (High Performance Liquid Chromatography). Quantification was made with a freshly prepared standard curve of the relevant (standard) pesticide. Analysis was done by High Performance Liquid Chromatography fitted with Photo Diode Array Detector [20].

3. Results and Discussion

Twenty-one soil samples collected from vegetables and paddy fields of the Sonagazi upazila of coastal Feni area (Fig 1) of Bangladesh were analyzed for the presence of different pesticide residues and to compare the data with IAEA/FAO/Codex Alimentarious Guideline value. HPLC technique was used as a method of choice for determining the organophosphorus, carbamate and organochlorine pesticide residues analysis in collected sample. A representative chromatogram of the studied samples showing peaks for diazinon (Fig 2a.) and carbaryl (Fig 2b.) has been presented. The analytical results reflected contamination of the soil samples with residues of diazinon, carbofuran and carbaryl pesticides. These results are summarized in Table 1. Table 1 reveals that 3 of 21 soil samples showed the contamination of diazinon compound. The presence of organophosphorus pesticide diazinon was analyzed in SS-11, SS-13 and SS-16 soil samples with a range of 0.01-0.235 µg/kg. The highest concentration (0.235 µg/kg) was found in SS-16 and the lowest concentration (0.01 µg/kg) was in SS-13. Excessive use of Basudin, an organophosphorus pesticide, is the main source of the residue. Table-1 also presents that of the 21 soil samples only 3 samples were contaminated with carbamate residue where 2 samples were

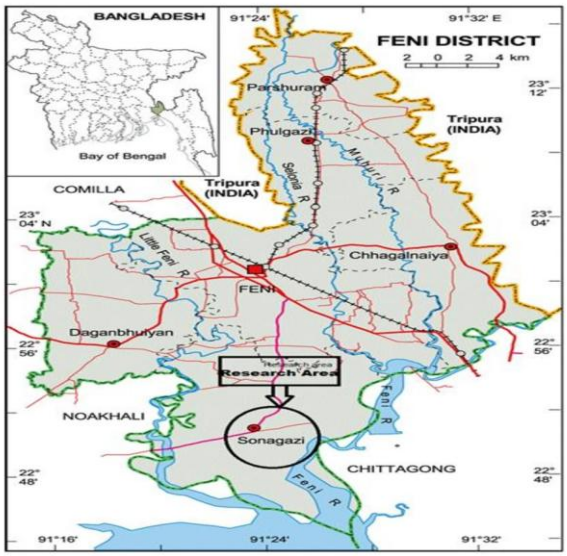

Fig. 1: Location map and sampling points of soil samples

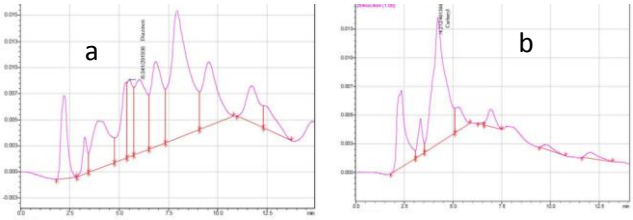

Fig. 2: Representative-chromatogram-of-the-analyzed-samples

Table 1: Amount of Organophosphorus and Carbamate Pesticide Residues in Soil Samples of Sonagazi Upazila in Feni

Sample No.	Pesticide Residues in Soil Samples (μg/kg)		
	Diazinon	Carbofuran	Carbaryl
SS-01	ND	ND	ND
SS-02	ND	ND	ND
SS-03	ND	ND	ND
SS-04	ND	ND	ND
SS-05	ND	ND	ND
SS-06	ND	ND	ND
SS-07	ND	ND	ND
SS-08	ND	ND	ND
SS-09	ND	ND	ND
SS-10	ND	3.21	0.381
SS-11	0.14	ND	ND
SS-12	ND	3.08	ND
SS-13	0.01	ND	ND
SS-14	ND	ND	ND
SS-15	ND	ND	ND
SS-16	0.235	ND	ND
SS-17	ND	ND	2.52
SS-18	ND	ND	ND
SS-19	ND	ND	ND
SS-20	ND	ND	ND
SS-21	ND	ND	ND

Detection limit for HPLC: 10μg/kg, ND: Not Detected

Table 2: Amount of Organochlorine Pesticide Residues in Soil Samples of Sonagazi Upazila in Feni

Sample No.	Pesticide Residues in Soil Samples (μg/kg)		
	DDD	DDE	DDT
SS-01	ND	ND	ND
SS-02	ND	ND	ND
SS-03	ND	ND	ND
SS-04	ND	ND	ND
SS-05	ND	ND	ND
SS-06	ND	ND	ND
SS-07	ND	ND	ND
SS-08	ND	ND	ND
SS-09	ND	ND	ND
SS-10	ND	ND	ND
SS-11	ND	ND	ND
SS-12	ND	ND	ND

Sample No.	Pesticide Residues in Soil Samples (μg/kg)		
	DDD	DDE	DDT
SS-13	ND	ND	ND
SS-14	ND	ND	ND
SS-15	ND	ND	ND
SS-16	ND	ND	ND
SS-17	ND	ND	ND
SS-18	ND	ND	ND
SS-19	ND	ND	ND
SS-20	ND	ND	ND
SS-21	ND	ND	ND

Detection limit for HPLC: 10μg/kg, ND: Not detected

found to be contaminated with carbaryl compound and 2 with carbofuran compound. Carbaryl residue was observed in SS-10 and SS-17 samples where the highest concentration (2.52 μg/kg) was found in SS-17 and the lowest concentration (0.381 μg/kg) was in SS-10. The carbofuran pesticide was detected in SS-10 and SS-12. The highest concentration of 3.21μg/kg was analyzed in SS-10 and the lowest concentration (3.08 μg/kg) was in SS-12. Different factors such as persistence of pesticides, availability in use, indiscriminate use and lack of consciousness are considered for the presence of these residues. However, the contamination level of organophosphorous and carbamate was relatively low compared to the IAEA/FAO/Codex Alimentarious Guideline value. The wide use of pesticides in the world causes major health and environmental problems. It is necessary to learn more about the problems caused by exposure to pesticides with respect to safety, health and the environment. It has been reported in the press and quoted from the farmers of grass roots level that pest from fields treated with pesticides move to the adjacent fields forcing the owners of these fields also to use chemicals as well. It was also mentioned quoting farmers that the pesticide company dealers try to motivate farmers of a village to use pesticide on their crops and naturally the other farmers also follow to avoid attack by pests [22]. The farmers and the inhabitants of the study areas should be educated on the dangers of pesticides for pest control. It should be noted that countries like Bangladesh did not have necessary resources and infrastructures to adequately regulate the use of pesticides. Proper regulatory enforcement of the relevant rules and provisions, and regular monitoring of residues would prevent misuses and could minimize the environmental problems.

Table-2 explores that the studied soil samples were free from organochlorine residues DDT, DDD and DDE. The absence of DDT along with its metabolite DDD and DDE indicated the growing awareness of its ill effects amongst the farmers.

The findings of this study suggest that the soil quality of Sonagazi upazila is better than those from other parts of Bangladesh in terms of pesticide residues [20]. This study can only provide some baseline data which deserve further investigation so that a concluding remark can be made regarding the present status of residual level in different environmental soil samples of the area.

4. Conclusion

The presence of various agrochemicals such as diazinon, carbofuran and carbaryl pesticides in the samples analyzed was an indication of the use of the pesticides by farmers in the study area to control pest and diseases. Though the soil was contaminated with organophosphate and carbamate pesticide residues, they were within the range of IAEA/FAO/Codex Alimentarious Guideline value. Despite the low level of contamination in the studied soils, the best environmental management in the vegetable and rice production area requires the regular monitoring of soil contamination level in the coastal Feni district.

References

1. K. Kannan, S. Tanabe, A. Ramesh, A. Subramanian and R. Tatsukawa, Persistent orgnochlorine residues in food stuffs from India and their implications on human dietary exposure, J. Agric. Food. Chem., **40**, 518–524 (1992).
2. A. Lakshmi, Pesticides in India: risk assessment to aquatic ecosystems, Sci Total Environ., **134**, 243–253 (1993).
3. R. J. Kuhr and H. W. Dorough, Carbamate Insecticides, Chemistry, Biochemistry and Toxicology. CRC Press, Boca Raton, **Fl,** 178 (1977).
4. D. K. Nath and B. B. Chakraborty, Control of Brinjal (Solanum melongena) fruit and shoot borer, Leucinodes orbonalis Gueen. (Pyralidae: Lepidoptera) by soil application of granular insecticides, Pesticides, **12** (10), 27-28 (1978).
5. N. Chowdhury, M. A. Malek, S. M. Ullah and M. M. Rahman, Fate of [^{14}C]-carbofuran pesticide studied in a sandy loam soil in laboratory conditions, J. Asiat. Soc. Bangladesh, Sci., **28** (1), 19-26 (1978).

6. M. Rahman, Pesticides and environmental pollution: Mitigation approach and measures 2007. T. M.: Support of the facilitating the development and spread of the IPM collaborative research support program, BARC, Dhaka, 4-12.
7. Yearbook of agricultural statistics-2016, Bangladesh Bureau of Statistics, 399 (2017).
8. M. A. Matin, Environmental pollution and its control in Bangladesh, TRAC Trends in Analytical Chemistry, **14** (10), 468-473 (1995).
9. S. K. Agbeve, P. Osei-Fosu and D. Carboo, Levels of organochlorine pesticide residues in Mondia whitei, a medicinal plant used in traditional medicine for erectile dysfunction in Ghana, Int J Adv Agric Res, **1**, 9–16 (2014).
10. J. C. Akan, L. Jafiya, Z. Mohammed and F. I. Abdulrahman, Organophosphorus pesticide residues in vegetable and soil samples from Alau Dam and Gongulong agricultural areas, Borno State, Nigeria. Int J Environ Monit Anal, **1** (2), 58-64 (2013).
11. V. F. Garry, D. Schreinemachers, M. E. Harkins and J. Griffith, Pesticide appliers, biocides, and birth defects in rural Minnesota, Environ. Health Perspectives, **104** (4), 394-399 (1996).
12. Y. P. Gupta, Pesticide poisoning, Sci, Rep., **26** (9), 491-492 (1989).
13. R. D. Johnson and D. D. Manske, Pesticide and other chemical residues in total diet samples (XI), Pestic. Monit. J., **11** (3), 116-131 (1977).
14. Anonymous, Survey of the Environment, The Hindu, (1991).
15. M. A. Matin, M. A. Malek, M. R. Amin, M. S. Rahman, J. Khatoon, M. Rahman, M. A. Uddin and A. J. Mian, Organochlorine insecticide residues in surface and underground water from different regions of Bangladesh. Agriculture, Ecosystems and Environment **69**, 11-15 (1998).
16. M. Tankiewicz, J. Fenik and M. Biziuk, Determination of organophosphorus and organonitrogen pesticides in water samples, Trends Anal. Chem., **29**, 1050–1063 (2010).
17. M. M. Rahman, Pesticide usage in field crop protection and its impact on environment. National workshop on conventional and nuclear techniques for pesticide residue studies in food and environment, IFRB, AERE, Savar, Dhaka (2000).
18. C. Dong, Z. Zeng and X. Li, Determination of organochlorine pesticides and their metabolites in radish after head space solid-phase microextraction using calix[4]arene fiber, Talanta, **66**, 721–727 (2005).
19. M. A. Z. Chowdhury, M. A. Zaman, Z. H. Khan, M. A. Uddin, M. A. Malek and S. M. Ullah, Detection of DDT residues in water samples from different locations of Dhaka metropolitan city by ELISA, Bangladesh J. Environ. Sci., **9**, 234-239 (2003).
20. M. A. Uddin, M. A. Z. Chowdhury, Z. Fardous and M. Hasanuzzaman, Quantification of pesticide residues in some soils of Narshingdi Area of Bangladesh, Bangladesh Journal of Scientific Research, **29** (1), 85-88 (2016).
21. DFG manual of pesticide residue analysis. Pesticide Commission, Weinheim, New York, NY: VCH. **1**, 297-307 (1987).
22. M. M. Alam, N. G. Das, M. M. Rahman and M. A. Malek, Organochlorine insecticide residues in water and soil of the Meghna Dhonagoda irrigation project of Bangladesh, J. Asiat. Soc. Bangladesh, Sci., **25** (1), 135-142 (1999).

Efficacy of Monosodium Glutamate Against Larvae of Culex Quiquefasciatus Say (1823) (Diptera: Culicidae)

D. Akter[1], H. R. Khan[1], M. M. Rahman[2] and M. Begum*[1]

[1]*Department of Zoology, University of Dhaka, Dhaka-1000, Bangladesh*
[2]*Bangladesh Atomic Energy Commission*

Abstract

The present experiment was done with 0.00, 0.01, 0.02, 0.03, 0.04 and 0.05 g/ml Monosodium Glutamate (MSG) solution (in 0.35mg of average body weight of larvae) against laboratory reared 4th instar larvae of *Cx. quinquefasciatus*. Mortalities of the larvae were recorded after 48 hours of application. Histo-morphological changes were observed in the untreated and treated larvae. Mean percentage of mortalities were subjected to one way ANOVA and multiple comparisons. Dose response curve were also produced by regression analysis. The highest (93.33%) and the lowest (7.22%) mortalities were recorded at dose 0.05 g/ml and 0.01 g/ml, respectively. Mean mortalities among different doses of MSG were found to be significantly ($p<0.05$) different. Histological study revealed that the tissue disruption in the stomodeal valve and the peritrophic membrane of anterior mid gut at 0.01 g/ml dose of MSG. The 0.3 and 0.5g/ml dose of the MSG caused the tissue destruction of the microvilli and muscular sheath of the rectal pad situated in the hindgut which indicates the major alteration of hind gut has been found at 0.05 g/ml dose of MSG. In untreated of MSG larvae, no such abnormalities were observed.

Keywords: *Culex quiquefasciatus*, monosodium glutamate, food additives, histology

1. Introduction

The various food additives and chemicals are used as preservatives or enhancer of palatability of food. Monosodium glutamate, one of the most common food additive largely consumed since 1909, has been doubted these last twenty years to potential adverse impact on health [19, 12]. As a food additive, it provides a flavoring function through the stimulation of organo sensory receptors and makes the food appetizingwhen added in the proper concentration [17]. MSG elicits a taste described in Japanese as umami, which is translated to ‘‘savory’’ and it is different from four basic taste (sweet, sour, salty and bitter) [22]. It is the naturally occurring amino acid containing 78% of glutamic acid 22% of sodium and water which is most used in India, China, Japan, Thailand,Vietnam and some other tropical countries including Bangladesh where it is generally known as testing salt [4]. MSG is currently found in thousands of diff erent processed foods, including soups, salad dressings, mayonnaise, canned vegetables and frozen dishes [4]. In 1991, the average intake of MSG in United Kingdom was 580 mg/day for general population individual and 4.68 g/day for extreme users [21]. The assessed average daily MSG intake per person in industrialized countries is 0.3–1.0 g, though it depends on the MSG content in foods and an individual’s taste preferences [13]. A typical Chinese restaurant meal contains between 10 and 1500 mg of MSG per 100 g [12]. Asia was responsible for approximately 88 percent of world MSG consumption, with China alone accounting for 55 percent of world consumption and approximately 65 percent of global production [2].

In spite of being flavor enhancer, different studies indicate that MSG is toxic to human and experimental animals [10]. In a review studies on animal and human, “MSG effects on central nervous system, adipose tissue, liver, reproductive organs and other systems have been found” [14]. An adverse reaction to MSG on nervous system, killing brain cells, causing retinal degeneration, endocrine disorder and other pathological symptoms have been reported [15]. Researches indicate potential adverse effects of glutamate may be due to its rapid assimilation and the resulting quick and large increase of glutamic acid in the organism. Histological studies have been showed that monosodium glutamate (MSG) has adverse effect on kidney of mammals (e.g. Adult Wister Rats) [10]. Besides these, monosodium glutamate also induced damage of stomach, testis, liver and kidney of mammals [20]. It has been claimed that MSG has physiological effects in both vertebrates and invertebrates [20]. A report showed that repeated use of MSG is responsible for constriction of Mulpighian tubules of *Lucilia cuprina* [4].That means long time use of MSG as a flavoring agent can cause tissue damage of any internal organ, which ultimate result is early death (4). Repeated application of MSG through ingestion instigated inhibition of ovarian development of *Chrysomya megacephala* [5]. MSG as a food additive increases the consumption of meat food of ants and largely decreases their precision of reaction, response to pheromones, cognition as well as their learning and memorization abilities [8]. Most biological processes are similar for all animals including humans (i.e. genetics, metabolism, nervous cells functioning). Besides vertebrates, invertebrates are used more because of being offered advantages to scientists such as a short life cycle [23]. Insects have similarities with the higher animals, in many cases in structure and physiological functions [23]. Present study on toxic effects of monosodium glutamate has initiated to investigate the efficacy of the stated material on *Cx. Quinquefasciatus* Say,which was used as a biological model.

2. Materials and Method

The experiment was carried out between May, 2016 and July, 2017 in the laboratory of Entomology, Department of Zoology, University of Dhaka in an ambient laboratory

Corresponding author: murshida.begum@du.ac.bd

condition (28 ± 2ºC temperature and 70-80% Relative Humidity).

2.1 Development of mosquito generations in the laboratory

To make sure constant supply of mosquito larvae for the experiment, mosquito rearing started after collecting larvae from their natural breeding places. By separating the larvae in different bowls with cleaned tap water, were provided routinely with baby cereal powder (Nestle Bangladesh), yeast etc. After 6-8 days larvae were moulted into a non-feeding pupal stage. To avoid movement a fixed numbers of pupae were kept in different bowls within adult rearing cages which were made by an iron rod frame (size: 30x30x30 cm). The cages were covered with mesh mosquito net and basal part of that cage made of wood. The pulpal period were lasted for about 2 to 3 days. Adult mosquitoes were provided with 10% glucose solution soaked cotton ball in a petridish as their food for first 2-3 days. Adult females were fed pigeon blood for oocyte development. Large numbers of eggs were observed in a raft by a stereomicroscope (Meiji SKT-3BT) [3]. The egg rafts were collected with the help of a spoon with water carefully and were transferred into several earthen bowls containing tap water to get emergenceof subsequently 1st, 2nd, 3rd and 4th instar larvae. It took one months in summer and one and half months in winter to establish a generations of mosquito for this experiment. The reared 4th instar larvae were used to determine the efficacy of monosodium glutamate against *Cx. quinquafasciatus.*

2.2 Treatment with MSG and mortality tests

Crude Monosodium Glutamate was added with fixed amount of tap water to prepare five doses (0.01, 0.02, 0.03, 0.04 and 0.05 g/ml). A number of 20 actively swimming larvae of 4th instar were taken into conical flask (250 ml) containing 100 ml different doses of MSG solution diluted in tape water. The flasks were stored at room temperature (28±2ºC) and 70-80% of relative humidity and at 12L: 12D (Photoperiod). A control was selected in which only tap water provided with larvae for each dose. The mortality of larvae in each concentration was recorded after 48 hours of exposure and the waning larvae were counted as dead and the mortality values were calculated. All experiments were replicated nine times. The percentage of mortality was calculated by using following formula-

Percentage of mortality

$$=\frac{Number\ of\ died\ in\ a\ test}{Number\ of\ used\ in\ test}\times 100$$

Test mortality records were corrected with the Abbott's formula, whenever there was some control mortality in a test. Abbott's correction formula [1]-

Corrected Mortality

$$=\frac{Mortality\ in\ treatment-Mortality\ in\ control}{100-Control\ mortality}\times 100$$

Histological procedure: Histological slides of MSG treated and untreated 4th instar larvae of *Cx. Quiquefasciatus* were prepared by transverse sectioning the tissues from the head to tail region. Ethanol, Myer's albumin and Xyline were used as fixatives. Serial transverse sections of the tissues were cut at 0.4 µm thickness with the help of a rotary microtome machine (model 08–260–02, ERMA INC, Japan). The tissue sections were stained with eosin and Heidenhein's haematoxylene in the laboratory condition. Histo-pathological observations were performed with the help of a compound microscope (Humascope Classic 2006/95/EC). Photographs were taken by a Canoon powershot S200 camera (16 mega pixel).

2.3 Statistical analyses

The data were reported as arithmetic mean ± Standard deviation (SD). One way of ANOVA and Multiple Range Test was applied on the data to assess the treatment effect [6, 7]. Dose response curve were prepared by regression analysis. All the statistical analyses were done on a computer using statistical software package for SPSS.

3. Results and Discussion

Different doses (0.00, 0.01, 0.02, 0.03, 0.04, and 0.05g/ml) of monosodium glutamate (in 0.35mg of average body weight of larvae) were used to study the efficacy of monosodium glutamate against 4th instar larvae of *Cx. quinquefasciatus* Say. Results of the mortality tests and hist-pathological observations are stated below.

3.1 Mortality of treated Culex quinquefasciatus (Say)

The mortalities of the treated 4th instar larvae of the *Cx. quinquefasciatus* after 48 hours exposure were presented in Table 1. The result of mortality test from these table showed that mortality was increasing along with increasing the doses of monosodium glutamate. Results indicated that the highest percent (93.33%) of mortality was taking place at 0.05 g/ml dose, while the lowest percent (7.22%) of mortality was observed at 0.01 g/ml. No larval mortality of the mosquito was observed in control treatment. The results of the one way ANOVA and multiple range test showed that mean mortalities were significantly different from each other ($p<0.05$) ($F = 431.143$). A dose response curve were produced from the regression analysis also expressed that increasing of the doses of MSG increased the mortality rate of 4th instar larval *Cx. quinquefasciatus* Say and decreased the mean percent of live larvae (Fig. 1).

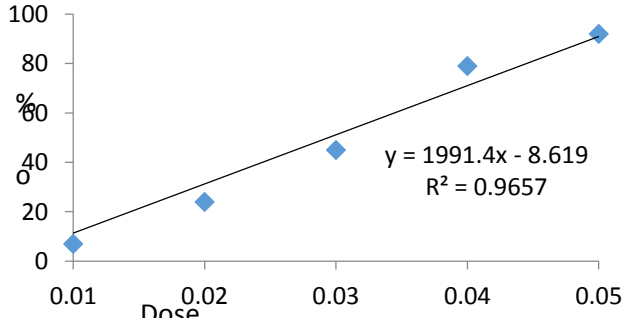

Fig. 1 Dose response curve showed the effectiveness of Monosodium Glutamate against 4th larval instar of C. quinquefasciatus

Table 1: Mortality of 4th instar larvae of *Culex quinquefasciatus* (Say) exposed to 48 hours at different doses of Monosodium Glutamate (N=180)

Dose (g/ml)	Total number of larvae survived	Mean no. of larvae survived (Mean±SD)	Larvae survived (%)	Total number of larvae died	Mean no. of larvae died (Mean±SD)	Mortality (%)
0.01	167	18.56±0.72a	92.78%	13	1.44±0.0.72e	7.22
0.02	138	15.33±1.00b	76.67%	42	4.67±1.00d	23.33
0.03	104	11.56±0.88c	57.78%	76	8.44±0.88c	42.22
0.04	47	5.22±1.39d	26.11%	133	14.78±1.39b	73.89
0.05	12	1.33±1.00e	6.67%	168	18.67±1.00a	93.33
Control	180	20.00±0.00	100%	0	0.00±0.00	0

*Mean larval mortalities after treated with different doses of MSG were compared by Multiple Range Test (Bonferoni, 1935 and 1936).
*Mean mortalities of different doses were significant different from each other ($p<0.05$)*MSG=Monosodium glutamate.

3.2 Histo-pathlogical observations

Permanent slides of transverse section of gut showed tissue damages at 0.05 g/ml and 0.03 g/ml and 0.01g/ml dose of MSG (Figs. 8, 6 and 4, respectively). In control, no such abnormalities were observed (Fig. 2 and 3).

After application of 0.01g/ml MSG, tissue damage was found in the stomodeal valve of anterior mid gut (Fig. 4). The major histological alterations were the structural disorganization hind gut tissue at 0.05 g/ml in which tissue damages found in rectal pads including destruction of

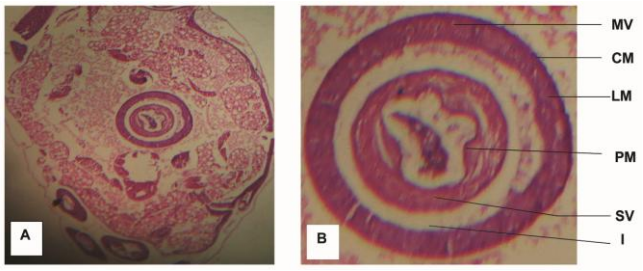

Fig. 2 A. Transverse section through the anterior mid gut area of an untreated 4th instar larvae of Cx. quinquefasciatus. B. Larger view of the transverse section through the anterior mid gut area of an untreated larvae. MV=microvilli, CM=circular muscle, LM=longitudinal muscle, PM= peritrophic membrane, MC= mid gut caeca and I= intima, SV=stomodeal valve

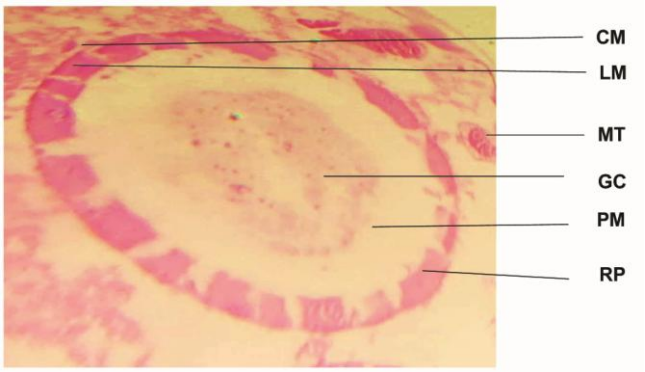

Fig. 3 Transverse section through the hind gut area of an untreated 4th instar larvae of Cx. quinquefasciatus. MV=microvilli, CM=circular muscle, LM =longitudinal muscle, PM= peritrophic membrane and RP= rectal pad, GC=gut content

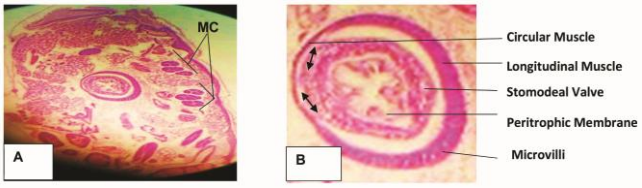

Fig. 4 Transverse section through the anterior mid gut area of a treated (0.01g/ml) 4th instar larvae of Cx. quinquefasciatus. B. Larger view of the transverse section through the anterior mid gut area the treated (0.01 g/ml) larvae.MC=mid gut caeca

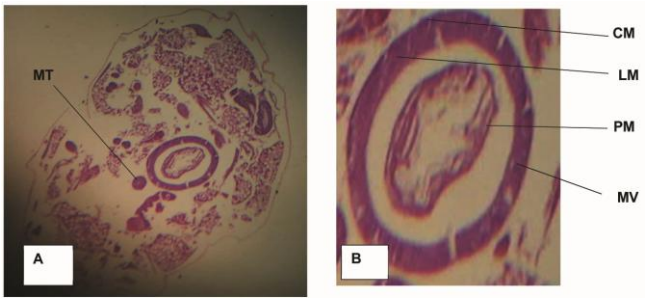

Fig. 5 A. Transverse section through the posterior mid gut area of an ttreated (0.02 g/ml) 4th instar larvae of Cx. quinquefasciatus. B. Larger view of the transverse section through the posterior mid gut area of the treated (0.02 g/ml) larvae. CM=circular muscle, LM =longitudinal muscle, PM= peritrophic membrane

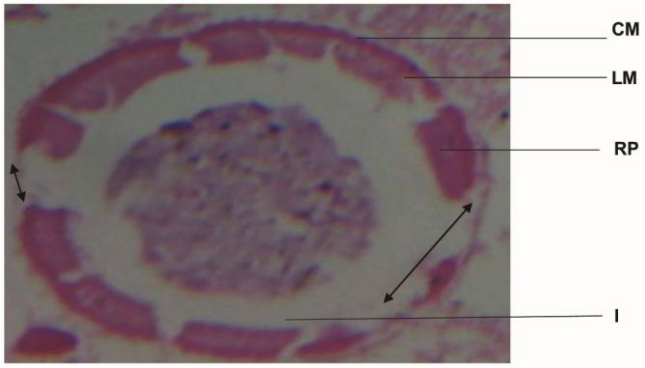

Fig. 6. Transverse section through the hind gut area of a treated (O.03 g/ml) 4th instar larvae of Cx. quinquefasciatus.MV= microvilli, I=intima, CM=circular muscle, LM=longitudinal muscle, and RP=rectal pad.(Arrow indicates the damage area)

peritrophic membrane, the inner longitudinal muscle and outer circular muscle disruption. The microvilli also had been damaged (Fig. 8). Lesions in some tissues occurred at 0.03 g/ml dose in the rectal pad of hind gut and had also longitudinal muscles disruption (Fig. 6). Scrapes in the peritrophic membrane were found in the tissues of treated animals from the doses of 0.02g/ml and 0.04 g/ml also (Fig. 5 and 7). The circular muscle, microvilli, peritrophic membrane, rectal pad were found to in their normal characteristic view in the untreated larval anterior mid gut and hind gut (Fig. 3 and 4).

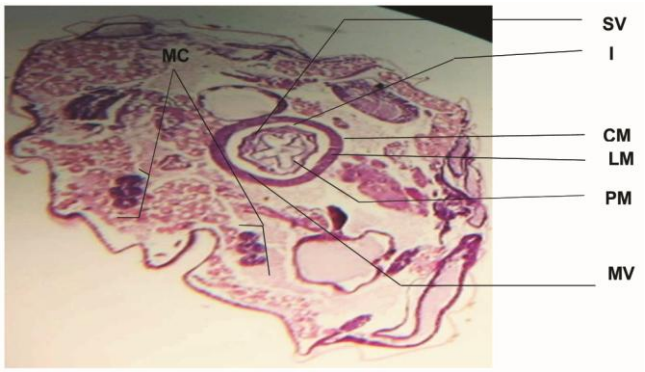

Fig. 7. Transverse section through the anterior mid gut area of a treated (0.04 g/ml) 4th instar larvae of Cx. quiquefasciatus. MV= microvilli, CM=circular muscle, LM=longitudinal muscle, PM= peritrophic membrane, MC= mid gut caeca and I=intima, SV=stomodeal valve

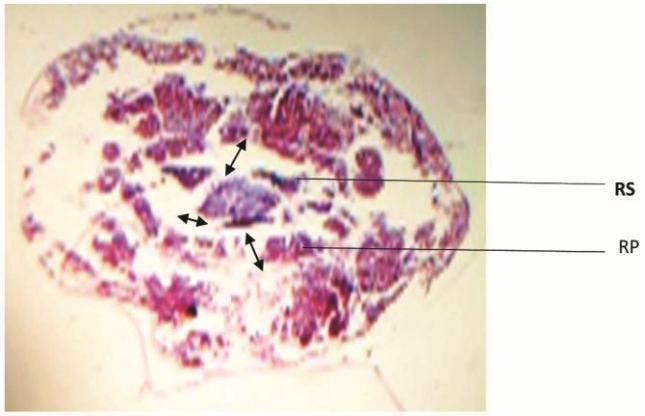

Fig 8.Transverse section through the hind gut area of a treated (0.05 g/ml) 4th instar larvae of Cx. quinquefasciatus. RP= Rectal Pad, RS=Rectal Spine. (Arrows indicate the damage area)

4. Discussion

Results indicated that 0.3 and 0.5g/ml dose of the MSG (in 0.35mg of average body weight of larvae) cause the tissue demolition of the rectal pad situated in the hindgut, microvilli, the peritrophic membrane and muscular sheath (Figs. 6 and 8). Hind gut of the alimentary canal is absorption site of the excretory material of insects [9]. The ionic balance of the body in insect through 'active transport' is maintained by malpighian tubules (MTs) [4]. Most likely the target of MSG is to the Na+/K+ channel of excretory system. The ionic balance of the body was broken down by the MSG and ultimately the MTs were constricted and tissue was also disrupted in the MTs of grey flesh fly *L. cuprina* [4]. However, in insects the MTs originate from the posterior mid gut and hind gut function as excretory organ somehow connected to the rectal pads [9]. Ingestion of any toxic material ionic balance of the body can be broken down [16]. Some of the former worker suggested that MSG somewhat may affect the renal system of vertebrates and invertebrates [18, 16]. Results of the present investigation had a precise connection to the results of the previous examiners. Apart from the renal system other internal organ arrangements of vertebrates were also affected by MSG. For instance, histological changes were observed in the stomach and testes of adult rat [10, 11]. Present researcher also observed the tissue disruption in the stomodeal valve of anterior mid gut at 0.01 g/ml dose of MSG (Fig. 4) which supports the previous results.

Being an Entomologist we have chosen the insects as a research model to observe the efficacy of Monosodium glutamate and assumed that may have some toxic effects on insect [4]. The present investigations have supported the assumption. Insects have similarities with higher animals, in many cases in structure and physiological functions [24]. Long term consumption of MSG exerts serious health hazards on oxidation state, antioxidant enzymes and the neurotransmitter cholinesterase which affects brain tissue structure [25]. So it can be concluded that MSG may effect on human health as well as vigor condition on other animals. Ultimate results may goes on the economic condition of our mother terrain.

References

1. W. S. Abbott, A method of computing the effectiveness of insecticides, J. Econ. Entomol., **18**(2), 267-269 (1925).
2. Anonymous, IHS chemical economics handbook, Monosodium Glutamate Report, pp. 79, (2014).
3. M. Bates, The natural history of mosquitoes, Macmillian Company, New York, NY. Pp. 379, (1949).
4. M. Begum, M. A. Kabir, H. R. Khan and M. F.Rahman, Efficacy of Monosodium Glutamate in the Australian Blowfly, Lucilia cuprina Wiedmann (Diptera: Culicidae)', Bangladesh J. Zool., **40**(1), 69-75 (2012).
5. M. Begum, M. K. Shorna, M. A. Rahman and H. R. Khan, Inhibition of ovarian development in Chrysomya megacephala (Fabricius, 1794) (Diptera: Calliphoridae) by monosodium glutamate, Physiol. Ecol. Envl. Sci., **5**(1&2), 33-38 (2014).
6. C. E. Boferroni, Teoria statistica delle classi e calcolo delle probabilità,Pubblicazioni del R Istituto Superiore di Scienze Economiche e Commerciali di Firenze. **8**, 3-62 (1936).
7. C. E. Bonferroni, Il calcolo delle assicurazioni su gruppi di teste, In Studi in Onore Del Professore Salvatore Ortu Carboni, Rome, Italy, pp. 13-60 (1935).
8. M. C. Cammaerts and R. Cammaerts, Effect of Monosodium Glutamate on behavior and cognition: A study using ants as biological models, Ann. Publ. Hlth. Res., **3**(3), 1044 (2016).

9. R. F. Chapman, The insects structure and function, 4th ed, Cambridge Univ. Press, UK, pp. 770 (1998).
10. A. O. Eweka, Histological studies on the effects of monosodium glutamate on the kidney of Adult Wister Rats, J. health, **6**(2), 7-12 (2007).
11. A. O. Eweka, Histological studies on the effects of monosodium glutamate on the testis of Adult Wister Rats, J. Urol, **5**(2), 41-145 (2008).
12. M. Freeman, Reconsidering the effect of monosodium glutamate; a literature review, Am. Acad. Nurs. Pract., **18**, 482-486 (2006).
13. R. S. Geha, A. Beiser, C. Ren, R. Patterson, P. A. Greenberger, L. C. Grammer, A. M. Ditto, K. E. Harris, M. A. Shaugsnessy, P. R. Yarnold, J. Corren and A. Saxon, Review of alleged reaction to Monosodium Glutamate and outcome of a multicenter double-blind Placebo-Controlled Study, The J. Nutn., **130 (**4S Suppl), 1058-1062 (2000).
14. V. Husarovan and D. Ostatnokova, Monosodium Glutamate toxic effects and their implications for human intake: A Review, J. Med. Res., **2013**, 1-12 (2013)
15. R. H. M. Kwok, The Chinese restaurant syndrome: Letter to the editor, N. Engl. J.Med., **278,** 796 (1968)
16. W. Lieberthat, S. A. Menza and J. S. Levine, Graded ATP depletion can cause necrosis or apoptosis of cultured mouse proximal tubular cells, Am. J. Physiol., **274,** 315-327 (1998).
17. J. Loliger, Function and importance of Glutamate for savory Foods, J. Nutrn., **130**, 915–920 (2000).
18. S. C. Malpas, G. A. Head and W. P. Anderson, Renal responses to increases in renal sympathetic nerve activity induced by brainstem stimulation in rabbits, J. Auton. Nerv. Syst., **61**(1), 70-78 (1996).
19. J. W. Olney, Excitotoxin-mediated neuron death in youth and old age,. Prog. Brain Res., **86**, 37-51 (1990).
20. G. G. Ortiz, O. K. B. Quintero and Z. C. Beas, Monosodium glutamate induced damage in liver and kidney: a morphological and biochemical approach, J. Biomed. Pharmacotherap., **60**(20), 86-91 (2006).
21. J. Rhodes, A. C. Titherley, J. A. Norman, R. Wood and D. W. Lord, A Survey of the Monosodium Glutamate content of foods and an estimation of the dietary intake of Monosodium Glutamate. Food additives & contaminants, Food Additvs. Contamts., **8**(5), 663-72 (1991).
22. K. Tori, H. Uneyama and E. Nakamura, Physiological role of diatary glutamate signaling via gut-brain axis due to efficient digestion and absorption, J. Gastroenterol., **48** (4), 442–451 (2013).
23. F. W. Wolf and U. J. Heberlein, Invertebrate models of drug abuse, Neurobiol. **54,** 161-178 (2003).
24. D. E. Alexander, On the Wing: Insects, pterosaurs, birds, bats and the evolution of animal flight, Integrtv. Comptiv. Biol, **56**(5), 1044-1046 (2016).
25. F. A. E. Shobaki, M. H. Mahmoud, A. E. Rahman, M. Attia, O. G. Refaat and E. F. E. Haggar, The effect of Monosodium Glutamate (MSG) on brain tissue, oxidation state, true cholinesterase and possible protection against health hazards using natural spices, Der Pharma Chemica, **8**(23), 44-50 (2016).

Synthesis and Characterization of Undoped and Aluminum Doped Zinc Oxide Thin Films using Thermal Evaporation Method

S. Hossain[1*], G. D. A. Quaderi[2], K. M. A. Hussain[3] and T. Faruqe[3]

[1*]*Atomic Energy Centre, Bangladesh Atomic Energy Commission, Chattogram, Bangladesh*
[2]*Department of Physics, University of Dhaka, Dhaka, Bangladesh*
[3]*Experimental Physics Division, Atomic Energy Centre, Dhaka, Bangladesh*

Abstract

The undoped and Aluminum doped Zinc Oxide (AZO) thin films were prepared on ultrasonically cleaned glass substrates by thermal evaporation method at a pressure of 1.33×10^{-5} Pascal (~10^{-6} Torr). The film thickness was kept constant at 100 nm and the substrate temperature was also kept constant at 350^0C with only varying the doping concentrations. The deposited thin films were annealed at 350^0C for 15 minutes. The transmittance of the films increased and the absorbance decreased with the increase of Al incorporation up to 1.2 at % but after further increase of Al content they showed reverse behavior. The maximum transparency was found 86.48% for 1.2 at % Al doped ZnO thin film. The refractive index showed slight variation in the visible region with the incorporation of Al but extinction coefficient decreased. The band gap varied from 3.06 eV to 3.49 eV for the variation of Al concentration in ZnO with the minimum band gap occurring for 0.3 at % of Al content. The conductivity at the room temperature varied from 5.26 $\Omega^{-1}cm^{-1}$ to 3.05×10^3 $\Omega^{-1}cm^{-1}$ for variation of Al concentration with a maximum conductivity occurring for the film with 0.3 at % Al content. The results can be used for optimizing the optical and electrical properties of AZO films by tuning the Al concentration. .

Keywords: Al doped ZnO thin film, thermal evaporation method, optical properties, electrical properties

1. Introduction

ZnO thin films have attracted considerable interest in recent years for application as a transparent conducting material in liquid crystal displays [1], solar cells [2], etc. Zinc Oxide (ZnO) is a direct band gap semiconductor with a band gap of 3.37 eV and large excitation binding energy of 60 meV at room temperature [3, 4]. The conventional transparent conductive oxide (TCO) material is indium tin oxide (ITO). However, ITO materials are very expensive and toxic, as well as unstable to H_2 plasma. In contrast, undoped and doped ZnO thin films are widely used in transparent conducting layers because of their non-toxicity, thermal stability and better resistance against H_2 plasma processing damage [5, 6]. The high heat capacity, heat conductivity and high melting temperature of ZnO are beneficial for ceramics. Among the tetrahedral semiconductors, ZnO has the highest piezoelectric tensor, or at least one comparable to that of GaN and AlN. This property also makes it a technologically important material for many piezoelectric applications. Among the possible dopants, Al (group-IIIA) is a popular one because of high-quality, low-resistivity properties of the AZO thin films [7].

Various techniques such as molecular beam epitaxy (MBE) [8], pulsed laser deposition (PLD) [9], magnetron sputtering [10], thermal evaporation [11-13], chemical vapor deposition (CVD) [14], sol-gel [15], spray pyrolysis [16] have been applied to AZO thin film preparation. Thermal evaporation has distinct advantages over other techniques. It is a simple, suitable and economically attractive deposition technique, in which the quality of the films grown is quite superior. Usually in this method we get uniform deposition of the coating material and hence the film shows smooth variation of the properties with respect to wavelength of the incident electromagnetic wave. Furthermore, in our experimental set up, thickness of the film can be controlled using a thickness monitor and hence the film thickness remains uniform over the exposed area of the substrate. The materials sublime at lower temperature under vacuum and it does not demand any catalyst.

In this work, undoped ZnO and AZO thin films were prepared by thermal evaporation with a wide range of Al concentrations. The surface morphological, optical and electrical properties of the AZO thin films were investigated. The present work is limited to variation of the doping concentration only, in order to isolate the effect of the Al doping on ZnO thin films.

2. Experimental Details

AZO thin films were deposited on ultrasonically cleaned glass substrates by thermal evaporation method. An Al wire was used for Al source and ZnO powder were used for ZnO source. The vacuum chamber was very carefully cleaned with clothes soaked in acetone and was let to dry. The source material, ZnO powder was inserted in a Molibdenum boat and Al wire was kept in a Tungsten boat of turret source. The substrate with the mask was then mounted with a clamp above the boat. The substrate was placed at a distance of 10 cm above the sources and this distance was kept constant for all the films. Vacuum was created in the chamber by using Rotary and Diffusion pumps. When high vacuum was achieved (~ 10^{-6} Torr), the substrate was heated with the help of a radiant heater to a certain substrate temperature which was kept fixed for a particular substrate. A low tension (LT) voltage source was switched on and a current of 30~32 Amps was passed through the boat making the boat red-hot and the materials in the boat evaporate. The

Corresponding author: shahadat.baec@gmail.com

thickness of the films was monitored. After getting the desired thickness, the evaporation was stopped by placing a shutter above the evaporator source. The boat was replaced by using a rotator to bring the Al containing boat in that position and Al was also deposited in a similar way. A pure ZnO thin film was prepared of thickness 100 nm keeping the substrate temperature at 350^0C. Then it was annealed at 350^0C for 15 minutes. Then we prepared another eight samples (0.3, 0.6, 0.9, 1.2, 2.0, 5.0, 10.0 and 20.0 at % Al doped ZnO) of the same thickness keeping the same substrate temperature and annealing time and temperature as in the pure ZnO film.

The surface morphology of the thin films was studied using JEOL JSM-6490LA analytical scanning electron microscope (SEM) [X20,000]. The optical properties of the films were investigated using a UV-3100 (dual beam) recording spectrophotometer. The wavelength range of the spectrophotometer is 310 nm to 3000 nm. The electrical properties were investigated using KEITHLEY 2401 source meter by linear four point probe method.

3. Results and Discussion

Surface morphology: Figure 1 shows SEM micrographs of the Al-doped ZnO thin films with different Al concentrations: (a) 0, (b) 2, (c) 10 and (d) 20 at %. All the Al-doped thin films exhibited a rough surface with three-dimensional (3D) island growth due to the lattice and chemical mismatches between the thin films and substrates whereas the undoped thin film had a relatively smooth surface. This may be due to the degradation of crystal quality or the presence of defects. Some grains are observed clearly for high Al contents.

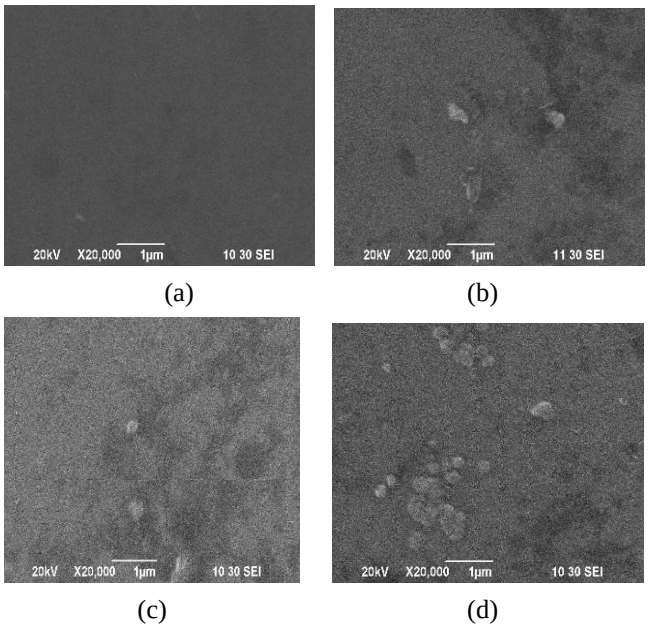

Fig. 1 SEM images of AZO thin films with different Al concentration: (a) 0, (b) 2, (c) 10 and (d) 20 at %

Optical properties and transmittance: Figure 2 gives the transmittance spectra for all the AZO thin films. For convenience of illustrations, they are displayed in figure 2(a) and 2(b). The optical transmittance spectra of all AZO films seem very similar and the transmittance in the UV region (310 - 380 nm) dropped abruptly for all the films as this is the absorption region. In this region, the incoming photons have sufficient energy to excite electrons from the valence band to the conduction band and thus these photons are absorbed within the material to decrease the transmittance. So this region carries the information of the band gap of the material [17]. In the visible region (380 - 700 nm), the transmittance increases logarithmically and all the films showed medium transmittance (40% - 55%). The variation of Al content does not show significant change in transmittance in this region. At higher wavelengths (2000 - 2500 nm) transmission exceeds 80%. In the near infrared region (700-2500 nm) all the films have high transmittance and which increase with the increase of Al content up to 1.2 at %. We get the highest transmittance (86.48%) at 2500 nm for 1.2 at % Al-doped ZnO thin film. But for 10 and 20 at % AZO film, the transmittance decreased slightly which might be due to the increment of scattering of photons by crystal defect [18]. These results imply that the optical transmittance can be increased by Al incorporation in the ZnO thin film but higher incorporation may degrade the crystal quality which will eventually decrease the transmittance.

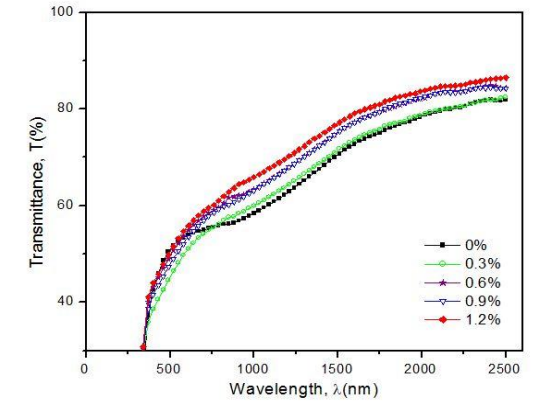

2(a)

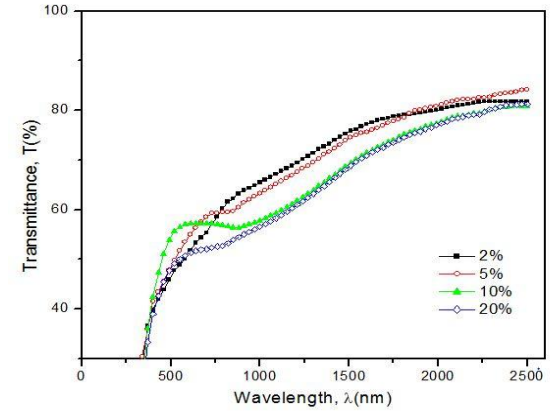

2(b)

Fig. 2 Optical transmittance spectra of AZO thin films prepared with different Al concentration

Reflectance: Figure 3(a) and 3(b) shows the reflectance spectra of Al-doped ZnO thin films. It is observed that in the UV region the reflectance increases smoothly for all the as-deposited thin films and lies in the range of 6% to 29%. The increasing points of reflectance shift gradually towards the lower wavelength with the increase of Al content in the films. The nature of increase gives an idea about the nature of the energy gap, which is ascertained further by the spectra of absorption coefficient. In the visible region we observe peaks for all the samples. These peaks indicate the maximum reflectance value for the respective films. The reflectance values start decreasing in the near infrared region as this region has high transparency. From both figures we see that, with the introduction of Al content in the film, the reflectance of the film has a decreasing trend. But all the AZO films have nearly equal reflectance values except 10 and 20 at % AZO. These two films have the reflectance values greater than other films in this region. A possible explanation for this is the increase of scattering of photons by crystal defects. Hence,

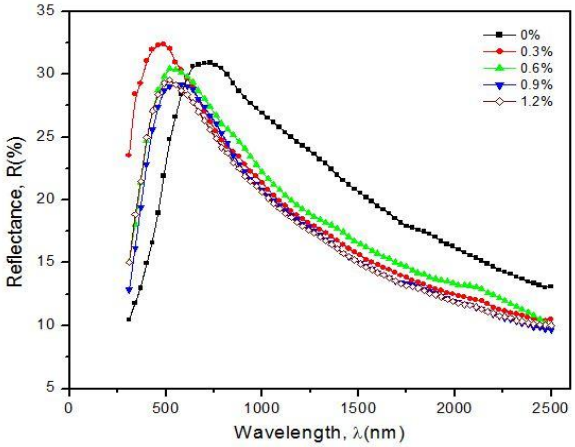

3(a)

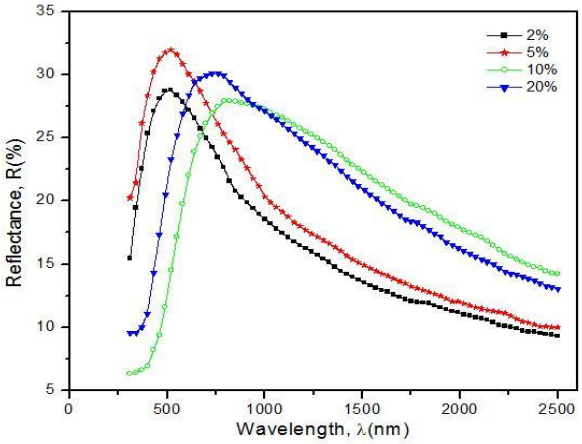

3(b)

Fig. 3 Optical reflectance spectra of AZO thin films prepared with different Al concentration

it can be said that the reflectance can be increased initially by incorporating Al in the ZnO thin film for the UV region and can be decreased by doing the same for the near infrared region. But higher incorporation of Al (≥ 10 at %) gives the opposite result in both cases.

Absorption Coefficient: The absorption coefficient characterizes how easily a material or medium can be penetrated by a beam of light and it can be obtained through $I = I_0 e^{-\alpha t}$, where I and I_0 are the intensities of the transmitted and incident light, respectively, and t is the thickness

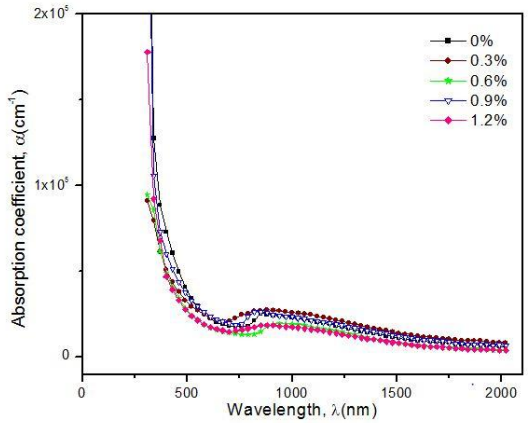

4(a)

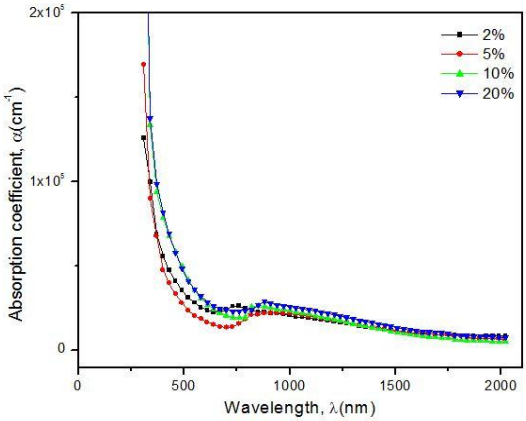

4(b)

Fig. 4 Optical absorption coefficient spectra of AZO thin films prepared with different Al concentration

of the AZO thin films. Figure 4(a) and 4(b) shows the absorption coefficient (α) of the AZO thin films with different Al concentrations. We see that the absorption coefficient is in the range of 1×10^5 to 3.5×10^5 cm^{-1} in the UV region and it is also observed that in this region the absorption coefficient exhibits higher values which clearly indicate that there is a large probability of the allowed direct transitions. The absorption coefficient falls exponentially in the visible region. With the increase in Al content the absorption coefficient decreases slightly but for 10 and 20 at % AZO thin film it increases. In the near Infrared region the absorption coefficient decreases with increasing photon wavelength and remains approximately constant at higher wavelengths. Al incorporation does not

affect α in this region. These results imply that the optical absorption in the visible region of the ZnO thin film can be reduced by incorporating low amount of Al and can be increased by incorporating higher amount of Al.

Band Gap: As a direct band gap semiconductor, ZnO has an absorption coefficient (α) obeying the following relation for high photon energies *(hν)*:

$$\alpha h\nu = A(h\nu - E_g)^{1/2} \quad (1)$$

Where *h* is Planck's constant, *ν* is the frequency of the incident photon and *A* is a constant that depends on the electron-hole mobility. The direct band gap energy of the deposited thin films have been obtained from the intercept on the energy axis, after extrapolation, of the tangent to the curve of $(\alpha h\nu)^2$ vs. $(h\nu)$ curve at large photon energies. Figure 5 shows the plots of $(\alpha h\nu)^2$ vs. photon energy of AZO thin films with different Al concentrations whereas fig. 6 shows the optical band gap variation of the AZO thin films as a function of Al-content in the ZnO thin film.

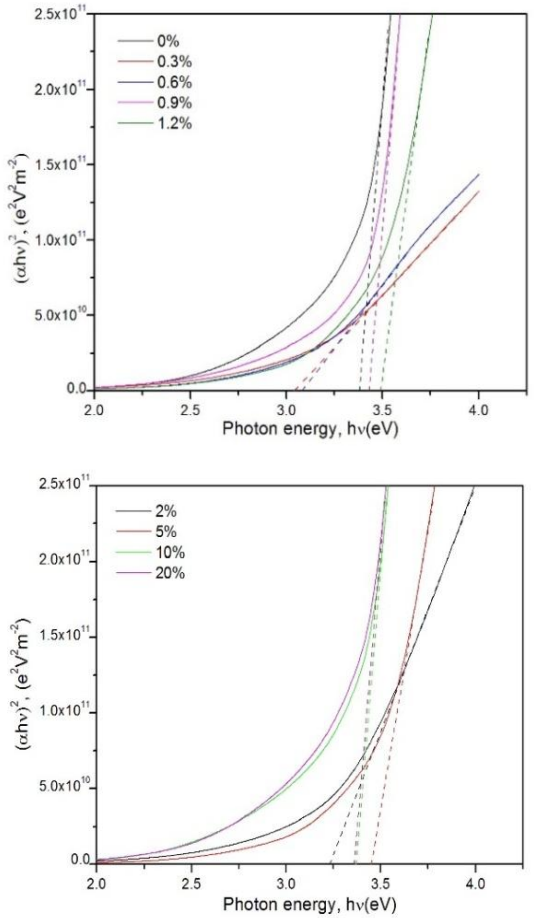

Fig. 5 Plot of $(\alpha h\nu)^2$ vs. photon energy (hν) of AZO thin films prepared with different Al concentration

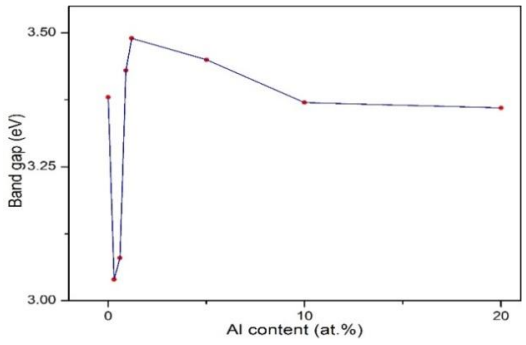

Fig. 6: Band gap of AZO films as a function of Al-content in the 0-20 at.% range

The optical band gap of the undoped ZnO thin film is found to be 3.38 eV. It is observed that the band gap sharply decreases for increase of Al-content at low concentration (~ 0.7 at.%) and increases up to a peak value 3.49 eV for concentration of 1.2 at.% and slowly decreases with further increase of Al-content. This movement of the band gap may be explained by the Burstein-Moss (BM) shift [19], an energy band widening (blue-shift) effect resulting from the increase of Fermi level in the conduction band of degenerate semiconductors [20].

Refractive Index: The refractive index is an important parameter for optical materials and applications. In materials where an electromagnetic wave can lose its energy during its propagation, the refractive index becomes a complex function of the frequency of the light wave. It is described by the following relation:

$$n = n(\omega) + ik(\omega) \quad (2)$$

Where *n* is the real part and *k* is the imaginary part (extinction coefficient) of the complex refractive index. We have calculated refractive index by using the following relation [21, 22].

$$n = \left(\frac{1+R}{1-R}\right) + \sqrt{\frac{4R}{(1-R)^2} - k^2} \quad (3)$$

Where k $(k = \alpha\lambda/4\pi)$ is the extinction coefficient and *R* is the reflectance. Figure 7a and 7b show the refractive index (*n*) of the AZO thin films with different Al concentrations. Refractive indices of the as deposited thin films first increase gradually in the UV and visible region; attaining a maximum peak (~ 4.0) at 700 nm they fall abruptly and finally tend to be a constant at 2.0 in the near infrared region. Incorporation of Al in the ZnO thin films shows slight variation in the UV and visible regions. The initial gradual increase and peak is due to the interaction that takes place between photons and electrons. The rapid change after peak indicates a change in the absorption energy of the material, which depends on the surface and volume imperfections. Constant refractive index occurs due to successive internal reflections or due to the trapped photon energy within the grain boundary [23].

Extinction Coefficient: Figure 8(a) and 8(b) shows the extinction coefficient (*k*) spectra of the AZO thin films. The behavior of the extinction coefficient is nearly similar to the corresponding absorption coefficient for AZO thin films. It is observed that, extinction coefficient falls abruptly with the increase of wavelength in the UV region. It may be due to the absorption of light at the grain boundaries. In the visible region, the extinction coefficient first decreases and

then increases for all the as deposited thin films. This change is also due to the variation of absorbance. The extinction coefficient decreases slightly with wavelength in the near infrared region for all the thin films. It is also seen that with the increase of Al content the extinction coefficient decreases. The extinction coefficient describes the attenuation of light in a medium and higher *k* value indicates the probability of raising the electron transfer across the mobility gap with photon energy. Therefore, the higher values are the representation of greater attenuation of light in a thin film.

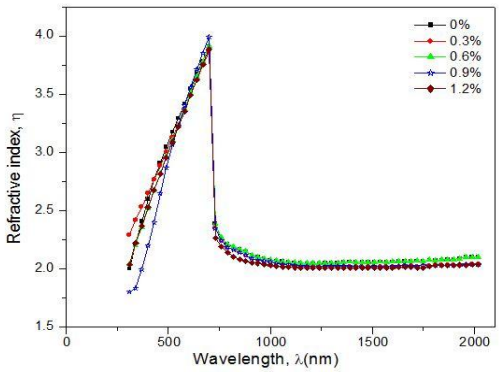

7(a)

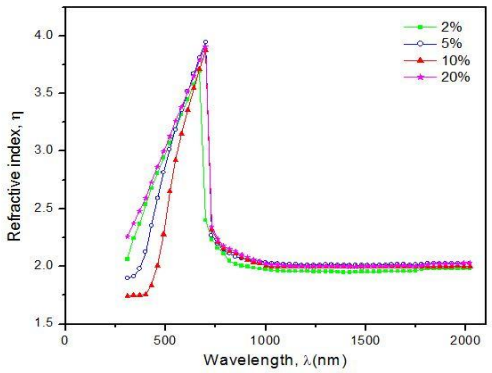

7(b)

Fig. 7: Refractive index spectra of AZO thin films prepared with different Al concentration

Electrical properties: From the I-V characteristics curve we have calculated the slope of each curve by making them linearly fit. The inverse of the slopes give us the value of resistances for each of the thin films. Then we calculated the resistivity using the following equation:

$$\rho = 4.532\, t\, (\frac{V}{I}) \quad (4)$$

Where *t* is the thickness of the sample, *V* is the applied voltage and *I* is the measured current. Then inverse of resistivity gives the value of conductivity and expressed by

$$\sigma = \frac{1}{\rho} \quad (5)$$

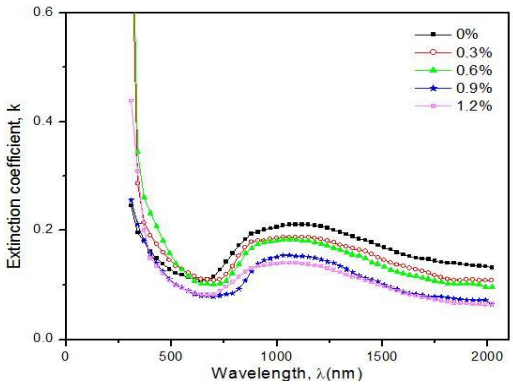

8(a)

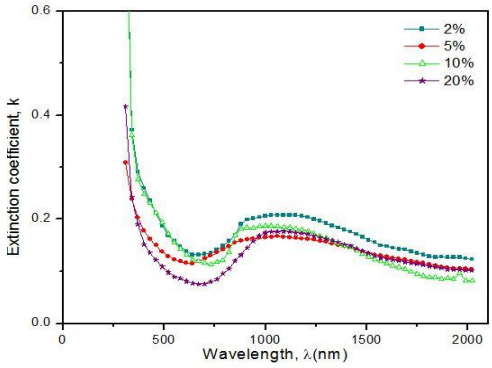

8(b)

Fig. 8: Extinction coefficient spectra of AZO thin films prepared with different Al concentration

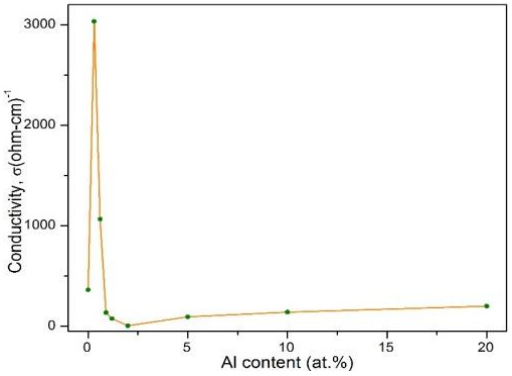

Fig. 9: Conductivity of the AZO films as a function of Al-content in the 0-20 at.% range

It is seen that by the introduction of 0.3 at % Al in ZnO, the electrical resistivity is reduced. With further increasing of Al up to 2.0 at % in ZnO, the resistivity increases. Then with the increase of Al content in ZnO the resistivity starts to decrease again and it continued to 20 at %. The resistivity of the AZO film is related to the Al doping concentration, intrinsic defects and various scattering centers [20]. Figure 9 shows the conductivity of the ZnO thin films as a function of Al content. It is seen that highly conducting AZO film is found in the low-Al content region. For 0.3 at % Al-doped ZnO thin film we found the highest conductivity which is 3.04×10^{3} $\Omega^{-1}cm^{-1}$. When a small

amount of Al impurities were added on ZnO, they mostly substitute Zn existing at lattice sites as donors, together with less Al atoms present at interstitial sites. However, when the Al content is around ~ 2.0 at.%, Al atoms in the film results in the intra-grain congregation and/or grain-boundary segregation forming Al–Al and Al–O clusters (e.g. AlO_x sub oxides) [20]. These Al atoms are electrically inactive, even acting as "electron killers" with such effects as donor passivation; thus the electron concentrations are limited. Similar suggestions were proposed by Chen et al. [24] and Choi et al. [25] for ZnO:Al and ZnO:Ga films, respectively. This is an indication that in order to get highly conducting AZO films, it is necessary to optimize the amount of Al in ZnO.

4. Conclusion

Al-doped ZnO thin films by thermal evaporation method in a wide range of Al - content from 0 to 20 at %. The AZO films were systematically studied for having a comprehensive knowledge of their behaviors. The SEM micrographs of Al-doped ZnO thin films have a rough surface with three dimensional island growths. Maximum transparency 86.48% was obtained for 1.2 at % Al-doped ZnO thin film in the near infrared region. For low Al-content (concentration < 2.0 at %), throughout the complete wavelength region, absorption coefficient decreases with increase of Al content. On the other hand, for moderate Al-concentration (> 2.0 at %), absorption coefficient slightly increases with increase of Al-concentration. Controlling Al-doping concentration, band gap of AZO thin film can be tuned at a suitable desired value. The refractive index (real part) shows slight variation with the incorporation of Al in the ZnO thin film in the visible region but extinction coefficient decreases with the increase of Al content in the ZnO thin films for all Al concentration. The conductivity also varied much for low-Al content region. Thus by varying the Al-content, we can tune band gap and can apply AZO thin films as front contact layer, buffer layer of thin film solar cell.

References

1. B. Y. Oh, M. C. Jeong, T. H. Moon, W. Lee and J. M. Myoung, Transparent conductive Al-doped ZnO films for liquid crystal displays, Journal of Applied Physics, **99**, 124505 (2006).
2. D. Nister, K. Keis, S. E. Lindquist and A. Hagfeldt, A detailed analysis of ambipolar diffusion in nanostructured metal oxide films, Sol. Energy Mater. Sol. Cells, **73**, 411-423 (2002).
3. K. Hümmer, Interband magnetoreflection of ZnO, Phys. Status Solidi B, **56**, 249-260 (1973).
4. E. M. Wong and P. C. Searson, ZnO quantum particle thin films fabricated by electrophoretic deposition, Appl. Phys. Lett., **74**, 2939-2941 (1999).
5. Y. Song, E. S. Kim and A. Kapila, Thermal stability of sputter-deposited ZnO thin films, J. Electron. Mater., **24**, 83-86 (1995).
6. K. Ip, M. E. Overberg, Y. W. Heo, D. P. Norton, S. J. Pearton, S. O. Kucheyev, C. Jagadish, J. S. Wiliams, R. G. Wilson and J. M. Zavada, Thermal stability of ion-implanted hydrogen in ZnO, Appl. Phys. Lett., **81**, 3996-3998 (2002).
7. D. C. Look, D. C. Reynolds, J. R. Sizelove, R. L. Jones, C. W. Litton, G. Cantwell and W. C. Harsch, Electrical properties of bulk ZnO, Solid state communications, **105**, 399-401 (1998).
8. M. S. Kim, T. H. Kim, D. Y. Kim, D. Y. Lee and S. Kim, Effects of annealing atmosphere and temperature on properties of ZnO thin films on porous silicon grown by plasma-assisted molecular beam epitaxy, Elec. Mat. Lett., **08**, 123-129 (2012).
9. E. M. Kaidashev, M. Lorenz, H. von Wenckstern, A. Rahm, H. C. Semmelhack, K. H. Han, G. Benndorf, C. Bundesmann, H. Hochmuth and M. Grundmann, High electron mobility of epitaxial ZnO thin films on c-plane sapphire grown by multistep pulsed-laser deposition, Appl. Phys. Lett., **82**, 3901-3903 (2003).
10. P. F. Carcia, R. S. McLean, M. H. Reilly and G. Nunnes Jr., Transparent ZnO thin-film transistor fabricated by rf magnetron sputtering, Appl. Phys. Lett., **82**, 1117-1119 (2003).
11. N. Bouhssira, S. Abed, E. Tomasella, J. Cellier, A. Mosbah, M. S. Aida and M. Jacquet, Influence of annealing temperature on the properties of ZnO thin films deposited by thermal evaporation, Appl. Sur. Sci., **252,** 5594-5597 (2006).
12. G. G. Rusu, A. P. Rambu, V. E. Buta, M. Dobromir, D. Luca and M. Rusu, Structural and optical characterization of Al-doped ZnO films prepared by thermal oxidation of evaporated Zn/Al multilayered films, Mat. Chem. Phys., **123**, 314-321 (2010).
13. M. Jin, J. Feng, Z. De-heng, M. Hong-lei and L. Shu-ying, Optical and electronic properties of transparent conducting ZnO and ZnO:Al films prepared by evaporating method, Thin Solid Films, **357**, 98-101 (1999).
14. C. R. Gorla, N. W. Emanetoglu, S. Liang, W. E. Mayo, Y. Lu, M. Wraback and H. Shen, Structural, optical and surface acoustic wave properties of epitaxial ZnO films grown on (0112) sapphire by metalorganic chemical vapor deposition, J. Appl. Phys., **85**, 2595-2602 (1999).
15. C. JianLin, C. Ding and C. ZhenHua, Optimization of the process for preparing Al-doped ZnO thin films by sol-gel method, Science in China Series E: Technological Sciences, **52,** 88-94 (2009).
16. A. El Manouni, F. J. Manjón, M. Perales, M. Mollar, B. Mari, M. C. Lopez and J. R. Ramos Barrado, Effect of thermal annealing on ZnO:Al thin films grown by spray pyrolysis, Superlattices and Microstructures, **42**, 134-139 (2007).
17. A. N. Banarjee, C. K. Ghosh, S. Das, K. K. Chattopadhyay, Elecro-optical characteristics and field-emission properties of reactive DC-sputtered p-$CuAlO_{2+x}$ thin films, Physica B: Condensed Matter, **370**, 264-276 (2005).
18. N. A. Hassan, M. S. Hashim and R. S. Khaleel, Optical characteristics of ZnO:Al thin films prepared by magnetron sputtering, Journal of Kerbala University, **8**, 224-230 (2010).
19. E. Burstein, Anomalous optical absorption limit in InSb, Phys. Rev., **93**, 632 (1954).
20. J. G. Lu, Z. Z. Ye, Y. J. Zeng, L. P. Zhu, L. Wang, J. Yuan and B. H. Zhao, Structural, optical and electrical properties of (Zn,Al)O films over a wide range of compositions, J. Appl. Phys., **100**, 073714 (2006).

21. J. A. Turner, J. K. Birtwistle and G. R. Hoffman, A method for the continuous measurement of thickness and deposition rate of conducting films during a vacuum evaporation, Journal of Scientific Instruments, **40**, 557-561 (1963).

22. E. A. Roth, E. A. Margerum and J. A. Amick, Evaporation of Silicon and Germanium by rf levitation, Review of Scientific Instruments, **33**, 686 (1962).

23. S. H. Baker, M. I. Manssor, S. J. Gurman, S. C. Bayliss and E. A. Davis, Structural investigation of the ternary alloys system a-GaAsP and correlation with optical properties, Journal of Physics: Condensed Matter, **4**, 2817-2830 (1992).

24. M. Chen, X. Wang, Y. H. Yu, Z. L. Pei, X. D. Bai, C. Sun, R. F. Huang and L. S. Wen, X-ray photoelectron spectroscopy and auger electron spectroscopy studies of Al-doped ZnO films, Appl. Sur. Sci., **158**, 134-140 (2000).

25. B. H. Choi, H. B. Im, J. S. Song and K. H. Yoon, Optical and electrical properties of Ga_2O_3-doped ZnO films prepared by r.f. sputtering, Thin Solid Films, **193-194**, 712-720 (1990).

Assessment of Background Radiation Level in Different Locations of Bangladesh

M. Begum*, M. A. Hoque[1], S. F. Mahal[1], S. Yeasmin, M. S. Rahman, A. Islam, J. Ferdous, A. K. M. M. Rahman
M. M. M. Siraz, S. Pervin, N. Hassan, Z. Hossain and A. Begum[1]

Health Physics Division, Atomic Energy Centre, Dhaka-1000, Bangladesh
[1]Ex Head, Health Physics Division, Atomic Energy Centre, Dhaka-1000, Bangladesh

Abstract

Environmental Radiation and Radioactivity monitoring has become important nationally and internationally to generate baseline database. In this study, the background radiation levels have been measured at 16 districts of Bangladesh along with the Rooppur Nuclear Power Plant area of Pabna and the sea-beach areas of Cox's Bazar. Calibrated beta-gamma survey meter and digital survey meter (GAMMA SCOUT) were used for the measurement of dose level where reading was taken by placing the survey meter at a height of 1m from the ground (gonad level). Natural background radiation is the main source of radiation for public. The observed average background radiation dose rate of 16 districts of Bangladesh is found to be (2 ± 0.66) $mSvy^{-1}$ (except Cox's Bazar beach side), whereas according to UNSCEAR-2000 the worldwide average background dose rate is 2.45 $mSvy^{-1}$. On the other hand, in the beach areas of Cox's Bazar region has contributed much higher background radiation level, where maximum background radiation level is 38.89 $mSvy^{-1}$. But apart from Cox's Bazar beach side the background radiation level is much lower in and around Cox's Bazar town, where minimum background radiation level is 1.40 $mSvy^{-1}$. So the background radiation level in Cox's Bazar district is varied from 1.40 $mSv.y^{-1}$to 38.89 $mSv.y^{-1}$. Presence of Monazite and Zircon in the sand of the beach areas of Cox's Bazar region has contributed such higher background radiation level. Moreover background radiation dose level of Dhaka region for 10 years from 2006 to 2015 have been measured on monthly basis, where no significant change has been observed even after the accident of Fukusima nuclear power plant in Japan.

Keywords: Background radiation level, beta-gamma survey meter, nuclear power plant area, base line study.

1. Introduction

Environmental Radiation and Radioactivity monitoring has become important nationally and internationally to generate baseline database. Naturally occurring radionuclides of terrestrial origin are present in the earth's crust since its origin. All living organisms of the planet are exposed to natural radiation, which is mainly due to the activity concentration of primordial radionuclides ^{232}Th, ^{238}U and their product of decay, in addition to the other natural radionuclide ^{40}K present in the earth' crust [1]. These primordial radionuclides have longer half-lives, that they survived since their creation and decaying to attain the stable state and produces ionizing radiation in various degrees. The cosmic component, on the other hand, originates from outer space as cosmic rays whose contribution to the background changes mainly with elevation and latitude. Cosmic radiation can also contribute significantly in areas at high altitudes [2-4]. The cosmic ray exposure becomes double for every 1500 meters above the earth's surface. Cosmic rays are the dominant source of ionization in the atmosphere from an altitude of 70 km down to around 1 km [5]. Apart from these naturally occurring radiation in the atmosphere and terrestrial sources, it has been reported and proven that human activities such as those due to the quest for technological advancement and comfort application, have gradually led to the increase of background ionizing radiation and even in some cases, much above recommended tolerable level [6]. Again human activities have led to the depletion of the ozone layer, increased the cosmic rays reaching the earth's surface and thereby affect the background radiation [7].

Corresponding author: mahbuba_hpd@yahoo.com

The natural or artificial radioactive nuclides that are present in the environment, constitute the background radiation level. Background radiation is the main source of radiation exposure for human beings. Natural background radiation contributes significantly (about 80%) to the annual effective dose received by the general population [1, 8]. There are few regions in the world, which are known for high background radiation areas (HBRAs), are due to the local geological and geochemical effects and cause enhanced levels of terrestrial radiation [1, 4]. Selected pockets of Brazil, China and India are reported under the grip of high background radiation [9]. Presence of monazite sand along the beaches of these regions, among other factors, has contributed to these dreaded radiations [10]. In most places on the earth, the natural radioactivity varies only within narrow limits, but in some places there are wide deviations from normal levels because of abnormally high levels of radioactive minerals. Excessive and prolonged exposure of live to radioactive elements however, have a general deteriorating side effect on health. So we can say, we all are in the midst of a radiation environment, however low it may be, and it is not possible to avoid radiation exposure from natural sources altogether. All what is needed and is possible is to be conscious of this fact with a constant endeavor to control the radiation from man-made sources to levels as low as is reasonably achievable.

In Bangladesh, to fulfill the increasing demand of electricity throughout the country there is no alternative of Nuclear Power Reactor. For the protection of population from nuclear hazards it is essential to know the base line data of environmental radiation and radioactivity. It is also regulatory prerequisite for the installation and operation of Nuclear Power Reactor. Therefore, the measurement of

natural background radiation is the most important and immediate concern to the general population.

For this study, the natural background radiation levels were measured at 16 districts of Bangladesh along with the Rooppur Nuclear Power Plant area of Pabna and the sea-beach areas of Cox's Bazar during the period from 2000 to 2015. Moreover background radiation dose level in and around Dhaka city for 10 years from 2006 to 2015 have been measured on monthly basis.

2. Materials and Method

The natural background radiation levels were measured at 16 districts of Bangladesh. Geiger-Muller based micro-Roentgen survey meter and digital survey meter (GAMMA SCOUT) were used for dose level measurements which are based on instantaneous techniques and we have employed this technique due to their versatility in the field work. Reading was taken by placing the survey meter at a height of 1 m from the ground. For Geiger-Muller based micro-Roentgen survey meter, the reading in μR/h were converted to nGy/h using the conversion factor of 8.7 nGy/μR (from the definition of Roentgen). The absorbed doses in nGy/h were further converted to annual effective doses (AED) in mSv/y by using the following formula:

$$AED\ (mSv/y) = D_{(out)} \times T \times OF \times CC$$

Where, $D_{(out)}$ is outdoor absorbed dose rate; T is time in hour for one year (8760 h); OF is the Occupancy Factor of 0.2 for the outdoor exposure and CC is the Conversion Coefficient, which is 0.7 Sv/Gy [1].

3. Results and Discussion

The overall annual average values of natural background radiation measured in different areas of Bangladesh are found to be lower than other areas of the world according to table-1. Total annual effective dose from natural radiation sources to Bangladeshi population is found to be (2 ± 0.66) mSv/y in comparison to the global value of 2.455 mSv/y [1]. Slightly higher background radiation dose levels are found in Dinajpur, Rangpur area which may be due to presence of hard rock i.e. basement rock at shallow depth. Slightly higher reading are also found in and around Sylhet area which may be due to contribution of uranium bearing sandstone. It may be noted that the background radiation are almost same for most of the areas of Bangladesh.

Table 1: Measurement of background radiation dose level in different location of Bangladesh

Location	Position		Average Backgroud Radiation Dose (mSv/y)
Dhaka	$23^0 42' 37.44'' N$	$90^0 24' 26.78'' E$	2.00 ± 0.47
Tangail	$24^0 14' 59.42'' N$	$89^0 54' 59.58'' E$	1.75 ± 0.38
Barisal	$22^0 42' 17.89'' N$	$90^0 22' 12.47'' E$	2.14 ± 0.24
Patuakhali	$22^0 27' 50.19'' N$	$90^0 20' 28.36'' E$	2.10 ± 0.26
Comilla	$23^0 27' 42.7'' N$	$91^0 11' 6.11'' E$	1.18 ± 0.42
Rangamati	$22^0 39' 26.46'' N$	$92^0 10' 23.77'' E$	2.10 ± 0.34
Chittagong	$22^0 20' 18.24'' N$	$91^0 49' 54.05'' E$	1.73 ± 0.48
Rangpur	$25^0 44' 47.9'' N$	$89^0 15' 5.98'' E$	3.17 ± 0.57
Mymenshing	$24^0 45' 22.9'' N$	$90^0 24' 23.26'' E$	1.75 ± 0.43
Pabna (Rooppur)	$24^0 0' 23.18'' N$	$89^0 14' 13.92'' E$	1.47 ± 0.36
Rajshahi	$24^0 22' 26.4'' N$	$88^0 36' 4.1'' E$	1.80 ± 0.18
Dinajpur	$25^0 37' 38.82'' N$	$88^0 38' 16.04'' E$	3.40 ± 0.47
Sylhet	$24^0 53' 56.54'' N$	$91^0 52' 19.13'' E$	2.74 ± 0.60
Jamalpur	$24^0 55' 10.74'' N$	$89^0 56' 53.23'' E$	1.27 ± 0.51
Kushtia	$23^0 54' 10.08'' N$	$89^0 7' 9.95'' E$	1.36 ± 0.34

In most places on the earth, the natural radioactivity varies only within narrow limits, but in some places there are wide deviations from normal levels because of abnormally high levels of radioactive minerals, such as monazites and zircons. From the table 2, in the beach areas of Cox's Bazar region has contributed much higher background radiation level, where maximum background radiation level is 38.89 $mSvy^{-1}$. But apart from Cox's Bazar beach side the background radiation level is much lower in and around Cox's Bazar town, where minimum background radiation level is 1.40 $mSvy^{-1}$. So the background radiation level in Cox's Bazar district is varied from 1.40 $mSvy^{-1}$ to 38.89 $mSvy^{-1}$. Presence of Monazite and Zircon in the sand of the beach areas of Cox's Bazar region has contributed such higher background radiation level.

Table 2: Minimum and maximum background radiation dose level in different location of Cox's Bazar district

Location	Position		Backgroud radiation dose level (mSv/y)	
			Minimum	Maximum
Cox's Bazar	$21^0$27′13.97″ N	$91^0$58′3.54″ E	1.40	38.89

Beach sands are mineral deposits formed through weathering and erosion of either igneous or metamorphic rocks. Among the rock constituent minerals are some natural radionuclides that contribute to ionizing radiation exposure on Earth. GB3 (Beach placer deposits around the world are known for their economic concentrations of heavy minerals such as monazite, zircon, ilmenite, rutile, garnet and sillimanite. Those enriched in radioactive minerals are of special interest for their use in nuclear industry [11, 12], and potential for environmental hazard engendered from natural radiation [12-14].

Table 3: The gamma dose rates in air of the Cox's Bazar District are compared with the values reported from other parts of the world and the World average

Area, Country	Minimum dose (mGy/y)	Maximum dose (mGy/y)	Refference
Cox's Bazar, Bangladesh	1.40	38.89 (Beach Area)	Present study
Ramsar, Iran	-	149	[1]
Ramsar, Iran	0.61	260	[15]
Kerala, India	1.75	35	[1]
Guarapari, Brazil	0.79	789	[1]
World Average	0.16	0.82	[1]

From table 3, the areas in Iran, India and Brazil are all due to local geologic and geochemical effects, giving rise to very high and very localized radiation exposure. UNSCEAR (2000) reports maximum dose rates of Guarapari, Brazil of 789 mGy/y on beaches of monazite sands [15]. The background radiation levels in different areas of Bangladesh are shown in fig. 1.

Background radiation dose level in and around Dhaka City for 10 years from 2006 to 2015 have been measured on monthly basis is shown in bar diagram of fig. 2, where no significant change has been observed even after the accident of Fukusima nuclear power plant in Japan.

Fig. 1 Background Radiation Levels in different areas of Bangladesh

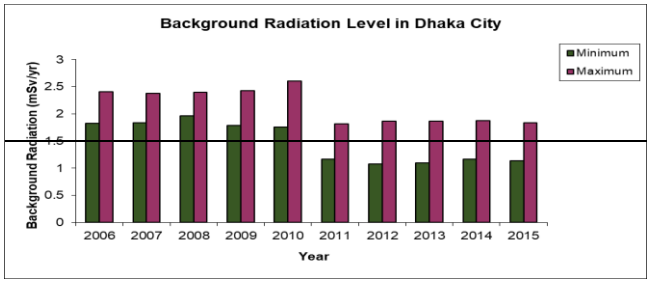

Fig. 2 Background Radiation Level in Dhaka City of Ten Years

4. Conclusion

From this study, the observed average background radiation dose rate of 16 districts of Bangladesh is found to be (2 ± 0.66) $mSvy^{-1}$ (except Cox's Bazar beach side). According to UNSCEAR-2000 the worldwide average background dose rate is 2.45 $mSvy^{-1}$. Moreover background radiation dose level of Dhaka region for 10 years from 2006 to 2015 have been measured on monthly basis, where no significant change has been observed even after the accident of Fukusima nuclear power plant in Japan. So these data could be taken as a baseline data. There is a need for continuous environmental monitoring program in order to determine any change due to artificial radioactivity releasing from the nuclear installation in case of incident/ accident. In future, multi method approach for more accuracy and comparison of results can be adopted.

References

1. UNSCEAR, Sources and effects of ionizing radiation, United Nations Scientific Committee on the Effects of Atomic Radiation, United Nations, New York (2000).

2. B. G. Bennett, Exposure to natural radiation worldwide, In: proceedings of the fourth international conference on high levels of natural radiation: Radiation doses and health effects, 1996, Beijing, China, Elsevier, Tokyo, 15–23 (1997).

3. NCRP, Exposure of the population of the United States and Canada from natural background Radiation, National Council on Radiation Protection and Measurements, Bethesda, Maryland, Report No. 94 (1987).

4. UNSCEAR, Sources and effects of ionizing radiation, United Nations Scientific Committee on the Effect of Atomic Radiation, United Nations, New York (1993).

5. T. V. Ramachandran, Background radiation, people and the environment, Iran. J. Radiat. Res., **9(2)**, 63-76, (2011).

6. B. Patel, Management of environment, Weiley eastern publications, **51-76,** 506-509 (1988).

7. C. K. Folland, T. R. Kirkland and K. Vinnikoov, Observed climatic variations and changes, IPCC scientific assessments, Cambridge university press. N.Y. , 101-105 (1995).

8. K. K. Narayan, D. K. Krishna and M. C. Subbaramu, Population exposure to ionizing radiation in India, ISRP (K)-BR-**3** (1991).

9. J. Malathi, S. Selvasekarapandian, G. M. Brahmanandhan, D. Khanna, V. Meenakshisundaram and R. Mathiyarsu, Radiat. Prot. Dosim., **113,** 415-420 (2005).

10. R. Ragel, M. Saroja and, D. V. Roy, High background radiation sweeping along the southwest coast of Tamil Nadu, India; Scientific Correspondence, **94(10)**, 1250-1251 (2008).

11. N. M. Alam, M. I. Chowdury, M. Kamal, S. Ghose, N. M. Islam, M. N. Mustafa, M. M. H. Miah and M. M. Ansary, The 226Ra, 232Th and 40K activities in beach sand minerals and beach soils of Cox's Bazar, Bangladesh, J. Environ. Radioact. **46,** 243-250 (1999).

12. A. C. Freitas and A. S. Alencar, Gamma dose rates and distribution of natural radionuclides in sand beaches-Ilha Grande, Southeastern Brazil, J. Environ. Radioact. **75**, 211-223 (2004).

13. A. S. Alencar and A. C. Freitas, Reference levels of natural radioactivity for the beach sands in a Brazilian southeastern coastal region, Radiat. Meas. **40**, 76-83 (2005).

14. C. Vassas, L. Pourcelot, C. Vella, J. Carpena, J. P. Pupin, P. Bouisset and L. Guillot, Mechanisms of enrichment of natural radioactivity along the beaches of the Camargue, France, J. Environ. Radioact. **91**, 146-159 (2006).

15. M. Ghiassi-nejad, S. M. J. Mortazavi, J. R. Cameron, A. Niroomandrad and P. A. Karam, Very high background radiation area of Ramsar, Iran: Preliminary biological studies, Jour. Health Phys. **82(1)**, 87-93, (2002).

Uranium Determination in Water, Soil and Stone Through Adsorptive Accumulation of U(VI)-chloranilic Acid Complex

A. K. M. A. Ullah[1], A. R. M. Tareq[1], A. T. Naziba[2], M. I. Khalil[3], M. T. Nafisa[4], H. M. B. Alam[5]
A. Imtiaz[5] and A. K. M. F. Kibria[5*]

[1]*Chemistry Division, Atomic Energy Centre, Ramna, Dhaka 1000*
[2]*Department of Electrical and Electronics Engineering, Bangladesh University of Business and Technology, Mirpur, Dhaka 1216*
[3]*Nuclear Minerals Unit, Atomic Energy Research Establishment, Savar, Dhaka 1349*
[4]*Department of Electrical and Electronics Engineering, American International University of Bangladesh, Kuril, Dhaka 1229*
[5]*Nuclear Safety, Security and Safeguards Division, Bangladesh Atomic Energy Commission, Agargaon, Dhaka 1207*

Abstract

Uranium concentrations in water, soil and stones collected from six different locations of Sherpur District, Bangladesh, were determined by adsorptive cathodic stripping (ACS) voltammetric technique. The technique is based on the adsorptive accumulation of the uranium(VI)-chloranilic acid (CA) complex onto a hanging mercury drop electrode, followed by reduction of the complex by cathodic voltammetric scan using differential pulse modulation. The set optimum experimental conditions were of pH value 2.5, CA concentration ~ 1.95 x 10^{-4} M, deposition potential + 90 mV, deposition time 120 s, scanned potential ranges – 35 mV to – 150 mV, pulse amplitude 25 mV and scan rate 2 mV/s. Solution of 0.02M KNO_3 was used as electrolyte and EDTA of concentration ~ 1.95 x 10^{-5} M was used to reduce the interferences of unwanted metal ions. 200 µl and 100 µl volumes of soil and stone digested samples in the investigation cell downed to 52- and 103-fold dilutions facilitated to determine uranium concentrations in trace element levels. The concentrations were found in ppb level. For example, 3.8 and 5.3 ppb values were obtained for a soil and a stone sample, respectively. For a water sample, 10.3 ppb value was obtained. The range of the calculated values of uranium concentrations in water, soil and stones were found to be 8.9-16.4 ppb, 16.3-31.7 ppm and 19.2-161.6 ppm, respectively.

Keywords: Uranium, water, soil, sand, stone, U(VI)-CA complex, adsorptive accumulation.

1. Introduction

Uranium is a naturally occurring radioactive element that exists in the form of isotopes with the quantity of U^{238} (99.27%), U^{235} (0.72%) and U^{234} (0.01%). The sources of uranium are generally rock, stone, soil, sand and water. A great amount of uranium is extracting from its source mine every year. It has been used industrially as a nuclear fuel for more than fifty years and has a great potential to be used for many years in the future. World reactor related uranium demands are projected to be as high as 122000 tons by 2035 [1]. Thus, uranium is considered to be one of the significant commercial items of the world energy market. However, as a deadly toxic element its exploration, extraction and utilization involve sophisticated technologies and techniques.

Air, soil, vegetations, aquatic media and the ecosystem can be contaminated by the uranium released from different sources. The effluent of nuclear industries, nuclear waste disposal sites, leached uranium from uranium rich matrices, dispersed uranium from the mining and processing sites, nuclear accident and lastly from the egoistic blasting of nuclear weapons and dirty bombs can be considered as the main sources of uranium contamination. Human body being contaminated by uranium severely suffers from uranium toxicity [2]. Ingestion, i.e., eating and drinking stuffs, is considered to be the main route among other ways of uranium intake by human. Thus, monitoring of uranium up to trace level is very important. Conversely, extraction of uranium for industrial application, obviously with maximum caution, is indispensable too. Therefore, extensive researches are being carried out worldwide on the environmental monitoring and concurrently searching deposits of uranium in its probable media for extraction [1].

It has been known that some areas of Bangladesh are moderately rich in uranium. A number of drives have also been given to quantify uranium in different matrices of different locations of Bangladesh [3-5]. It is well documented that India has a big uranium deposit at its West Khasi Hills in Meghalaya District which is adjacent to the northern part of Bangladesh. Almost alike geological structure of the northern part of Bangladesh with that of Meghalaya District, provides good indication of having uranium deposits at the northern areas of Bangladesh. With a view to find out the facts and concurrently to achieve a database, and also keeping in mind the high commercial values of uranium, plan has been taken to search uranium in different locations of Bangladesh as well as to quantify uranium concentrations in different matrices such as water, beach sand, soil, rock and stones [4, 5].

Uranium can be determined through various techniques. But, determination of uranium in trace level by electrochemical means is an innovative technology. High sensitive voltammetric techniques such as various forms of stripping voltammetry are reported to be able to quantify uranium with relatively simple and less expensive way [6, 7]. Among stripping voltammetry, the adsorptive stripping voltammetry (ASV) is reported to be a powerful technique for trace uranium analysis [7]. In this technique, uranium is pre-concentrated on to the surface of a fresh mercury drop at a fixed potential by adsoroption and then it is allowed for measurements between the chosen potential regions through decomposition. To minimize the bad impact of other

Corresponding author: kibriaf@yahoo.com

electroactive species, when they are remarkably present in the sample, and concurrently to enhance the efficiency of the technique, nowadays various complex forming organic ligands are utilized too. Among them catechol [8], oxine and cupferron [9], aluminon [10], pyromellitic acid [11], thioglycolic acid [12] and chloranilic acid (CA) [5, 13-17] are extensively investigated. In case of CA, at an optimum experimental condition, its adsorption range of potential onto a mercury drop and the mechanism of formation of U(VI)-CA complex are almost clear [5, 13, 17]. The limiting concentration of uranium to be determined by using CA is also anticipated [5, 17]. These valuable findings and information enable one to apply its relatively selective accumulation at potentials where usual nonionic organic contaminants and all other metal-CA complexes are hardly adsorbed [5, 17].

The present study attempts to determine uranium in water, soil and stones of different locations of the Sherpur District, Bangladesh. This district is situated near the border of India and not too far from the uranium deposit of West Khasi Hills present in the Meghalaya District of India. Almost alike geological formation of Meghalaya and Sherpur may be a fact of having uranium deposits in this part of Bangladesh. The chosen method is the cathodic adsorptive stripping voltammetry (CASV) which seems to be a user friendly technology for trace uranium determination in such matrices.

2. Materials and Method

2.1 Sampling location and sample collection

Fig. 1 shows the sampling locations are Poragaon, Kakrakandi, Bheula, Garjaripa, Jhenaigati and Dhansail, as marked by circles, which situated in the north part of Sherpur District, Bangladesh. Water, soil and stone samples were collected from these places.

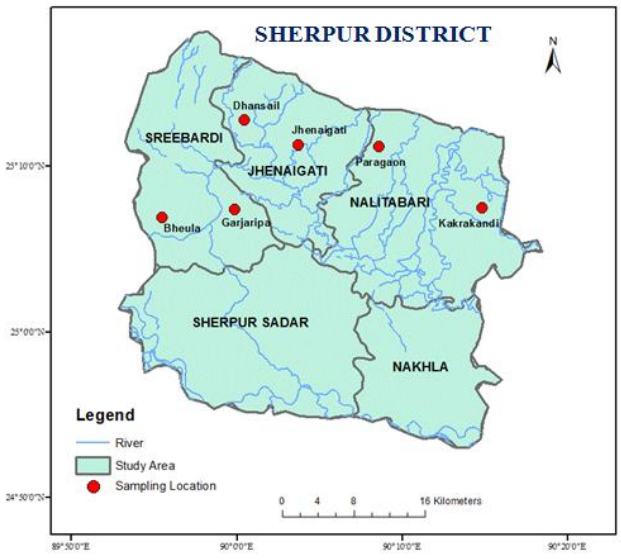

Fig. 1 Sampling locations: Kakrakandi, Garjaripa, Bheula, Poragaon, Jhenaigati and Dhansail (marked by circles) of Sherpur District, Bangladesh

Water samples included surface and underground water were collected in acid washed polythene bottles. Each sample (~ 500ml) was immediately acidified by adding 100 µl of 1M HNO_3. Soil samples were collected from around one feet depth of surface. Stone samples were collected from the earth surface of hilly areas. Both the soil and stone samples were collected in clean polythene bags with adequate precautions.

2.2 Chemicals

All the chemicals used were of analytical reagent grade and/or suprapur. Distilled water was used to prepare the reagent solutions and for rinsing the glass wares and the three-electrode cell system. 1000 ppm uranium standard solution acidified with 1M HNO_3 of volume 100 ml was prepared by dissolving Uranyl Nitrate $[UO_2(NO_3)_2.6H_2O]$ (May and Baker Ltd., Dagenham, England). 100 ml 0.01M Chloranilic acid (CA) (Alpha Aesar, USA) solution, 100 ml 0.01M EDTA solution (Merck, India), 250 ml 0.2M KNO_3 solution (Merck, India), 100 ml 1M HNO_3 (Merck, India), 250 ml 5M HNO_3, 250 ml 2M HF (BDH), 250 ml 2M $HClO_4$ (Merck, India) and 100 ml 1M NaOH (BDH) were duly prepared.

2.3 Sample preparation

2.3.1 Water sample preparation

For the adsorption accumulation studies of uranium, each water sample was made ready by filtering through filter paper of porosity 0.45 µm. It was done to separate any plotting and particulate materials. Then the pH value was adjusted to 2.5 by adding 1M HNO_3 drop wise.

2.3.2 Soil sample preparation

Each soil sample was oven dried to a constant weight at 333 K. Then about 1.0 g of soil was taken into a perfluoroalkoxy polymer container and reacted with 2 ml 2M HF and 3 ml 5M HNO_3 for a 12 h. After then, the container with the generated mass was placed in a microwave pressure vessel. There 10 ml 5M HNO_3:2M $HClO_4$ (4:1v/v) was added with it and digested at 180°C for 10 minutes. After cooling, the produced solution was filtered through a 0.45 µM syringe and diluted to 100 ml by adding water. But, before adjusting this volume, pH value of the solution was adjusted to 2.5 by adding 1M NaOH drop wise and stirring.

2.3.3 Stone sample preparation

Each stone sample as collected was crushed and then grinded to powder in a PTFE mortar. Powder was then oven dried at 333 K to a constant weight. After that, around 0.5 g powder was subjected to acid treatment and successively followed microwave digestion. The procedure was identical to that applied for soil sample as described in the sub-section 2.3.2. The sample volume and sample pH were kept to 100 ml and 2.5, respectively.

2.4 Apparatus

Uranium concentration determination was carried out by using Princeton Applied Research (PAR) model 174A polarographic analyzer. PAR 303 hanging mercury drop

electrode (HMDE) was used as the working electrode, i.e., electrode for adsorption and desorption of uranium, Ag/AgCl as the reference electrode and a platinum wire as the counter electrode. An XY recorder of model RE0089 was used for sketching the voltammograms [current *(i)* vs. potential relationships *(c)*] of the reduction of U(VI)-CA complex. A magnetic stirrer of Model 305 was used for the mixing of the sample and added uranium standard with the electrolyte solutions in the cell sample cup. A Metrohom 692 digital pH meter was used for the pH measurement.

2.5 Analytical Procedure

2.5.1 Understanding the feature of U(VI)-CA complex reduction peak current (i) vs. uranium concentration (c) for blank solution and uranium standards

At first 25 ml 0.02 M KNO_3 electrolyte solution was prepared from 0.2 M KNO_3 solution by dilution. Then 0.5 ml CA and 50 µl EDTA solutions were added with it and mixed. The pH value of this mixture was adjusted to 2.5 by adding 1M HNO_3 drop wise and stirring. As a result, a mixture of volume around 25.6 ml became ready. In the mixture, the concentrations of CA and EDTA downed to 1.95×10^{-4} M and 1.95×10^{-5} M, respectively. Then 10 ml mixture was pipetted into the cell cup and set it to the three-electrode cell system of the voltammetric analyzer. The mixture was then deaerated with nitrogen for 10 minutes under stirring. The stirrer was then switched off and for stripping analysis deposition potential was set to + 90 mV. After then on a fresh mercury drop, the accumulation of CA, and concurrently U(VI)-CA complex if any trace uranium is present in the mixture, was continued for 120 s under stirring condition. Following the accumulation step, stirring was stopped and after a quiescent period of 30 s a negative potential scan i.e., cathodic stripping was made using differential pulse modulation at a scan rate of 2 mV/s with pulse amplitude of 25 mV in the scanning potential range from-35 mV to-150 mV. As a result, a voltammogram (current vs. potential curve) for the blank mixture is obtained through the XY recorder. Then 10 µl uranium standard solution of concentration 10 ppm was added to the cell cup. This standard was made from 1000 ppm uranium standard solution by dilution. So, the uranium standard addition became to 10 ppb. The mixture was then stirred for 5 minutes and stopped. Thereafter, successively setting up the deposition potential, by producing a fresh mercury drop, completing of accumulation, setting up scanning potential range and starting scanning a voltammogram for the U(VI)-CA complex reduction peak current *(i)* vs. uranium concentration *(c)* for the first standard addition was obtained. In such a way five consecutive uranium standard additions (10, 20, 30, 40 and 50 ppb) were carried out with a view to obtain *i vs. c* feature of U(VI)-CA complex.

2.5.2 Behavior of U(VI)-CA complex reduction peak current (i) vs. uranium concentration (c) for the water samples

In case of water samples, 10 ml water was pipetted into the cell cup and set it to the three-electrode cell system of the voltammetric analyzer. After then 0.2 ml CA and 20 µl EDTA solutions were added with it. After that all the successive steps starting from deaeriation to sketching voltammogram as carried out for the blank solution were followed and the U(VI)-CA reduction peak for the unknown uranium present in the water sample was obtained. Thereafter, uranium standard addition was continued for three times (10 ppb, 15 ppb and 20 ppb). From the *i vs. c* relationships of the U(VI)-CA reduction peaks, the amount of uranium present in the water in ppb level was obtained. Using this value, uranium contained in 10.22 ml mixture present in the cell cup, at the zero addition level, was found out. This amount of uranium is the uranium present in the 10 ml water sample. From it uranium present per liter water was calculated.

2.5.3 Behavior of U(VI)-CA complex reduction peak current (i) vs. uranium concentration (c) for soil samples

In case of soil samples, 10 ml 0.02 M KNO_3 electrolyte solution of pH 2.5 was taken in the cell cup and set to the cell of the analyzer. Then 0.2 ml CA, 20 µl EDTA and 200 µl soil sample solutions were added with it. After that by adopting earlier procedure, voltammograms of U(VI)-CA reduction peak for the unknown uranium and three successive uranium standard additions (10 ppb, 20 ppb and 30 ppb) were obtained. The *i vs. c* relationships of the U(VI)-CA reduction peaks cleared about the amount of uranium present in the added sample in ppb level. Using this value, uranium contained in 10.42 ml solution present in the cell cup, at the zero addition level, was found out. This amount of uranium is the uranium present in the 200 µl soil sample. From this value uranium present in 100 ml sample was calculated. This amount of uranium is present in the digested amount of soil. Using this value, the amount of uranium present per Kg soil was obtained.

2.5.4 Behavior of U(VI)-CA complex reduction peak current (i) vs. uranium concentration (c) for stone samples

In case of stone samples, 10 ml 0.02 M KNO_3 electrolyte solution of pH 2.5 was taken in the cell cup and set to the cell of the analyzer. Then 0.2 ml CA, 20 µl EDTA and 100 µl stone sample solutions were added with it. Voltammograms for the unknown sample and three successive uranium standard additions (10 ppb, 20 ppb and 30 ppb) were sketched. From the *i vs. c* relationships of the U(VI)-CA reduction peaks, the amount of uranium in ppb level was obtained. Using this value uranium contained in 10.32 ml solution present in the cell cup, at the zero addition level, was found out. This amount of uranium is the uranium present in the 100 µl stone digested solution. By using this value, the amount of uranium present in the digested amount of stone and then uranium present per Kg stone was obtained.

3. Results and Discussion

Fig. 2 shows the adsorptive cathodic stripping (ACS) voltammograms obtained for the U(VI)-CA complex reduction at different uranium concentrations. It can be seen that a well defined U(VI)-CA complex reduction peak is

appeared in between the potential range of – 55 mV to – 125 mV. Reduction peak current value *(i)* gradually increased with increasing the concentrations of uranium *(c)*. The inset Fig. 2(a) shows the *i vs. c* relationships of the U(VI)-CA complex reduction. It can be seen that the relationships show linearity up to 42 ppb added uranium with R^2 value of 0.996 beyond which a clear non-linearity is appeared. This is a long linearity range and seems will allow the method to be used to measure unknown sample having appreciable amount of uranium in trace level.

Linearity up to 30 ppb uranium with R^2 value of 0.99 and up to 50 ppb uranium with R^2 value of 0.89 was reported by the authors [15]. The method was used to quantify uranium in the lichen sample. Nevertheless, present study informs that 42 ppb is the limiting uranium concentration to be present in the investigated solution to avoid experimental inaccuracy. This value is equal to the value of the total uranium present in an unknown sample plus added uranium standard. The inset Fig. 2(b) shows the enlarge version of the fraction of the (i) vs. (potential, mV) relationships obtained for the blank solution. The appearance of a very small peak hump is indicating that the used water, electrolyte, reagents and ligands are almost free from uranium contamination. It is signifying that without any major interruption effect, the mixture of the set electrolyte, reagents and ligands to be applied to quantify uranium concentrations in the targeted samples in trace level.

Fig. 3 shows the ACS voltammograms of the U(VI)-CA complex for a water sample with 10 ppb, 15 ppb and 20 ppb uranium standard additions. It may be seen that a smooth and a well defined voltammogram with a reduction peak is appeared for the water sample. The peak appeared at the potential of – 90 mV as that obtained for the reduction peak of uranium(VI)-CA complex when 10 ppb uranium standard was added in the mixture solution as shown in Figure 2. It indicates that the water sample consists of uranium.

The inset Fig. 3 shows the *i vs. c* relationships of the U(VI)-CA complex reduction. It may be seen that *i vs. c* shows a linear relationship which passes through the *i* line (Y-axis) and touches the *c* line (X-axis) at the concentration of 10.3 ppb. It means that 10 ml water sample consists of 105.27 ng uranium (solution volume in the cell cup was 10.22 ml). Therefore, 10.53 μg of uranium is present in one liter of water. In such a way, uranium concentrations in 36 water samples were determined. The obtained uranium concentration values are presented in the Table 1. It may be seen that the values lies in between 8.9-16.4 ppb. For drinking water, the permissible intake level of uranium is very low. As for example, United States Environmental Protection Agency (EPA) suggests maximum uranium contaminant level of 30 ppb [18] and the World Health Organization (WHO) harshly recommended the level of 15 ppb only [19]. At around 20% cases, the presently obtained values are higher than the recommended value of WHO [19]. The peoples living in this area are directly drinking this water and using it for their cooking and daily works. It seems that uranium concentrations in water of those areas are not so alarming yet.

Fig. 4 shows the ACS voltammograms of the U(VI)-CA complex for a soil digested sample of volume 200 μl with 10 ppb, 20 ppb and 30 ppb uranium standard additions. The amount of soil sample taken for the microwave digestions is listed in the Table 1. It is notable that the amounts were fixed up by carrying out a series of ACS analysis on the reduction behavior of the U(VI)-CA complex. It can be seen that a smooth and a well defined voltammogram with a reduction peak is appeared for the sample. The appearance of such a smooth peak is obviously the positive effect of appropriate dilution of the sample (1:52 fold) and the use of masking agent EDTA. However, the appearance of the U(VI)-CA reduction peak informs that the added soil digested sample consists of uranium. With increasing uranium concentration, increase in peak current behavior is analogous to that observed for the blank sample (Fig. 2) and water sample (Fig. 3).

The inset Fig. 4 shows the *i vs. c* relationships of the U(VI)-CA complex. The linear line of the *i vs. c* touches the uranium concentration line (X-axis) at the concentration of 3.8 ppb. It means that 200 μl soil digested sample consists of 39.59 ng uranium (volume in the cell cup is 10.42 ml). Amount of uranium in 100 ml prepared sample is 19.79 μg. This amount of uranium is present in 0.9016 g of soil which corresponds to 21.95 mg uranium/Kg soil i.e. 21.96 ppm uranium in the soil. Table 1 summarizes the uranium content found in the soil samples collected from different locations. It may be seen that the obtained values lie in between 16.3-31.7 ppm. At around 5% cases, the presently obtained values are higher than 30 ppm. Actually, there are no guidelines of EPA or WHO for the safe level of uranium in soil as that provided for water. Canadian Council of Ministers of the Environment (CCME) has a published guideline on the safe level of uranium in soil [20]. According to this guide line, it seems that uranium concentrations present in the soils of the investigated areas are not so alarming.

Table 1: Data for the amount of digested soils and stones, volumes of sample prepared, volumes of sample taken and added and the concentrations of uranium obtained in water, soil and stones collected from the different locations of Sherpur District, Bangladesh

Sample name	Number of samples studied	Weight of digested sample (g)	Sample volume made (ml)	Added sample volume (μl)	Uranium concentration μg/L (ppb)	Uranium concentration mg/Kg (ppm)
Water	36	-	25.0	10×10^3	8.9 - 16.4	-
Soil	30	0.9016 - 1.0013	100	200	-	16.3 - 31.7
Stone	30	0.5026 - 0.5221	100	100	-	19.2 - 161.6

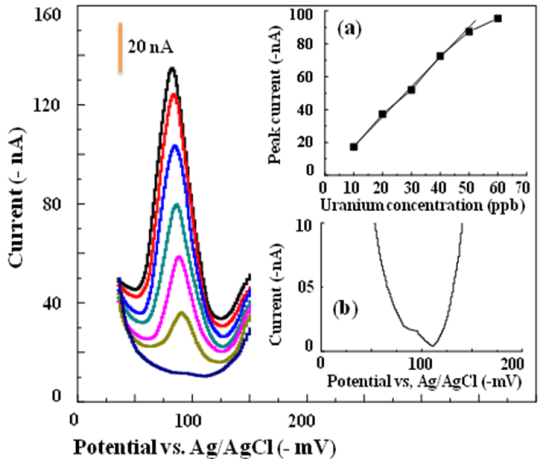

Fig. 2. ACS voltammograms of the U(VI)-CA reduction during uranium standard additions (0, 10, 20, 30, 40, 50 and 60 ppb) [pH 2.5, 0.02 M KNO_3 electrolyte, 1.95 x 10^{-4} M CA and 1.95 x 10^{-5} M EDTA]. Inset Figures: (a) U(VI)-CA reduction peak current (i) and uranium concentration (c) relationships and (b) (i) vs. (potential) relationships for the blank solution

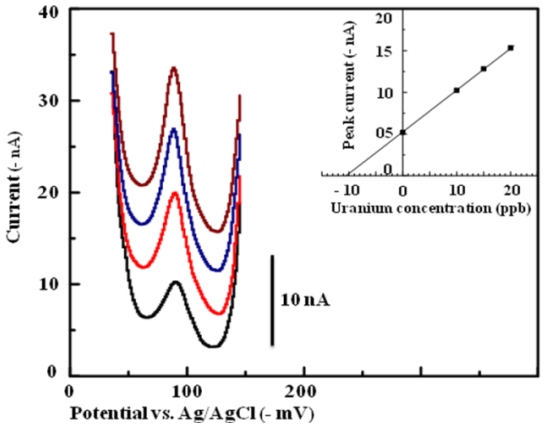

Fig. 3 ACS voltammograms of the U(VI)-CA reduction for a water sample with 10, 15 and 20 ppb uranium standard additions [pH 2.5, 0.02 M KNO_3 electrolyte, 1.96 x 10^{-4} M CA and 1.96 x 10^{-5} M EDTA]. Inset Fig.: Relationships between the U(VI)-CA reduction peak current (i) and concentration of uranium (c)

Fig. 5 shows the ACS voltammograms of the U(VI)-CA complex for 100 µl stone digested sample with three successive uranium standard addition (10, 20 and 30 ppb). The amounts of stone powder taken for the microwave digestions are enclosed in the Table 1. These amounts were fixed up by carrying out a series of ACS analysis on the reduction behavior of the U(VI)-CA complex. The purpose of series of analysis was to optimize the least volume of digested sample need to be added to 10 ml mixture of electrolyte and ligand to obtain around 10 ppb uranium concentration i.e. trace level uranium. The second purpose was to minimize as possible as the unwanted effect of other metal ions present in the sample on the desired U(VI)-CA complex. It was observed that the optimized condition (pH 2.5, CA concentration 1.95 x 10^{-4} M and EDTA of concentration 1.95 x 10^{-5} M) was enabled in suppressing the side effect of foreign materials on the U(VI)-CA complex. Such a benefit was also achieved by the authors [8, 9] to inactivate unwanted metal ions such as Cu(II), Fe(III), Mn(II), Zn(II) and Pb(II) present in digested sample.

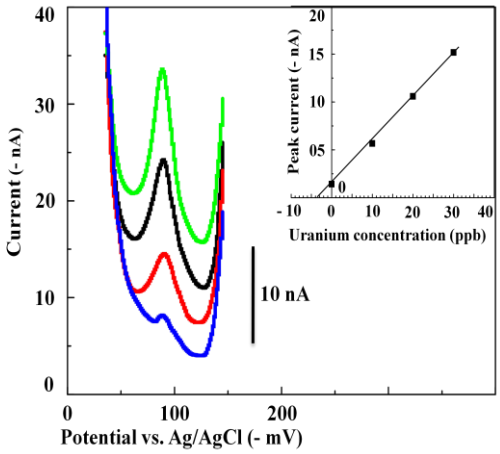

Fig. 4 ACS voltammograms of the U(VI)-CA reduction for a soil sample with 10, 20 and 30 ppb uranium standard additions [pH 2.5, 0.02 M KNO_3 electrolyte, 1.92 x 10^{-4} M CA and 1.92 x 10^{-5} M EDTA]. Inset Fig.: Relationships between the U(VI)-CA reduction peak current (i) and concentration of uranium (c)

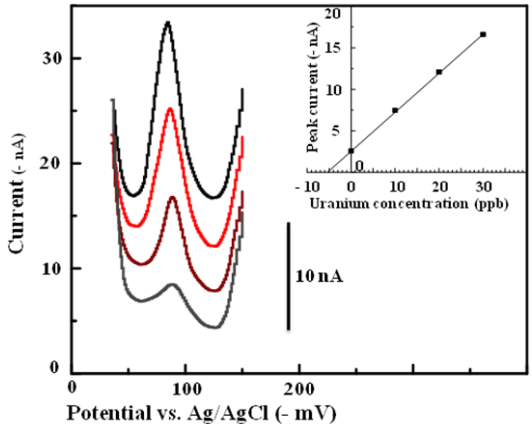

Fig. 5 ACS voltammograms of the U(VI)-CA reduction for a stone digested sample with three successive uranium standard additions (10, 20 and 30 ppb) [pH 2.5, 0.02M KNO_3 electrolyte, 1.94 x 10^{-4} M CA and 1.94 x 10^{-5} M EDTA]. Inset Fig.: Relationships between the U(VI)-CA reduction peak current (i) and concentration of uranium (c)

From the Fig. 5, it can be seen that a well defined voltammogram with a reduction peak is appeared for the unknown stone digested sample. The appearance of smooth peak is obviously the positive effect of appropriate dilution (1:103 fold) of the digested sample solution and the use of EDTA [8, 9]. The peak appeared at the potential of – 89 mV which can be taken equal to the potential – 90 mV obtained for the reduction peak of uranium(VI)-CA complex when 10 ppb uranium standard was added with the blank solution as shown in Fig. 2. It may be taken as an indication that the stone digested sample consists of uranium.

The inset Fig. 5 shows the *i vs. c* relationships of the U(VI)-CA complex. Linear line of the *i vs. c* touches the uranium concentration axis (X-axis) at the concentration of 5.3 ppb. It means that 100 μl stone digested sample consists of 54.69 ng uranium (volume in the cell cup is 10.32 ml). So, amount of uranium in 100 ml prepared sample is 54.69 μg. This amount of uranium is present in 0.5221 g of stone which corresponds to 104.75 mg uranium/Kg stone i.e. 104.75 ppm.

Table 1 summarizes the uranium content found in the stone samples collected from different locations. It may be seen that the obtained values lie in between 19.2 - 161.6 ppm. At around 9% cases, the presently obtained values are higher than 150 ppm. Although, this concentration is not economically viable to extract uranium from these stones but it requires an extensive study to find out the uranium crust layer if any to understand the leaching property and to estimate uranium abundances. It is noteworthy to mention here that the long-term retention of the high content of uranium as observed in the soil and stone of some investigated areas may experience a radiation risk in the human health living in those areas in near future [2]. Therefore, monitoring, i.e., uranium quantification, radiation dose estimation and activity regarding radioactive remediation seems to be essential.

4. Conclusion

The present study demonstrates that CAS voltammetric determination of uranium based on accumulation of the U(VI)-CA complex can be used to quantify uranium concentrations in water, soil and uranium rich stones by measuring uranium in trace level as selected. It seems that the adopted experimental optimum conditions are quite suitable to minimize the interferences of other metal-ions present in water and especially soil and stones during uranium determination. The method is not complex and highly selective. Success of this study seems to be opened a new scope to enhance the uranium exploration and quantification studies at various geographical locations of Bangladesh. However, more investigations are needed to be carried out because soil and stones of different locations of Bangladesh may contain different elemental compositions and may impart different complexities in the measurements.

Acknowledgement

The financial support from the Ministry of Science & Technology, Government of the People's Republic of Bangladesh, in the session 2016-2017 under special allocation (No. Physical Science 368-2), in the form of chemicals and small accessories, is thankfully acknowledged. The authors are grateful to Professor K. S. Nahm, Faculty of Chemical Engineering and Technology, Chonbuk National University, Republic of Korea, for his valuable advice and suggestion during the experiments.

References

1. Uranium 2014: Resources, Production and demand, A joint report by the OECD Nuclear Energy Agency and the International Atomic Energy Agency, NEA No. 7209, OECD 2014.
2. N. K. Sethy, R. M. Tripathi, V. N. Jha, S. K. Sahoo, A. K. Shukla and V. D. Puranik, Assessment of natural Uranium in the ground Water around Jaduguda Uranium Mining Complex, India, J. Environmental Protec., **2,** 1002-1007 (2011).
3. M. Rahman, N. I. Molla, A. K. M. Sharif, S. Basunia, S. Islam, R. U. Miah, S. M. Hossain, M. I Chowdhury, A. D. Bhuiyan and P. Stegner, Determination of U and Th in rock samples from Harargaj anticline by instrumental neutron activation analysis, J. Radioanal. Nuclear Chem., **1**, 17-22 (1993).
4. A. K. M. A. Ullah, M. I. Khalil and A. K. M. F. Kibria, Determination of uranium in stones by stripping voltammetry following adsorptive accumulation of the U(VI)-chloranilic acid complex, Int. Res. J. Eng. Tech., **2(7)**, 705-712 (2015).
5. A. K. M. A. Ullah, M. I. Khalil and A. K. M. F. Kibria, Determination of Uranium in stream water, beach sand and rocks by stripping voltammetry following adsorptive accumulation of the U(VI)-chloranilic acid complex, Int. Res. J. Eng. Tech., **2(8)**, 54-63 (2015).
6. J. Wang and R. Setradji, Selective determination of trace uranium by stripping voltammetry following adsorptive accumulation of the uranium-cupferron complex, Anal. Chim. Acta, **264**, 205-211 (1992).
7. M. I. C. Cantagallo and M. A. de Sousa, Voltammetric determination of Uranium in rocks, soils and sediments by using the catalytic nitrate reduction, J. Radioanal. Nucl. Chem., **218**, 117-118 (1997).
8. C. M. G. V. D. Berg and Z. Q. Huang, Determination of Uranium in sea water by cathodic stripping voltammetry of complexes with catechol, Anal. Chim. Acta, **164**, 209-222 (1984).
9. J. Wang, J. Wang, J. L. and K. Olsen, Adsorptive stripping voltammetry of trace Uranium: Critical comparison of various chelating agents, Anal. Chim. Acta,**292**, 91-97 (1994).
10. K. W. Cha, C. I. Park and S. H. Park, Simultaneous determination of trace Uranium(VI) by adsorptive cathodic stripping voltammetry with aluminon ligand, Talanta, **52**, 983-989 (2000).
11. M. B. Gholivand and H. R. Nassab, Highly selective adsorptive cathodic stripping voltammetric determination of Uranium in the presence of pyromellitic acid, Electroanalysis, **17**, 719-723 (2005).
12. S. K. Rajusth, P. Sharma, C. Srilakshmi and A. K. Shukla, Voltrametric ultra trace determination of Uranium: Method development, application and validity, J. Eng. Sci. and Tech., **2**, 39-42 (2013).
13. S. Sander and G. Henze, Adsorptive voltammetric techniques for the determination of Uranium(VI) with 2,5-dichloro-3,6-dihydroxy-1,4-benzoquinonoe as complex forming reagent, Fresenius J. Anal. Chem., **349**, 654-658 (1994).
14. S. Sander, W. Wagner and G. Henze, Direct determination of Uranium traces by adsorptive stripping voltammetry, Anal. Chim. Acta,**305**, 154-158 (1995).

15. S. Sander, W. Wagner and G. Henze, Possibilities for the automated determination of trace concentrations of Uranium in water samples by adsorptive stripping voltammetry, Anal. Chim. Acta, **349**, 93-99 (1997).

16. S. Rout, M. K. Mishra, A. Kumar and P. M. Ravi, Determination of ultra trace Uranium in lichen by asorptive-cathodic stripping volammetric technique, Int. J. Environ. Sci., **4**, 605-613 (2014).

17. L. Novotny, T. Navratil, S. Sander and P. Basova, Electrocapillary activity and accumulation of U(VI)-Cupferron and U(VI)-Chloranilic acid complexes on mercury electrode, Electroanalysis, **15**, 1687-1692 (2005).

18. U. S. EPA, Draft guidelines for carcinogen risk assessment (Review Draft, July 1999), U. S. environmental protection agency, risk assessment forum, Washington, D. C., 1999.

19. World Health Organization (WHO), Water guidelines for drinking quality, **1,** Recommendations, 3rd Edition, WHO, Geneva, 2006.

20. Canadian soil quality guidelines for the protection of environmental and human health, Uranium 2007.

Distribution and Contamination of Trace Elements in Core Sediments of the Karnaphuli River using Neutron Activation Analysis

R. Das[1, 2], M. A. Islam[2*], K. Naher[2], R. Khan[2], U. Tamim[2] and M. A. Rashid[1]

[1]*Department of Physics, Chittagong University of Engineering & Technology, Chittagong-4349, Bangladesh*
[2]*Institute of Nuclear Science & Technology, Atomic Energy Research Establishment, Ganakbari, Ashulia, Dhaka-1349, Bangladesh*

Abstract

The present study investigates the distribution and contamination of trace elements in core sediments collected from 3 locations of the Karnaphuli river. Total concentrations of 15 major and trace elements (Na, Al, K, Sc, Ti, V, Cr, Mn, Fe, Co, Zn, As, Rb, Th and U) were determined in sediments of the Karnaphuli river by neutron activation analysis (NAA) method. When compared with upper continental crustal (UCC) values, it is observed that mean concentrations of Al, Ti, V, Zn, Rb and that most of the cores show elevated values. In this study, pollution level of pollutants in core sediments evaluated by different pollution indices suggests that recent pollution level of the sediments is higher than the previous levels. This study will be helpful to quantify levels of trace elements pollution, to identify their tentative sources as well as to mitigate future pollution risks of the river.

***Keywords*:** Trace element, core sediments, neutron activation analysis, Karnaphuli river

1. Introduction

Sediments are important carriers of trace elements in the hydrological cycle. Since trace elements are partitioned with the surrounding waters, they reflect the quality of an aquatic system. Moreover, sediments play a major role in determining pollution pattern of aquatic systems [1, 2], reflecting the history of pollutants deposition and providing a record of catchment inputs into aquatic ecosystems [3, 4]. Therefore, by analyzing sediments, it is possible to determine the provenance, distribution and possible hazards of element contaminations in the river system [5-7]. The concentration of trace elements in sediments are varied according to the rate of particle sedimentation, the rate of heavy metals deposition, the particle size and the presence or absence of organic matter in the sediments.

Environmental research using nuclear techniques for the determination of trace and ultra-trace element pollutions has a great potential in relation to human health. Generally, different analytical techniques have been extensively employed for elemental pollution monitoring of sediments like atomic absorption spectrometry, inductively coupled plasma optical emission spectrometry, and inductively coupled plasma mass spectrometry. These chemical methods involve digestion of the samples. There are also some other methods that use only finely grinded homogenized powder samples without further chemical treatments [8]. Neutron activation analysis (NAA) is one of them. NAA is a specific and accurate analytical technique due to its high sensitivity and multi-element determination nature [9, 10], recently classified as a primary ratio method by metrology [11].

The increasing urbanization and industrialization of Bangladesh have negative implications in river sediment and water quality. The Karnaphuli is the principal river of the Chattogram region. A water treatment plant has been set up by Chattogram Port Authority to source water from the Karnaphuli river for its uses. The plant will make the port self-reliant in its water needs. Like many rivers in Bangladesh, Karnaphuli is heavily polluted by agricultural runoff and industrial effluents. Although some studies on spatial metal distributions of the Karnaphuli river have been carried out [12, 13], but core sediment analysis of this river is rare. Therefore, in this study an attempt has been taken to investigate the concentration and distribution of major and trace elements in core sediments of the Karnaphuli river using NAA technique. This study also assesses the depth-wise elemental pollution status of the river by calculating different environmental pollution indices.

2. Experimental Details

2.1 Study area and sample collection

The Karnaphuli river is located (22 ° 12 ′33 ′′ N to 91 °48 ′54 ′′E) in the southeastern region of Bangladesh. Karnaphuli river is the major watercourse of the Chattogram region of Bangladesh. Rising in the Mizo Hills of Mizoram state, northeastern India, flows about 270 km south and southwest through the southeastern arm of Bangladesh to empty into the Bay of Bengal, 19 km below the city of Chittagong. Three core sediment samples were collected from 3 locations of the Karnaphuli river (Core-1: 22 °37 ′1 ′′N and 91 °88 ′6 ′′E, Core-2: 22 °35 ′3 ′′N and 91 °87 ′8 ′′E, Core-3:22 °35 ′2"N and 91 °86'9 ′′E). The sediment samples were collected using an acrylic pipe sampler during ebbs. Each core sample was sliced into 5 cm interval (for example, K-1.1=surface (0-5cm), K-1.2= 5-10 cm, K-1.3=10-15 cm etc.) to study depth-wise distribution of trace elements in the cores and each sediment slice was stored in cleaned polyethylene bag. The length of core-1 was 60 cm whereas core-2 and core-3 were 70 cm.

2.2 Sample preparation

The aggregates and organic species from the sediment samples were removed and dried at about 50 °C in an

Corresponding author*:* liton80m@yahoo.com

electric oven in the laboratory to obtain constant weight. The dried samples were then ground into small grain size and homogeneously mixed using anagate mortar and pestle. The homogenous powdered samples were sieved and stored in labeled glass bottles as stock samples for elemental analyses.

2.3 Sample irradiation and analysis

Approximately 50 mg of each dried powder sample was weighed in polyethylene bag and heat sealed. For relative standardization approach of instrumental neutron activation analysis (INAA), two certified reference materials (CRMs) from International Atomic Energy Agency (IAEA): IAEA-Soil-7 and IAEA-SL-1 (Lake Sediment) and one standard reference material NIST-1633b along with the sediment samples were analyzed in this study. IAEA-Soil-7 was used as the standard, while IAEA-SL-1 and NIST-1633b were used as the control samples. Two types of neutron irradiation (short and long) were performed at 3 MW TRIGA MARK II research reactor of Bangladesh Atomic Energy commission. Short irradiation was perform to investigate the short-lived radionuclidesof the elements Na, K, Al, Mn,Ti, V which was performed separately for each sample with the thermal neutrons (flux:~5.28×10^{12} cm^{-2} s^{-1}) for 1min. at 250 kW reactor power. The dead time of the counting system was kept within 10%.

Long irradiation was perform to investigate medium and long lived radionuclidesof the elements which was performed simultaneously with all the samples and standards with the thermal neutrons (flux: ~2.11×10^{13} cm^{-2} s^{-1}) for 7 minutes at 2.4 MW power of the reactor. In that irradiation tube, three Al-0.1% Au (0.1 mm foil) were also stacked at the top, middle and bottom of the samples and standards for monitoring neutron flux variation in the tube. After long irradiation, two timesgamma ray countingswith different decay intervals were performed for medium and long-lived radionuclides with a high purity germanium (HPGe) detector (40% relative efficiency, 1.8 keV resolution at 1332.5 keV of ^{60}Co source) coupled with a gamma spectrometer (ORTEC, DSPEC JrTM). Peak counts were calculated using Hypermet PC software. For the calculation of trace element concentrations, the considered product radionuclides with their half-lives and gamma-ray energies are given in Table 1.

Table 1. Radionuclides with their half-lives and gamma ray energies for NAA determination of the elements [22]

Elements	Product nuclide	Half-life	Gamma-ray energy (keV)
Na[a]	^{24}Na	14.7 h	1369
Al[a]	^{28}Al	2.24 min	1779
K[a]	^{42}K	12.4 h	1525
Sc	^{46}Sc	83.8 d	889 , 1121
Ti[a]	^{51}Ti	5.76 min	320
V[a]	^{52}V	3.75 min.	1434
Cr	^{51}Cr	27.7 d	320
Mn[a]	^{56}Mn	2.58 h	847, 1811
Fe	^{59}Fe	44.5 d	1099,1292
Co	^{60}Co	5.27 y	1173, 1332
Zn	^{66}Zn	244 d	116
As	^{76}As	26.3 h	559
Rb	^{86}Rb	18.7 d	1077
Th	^{233}Pa	27 d	312
U	^{239}Np	2.36 d	106 , 278

[a]Elements are determined by short irradiation

2.4 Quantification of sediment pollution

2.4.1 Enrichment factor (*EF*)

Metal contamination in the studied sediments can be evaluated in more comprehensive way by using enrichment factor (EF), which can be calculated by using the following equation [14].

$$EF = \frac{\left(\frac{Metal}{Al}\right)sample}{\left(\frac{Metal}{Al}\right)Background}$$

In this study, Al was used as reference element for geochemical normalization and upper continental crustal (UCC) average values from literature [15] were used as the geochemical background concentration. EF values 1.5-3.0, 3.0-5.0, 5.0-10 and >10 are the evidence of minor, moderate, severe and very severe enrichment of the elements in sediments, respectively.

2.4.2 Geo-accumulation index (I_{geo})

Geo-accumulation index (I_{geo}) can be defined by the following equation [14]:

$$I_{geo} = Log_2\left(\frac{C_x}{1.5\ XB_x}\right)$$

Where, C_x is the measured concentration of the metal x, B_x is the geochemical background concentration of metal x.

Factor 1.5 is the background matrix correction factor due to lithospheric effects. The I_{geo} consists of seven classes. Class 0 (practically uncontaminated): $I_{geo}<0$; Class 1 (uncontaminated to moderately contaminated): $0 < I_{geo}<1$; Class 2 (moderately contaminated): $1 < I_{geo}< 2$; Class 3 (moderately to heavily contaminated): $2 < I_{geo}< 3$; Class 4 (heavily contaminated): $3 < I_{geo}< 4$; Class 5 (heavily to extremely contaminated): $4 < I_{geo}< 5$; Class 6 (extremely contaminated): $5 <I_{geo}$.

2.4.3 Pollution load index **(***PLI***)** *and modified degree of contamination* **(***mC_d***)**

Pollution load index (PLI) is calculated from the contamination factors (CF) of the studied elements for a specific sampling site, which can be defined as follows [16]:

$$CF = \frac{(Metal\ concentration)_{Sample}}{(Metal\ concentration)_{Background}}$$

Then, PLI is represented by the following equation [16]

$$PLI = (CF_1 X\ CF_2 X\ CF_3\ X \dots\dots\dots\ CF_n)^{1/n}$$

Where, CF_1 to CF_n represents the contamination factors for the studied elements and n is the total number of contamination factors considered.

The modified degree of contamination (mC_d) index can be calculated as follows [14]:

$$mC_d = \frac{1}{n}\sum_{i=1}^{n} CF_i$$

Where, n is the total number of contaminants; CF is the contamination factor of each element at a point. The mC_dconsists of following gradation: $mC_d<1.5$ is nil to a very low degree of contamination; $1.5\leq mC_d< 2$ is a low degree of contamination; $2\leq mC_d<4$ is a moderate degree of contamination; $4\leq mC_d<8$ is a high degree of contamination; $8\leq mC_d<16$ is a very high degree of contamination; $16\leq mC_d<32$ is an extremely high degree of contamination; $mC_d\leq 32$ is an ultra-high degree of contamination.

3. Results and Discussion

3.1 Elemental concentration in sediments

In this study, total concentrations of 15 major and trace elements (Na, Al, K, Sc, Ti, V, Cr, Mn, Fe, Co, Zn, As, Rb, Th and U**)** in core sediments of the Karnaphuli river are determined by NAA. To ensure quality of the analytical data, comparisons of trace element analyses results for single measurement in this study to the certified/ information values of the reference materials are given in Table 2. It is observed that concentrations for most of the studied elements obtained in this study are within 10% deviation from their certified/information values which assures accuracy of the analysis. The elemental concentrations, their descriptive statistics, PLI values as well as the literature data of UCC [15] for the respective elements in core sediments of the Karnaphuli river are given in Table 3-5. If we observe the concentration variations of the elements in different cores, it is observed that for core-1, most of the element contents do not vary over a long range (RSD: 6.8–46.7%), whereas Al and Rb contents vary widely(RSD: 61.4% and 69.4% respectively,Table 3); for core-2 all element contents varywith RSD: 4.3-39.4% except Al and Rb contents (RSD: 42.4% and 45.1%, respectively, Table 4) whereas for core-3 element contents vary with RSD: 10-36.8% except Al contents (RSD: 46.9%, Table 5) varies over a relatively long range.

Table 2. Comparison of results (mg kg^{-1}) of the element analyses in this study to the certified values of those elements in the reference materials

Element	IAEA-CRM-SL-1			NIST-SRM-1633b		
	Study value	certified value	ratio	study value	certified value	ratio
Na	1707 ± 60.1	1700 (1600-1800)	1.00	2159 ± 25.3	2010	1.07
Al	96625 ± 3091	89000	1.09	151478 ± 4821	150500	1.01
K	12623 ± 675	14500 (12400-16600)	0.87	20861 ± 1065	19500	1.07
Sc	14.9 ± 0.48	17.3 (16.2-18.4)	0.86	39.0 ± 1.26	41.0	0.95
Ti	5937 ± 413	5170 (4740-5600)	1.15	7799 ± 459	7910	0.99
V	186 ± 8.78	170	1.09	237 ± 10.7	296	0.80
Cr	92.6 ± 4.24	104 (95-113)	0.89	183 ± 7.82	198	0.92
Mn	3529 ± 121	3460	1.02	145 ± 6.26	132	1.09
Fe	58649 ± 2119	67400	0.87	74252 ± 2649	77800	0.95
Co	19.5 ± 1.03	19.8 (18.3-21.3)	0.99	49.8 ± 2.6	50	1.00
Zn	207.9 ± 14.88	223	0.93	200.2 ± 15.1	210	0.95
As	29.2 ± 1.20	27.6 (24.7-30.5)	1.06	9 ± 0.3	136	0.07
Rb	96 ± 8.50	113 (102-124)	0.85	145 ± 11	140	1.04
Th	12.4 ± 0.5	14 (13-15)	0.89	26.1 ± 1.0	25.7	1.02
U	4.13 ± 0.3	4.02 (3.69-4.35)	1.03	9.01 ± 0.41	8.79	1.03

ratio = **s**tudy value/certified value

Table 3. Concentrations of the elements (mg kg^{-1}) in sediments of core-1 of the Karnaphuli river

Sample	Na	Al	K	Sc	Ti	V	Cr	Mn	Fe	Co	Zn	As	Rb	Th	U	PLI
K-1.1	7933	166622	25615	18.2	7257	168	165	749	61307	19.1	116	10.9	393	31.9	4.25	1.52
K-1.2	8581	192687	21742	15.5	7379	190	161	877	53723	16.2	96.6	7.17	318	30.6	2.65	1.46
K-1.3	6915	223716	24719	15.7	7844	208	102	883	46034	19.9	102	9.05	153	20.4	3.95	1.32
K-1.4	7935	215763	25267	16.7	7409	198	101	816	48235	21.6	113	8.25	155	19.1	3.53	1.34
K-1.5	8580	177954	22578	12.9	6064	156	82.4	647	37018	17.0	110	5.35	119	15.7	4.05	1.12
K-1.6	8597	217343	23400	12.4	9051	181	78.2	663	34923	15.6	97.6	4.36	111	14.9	3.33	1.15
K-1.7	8608	281713	22975	12.0	7230	189	77.5	635	33808	15.8	80.8	4.81	111	15.7	2.97	1.13
K-1.8	7714	157548	22210	11.9	6317	140	62.5	665	31247	17.0	82.9	5.94	82.7	11.6	2.52	1.00
K-1.9	7558	156169	22395	13.4	6345	147	68.8	699	35034	18.8	101	5.46	96.6	12.8	2.48	1.05
K-1.10	7647	257490	22954	13.1	9300	216	68.8	720	34972	18.6	110	4.11	73.1	12.5	1.96	1.14
K-1.11	7525	268285	24383	13.5	7205	207	66.2	796	34828	18.3	89.7	4.62	77.7	11.5	2.62	1.11
K-1.12	8151	238502	24384	11.7	7928	177	60.7	718	30862	17.6	87.3	3.64	64.6	10.7	3.03	1.04
Min	6915	156169	21742	11.7	6064	140	60.7	635	30862	15.6	80.8	3.6	64.6	10.7	1.96	1.00
Max	8607	281713	25615	18.2	9300	216	165	883	61307	21.6	116	10.9	393	31.9	4.25	1.52
UCC	24300	81500	23200	14	3800	97	92	775	39200	17.3	67	4.8	84	10.5	2.7	
Mean	7979	125617	22664	12	4896	116	74	722	32159	17	88	4	98	14	3	1.20
SD	542	43322	1280	2	997	25	36	86	9798	2	12	2	103	7	1	
RSD,%	6.8	61.4	11.1	20.9	43.7	44.8	37.3	12.7	27.4	11.7	18.3	46.7	69.4	38.3	28.5	

UCC= Upper continental crustal average; SD= Standard deviation; RSD= Relative standard deviation; PLI = Pollution load index

Uncertainties associated with elemental concentrations due to estimated uncertainty budget of NAA are**:** Na, Al, K, Sc, Mn, Fe, As, Th and U = 3-4%; V, Cr and Co = 4-5%; Ti, Zn and Rb = 6-7%

Table 4. Concentrations of the elements (mg kg^{-1}) in sediments of core-2 of the Karnaphuli river

Sample	Na	Al	K	Sc	Ti	V	Cr	Mn	Fe	Co	Zn	As	Rb	Th	U	PLI
K-2.1	6744	155864	18596	7.87	5361	114	53.9	631	21746	13.8	73.2	2.05	47.5	8.28	1.86	0.78
K-2.2	6993	197654	21454	8.90	6720	151	45.8	653	23266	15.5	80.9	3.20	49.4	7.33	1.60	0.85
K-2.3	7339	178303	19178	7.47	6727	143	39.4	616	19459	13.1	72.9	2.06	33.2	7.47	1.53	0.76
K-2.4	896	216092	19837	7.18	6616	146	35.0	553	18881	12.9	72.4	2.17	34.6	7.46	1.99	0.65
K-2.5	7123	178695	19922	9.40	7251	143	34.9	697	23871	15.7	80.4	2.30	49.5	8.05	1.97	0.84
K-2.6	7561	84990	20417	8.27	4657	93.5	40.7	650	20644	14.1	73.3	2.22	33.1	6.88	1.92	0.70
K-2.7	6588	99547	19651	10.9	3703	84.4	87.4	654	33694	16.7	62.6	6.32	122	16.8	3.04	0.90
K-2.8	7167	121251	21598	12.5	3933	102	105	777	36435	17.6	91.2	6.00	136	17.1	3.03	1.03
K-2.9	7458	85828	20645	10.8	3464	76.9	88.0	635	30932	15.1	60.8	4.91	100	14.9	2.49	0.86
K-2.10	7105	92211	20708	11.3	3237	85.6	78.3	729	31206	16.6	84.3	3.89	96.6	12.9	2.65	0.88
K-2.11	5919	112242	20997	11.8	3676	94.0	86.6	739	33511	17.6	89.6	3.88	95.3	15.0	2.75	0.93
K-2.12	7782	57853	20970	11.2	2549	59.2	86.3	657	30413	16.4	84.4	4.70	90.1	13.5	2.49	0.81
K-2.13	6730	44317	20754	11.6	2322	50.1	78.8	655	31994	18.0	80.6	3.79	99.0	13.7	2.59	0.78
K-2.14	7355	120437	21318	11.1	3768	94.2	76.3	793	30878	17.3	73.2	3.57	92.1	13.0	2.79	0.91
Min	896	44317	18596	7.18	2322	50.1	34.9	553	18881	12.9	60.8	2.05	33.1	6.88	1.53	0.65
Max	7782	216092	21597	12.5	7251	151	105	793	36435	18.0	91.2	6.32	136	17.1	3.04	1.03
UCC	24300	81500	23200	14	3800	97	92	775	39200	17.3	67	4.8	84	10.5	2.7	
Mean	6626	124663	20432	10	4570	103	67	674	27638	16	77	4	77	12	2	0.84
SD	1714	52861	885	2	1664	33	24	66	6012	2	9	1	35	4	1	
RSD,%	25.9	42.4	4.3	17.8	36.4	31.8	36.0	9.7	21.8	10.9	11.7	39.4	45.1	33.0	21.9	

Table 5. Concentrations of the elements (mg kg^{-1}) in sediments of core-3 of the Karnaphuli river

Sample	Na	Al	K	Sc	Ti	V	Cr	Mn	Fe	Co	Zn	As	Rb	Th	U	PLI
K-3.1	8049	39087	25858	13.8	4039	105	84.1	1015	37558	19.3	104	4.30	101	15.0	3.63	0.97
K-3.2	8071	40148	22829	13.0	3086	76.3	77.8	745	35785	18.7	112	4.22	102	14.8	2.80	0.89
K-3.3	8260	48162	22977	12.7	2764	62.5	78.8	651	33983	16.6	97.9	4.87	96.9	15.2	2.95	0.85
K-3.4	7995	38935	22267	12.7	3775	91.6	76.6	725	33988	18.7	83.4	4.98	88.1	14.2	3.05	0.87
K-3.5	8393	4153	23139	12.0	3420	65.6	67.8	801	31356	17.7	99.0	<0.82	87.4	12.7	<1.5	0.84
K-3.6	8390	40331	25434	12.7	3133	80.4	69.5	793	33525	19.3	104	3.88	96.9	13.1	2.62	0.88
K-3.7	8768	39894	2658	11.9	2783	69.4	72.9	764	31510	17.8	98.8	3.83	88.6	12.7	2.65	0.84
K-3.8	9523	43410	24289	10.5	2407	56.8	59.3	718	26095	16.4	85.4	3.45	59.1	11.1	2.69	0.74
K-3.9	8636	40087	27099	12.7	2390	59.4	63.3	860	31292	19.9	91.1	3.71	73.8	12.1	2.93	0.81
K-3.10	9803	31662	26623	11.5	2618	46.6	63.4	750	28478	17.7	103	4.03	66.9	10.6	2.72	0.76
K-3.11	8899	51095	25371	10.4	2412	60.8	58.3	796	27123	17.3	96.2	3.34	58.0	14.4	3.81	0.79
K-3.12	9282	116318	26313	11.0	3766	104	54.1	724	26808	17.6	72.2	3.52	57.9	10.5	3.06	0.86
K-3.13	647	96584	15934	7.70	3173	79.8	43.4	662	20386	14.0	46.9	2.60	44.8	8.57	2.23	0.66
K-3.14	7525	58343	23184	7.99	2758	58.6	42.5	569	19537	13.4	60.0	1.96	46.4	9.01	2.55	0.64
Min	6477.3	31662	15934	7.70	2390	46.6	42.5	569	19537	13.4	46.9	<0.82	44.8	8.57	<1.5	0.64
Max	9803.1	116318	27099	13.8	4039	105	84.1	1015	37558	19.9	112.2	5.0	102.4	15.2	3.8	0.97
UCC	24300	81500	23200	14	3800	97	92	775	39200	17.3	67	4.8	84	10.5	2.7	
Mean	8434	51828	24136	11	3037	73	65	755	29816	17	89	3	76	12	3	0.82
SD	846	24305	2877	2	545	18	13	104	5392	2	18	1	21	2	1	
RSD,%	10.0	46.9	11.9	15.8	17.9	24.6	19.6	13.8	18.1	10.7	20.6	36.8	26.9	17.7	32.6	

When compared with UCC values, it is observed that mean concentrations of Al, Ti, V, Zn, Rb and Th (core-1), mean concentration of Al, Ti, V, Zn and Th (core-2) and mean concentration of K, Co, Zn and Th (core-3) show elevated values. Recently, distributions of trace elements in surface sediments of the Buriganga and Poshur rivers have been reported [5, 9]. The elevated concentration levels of Ti, V, Th and U are also reported in those studies. The overall mean elemental concentrations for rest of the studied elements in this study are comparable to that of their concentrations in surface sediments of the Bangladeshi rivers [17, 18].

For core-1, the concentration of Al varied from 156169 (K-1.9) to 281713mg kg^{-1} (K-1.7), with a mean concentration of 125617 mg kg^{-1}. The concentration of Ti varied from 6064(K-1.5) to 9300mg kg^{-1} (K-1.10), with a mean concentration of 4896mg kg^{-1}. The concentration of V varied from 140 (K-1.8) to 216mg kg^{-1} (K-1.10), with a mean concentration of 116mg kg^{-1}. The concentration of Zn varied from 80.8 (K-1.7) to 116mg kg^{-1} (K-1.1), with a mean concentration of 88mg kg^{-1}. The concentration of Rb varied from 64.6 (K-1.12) to 393mgkg^{-1}(K-1.1), with a mean concentration of 98 mg kg^{-1}. The concentration of Th varied from 10.7 (K-1.12) to 31.9 (K-1.1) mg kg^{-}1, with a mean concentration of 14mg kg^{-1}. For core-1, relatively higher concentrations of trace elements were found in K-1.1 (surface, 0-5 cm), whereas K-1.12 (55-60 cm depth) shows the overall lowest concentrations of the studied trace elements. The higher concentrations of the trace elements in surface sediments of core-1 indicate more contamination in the present time than previous periods in the Karnaphuli river. In core-2, the concentration of Al varied from 44317(K-2.13) to 216092 mg kg^{-1} (K-2.4), with a mean concentration of 124663 mg kg^{-1}. The concentration of Ti varied from 2322 (K-2.13) to 7251 mg kg^{-1} (K-2.5), with a mean concentration of 4570 mg kg^{-1}. The concentration of V varied from 50.1 (K-2.13) to 151 mg kg^{-1} (K-2.2), with a mean concentration of 103 mg kg^{-1}. The concentration of Zn varied from 60.8 (K-2.9) to 91.2mg kg^{-1} (K-2.8), with a mean concentration of 77 mg kg^{-1}. The concentration of Th varied from 6.88 (K-2.6) to 17.1mg kg^{-1} (K-2.8), with a mean concentration of 12mg kg^{-1}. For core-2, relatively higher concentrations of the studied elements were found in K-2.8 (35-40 cm), whereas lowest concentrations were found in K-13 (60-65 cm). In the case of core-3, the concentration of K varied from 15934 (K-3.13) to 27099mg kg^{-1} (K-3.9), with a mean concentration of 24136 mg kg^{-1}. The concentration of Co varied from 13.4 (K-3.14) to 19.9 mg kg^{-1} (K-3.9), with a mean concentration of 17 mg kg^{-1}. The concentration of Zn varied from 46.9 (K-3.13) to 112 mg kg^{-1} (K-3.2), with a mean concentration of 89 mg kg^{-1}. The concentration of Th varied from 8.57 (K-3.13) to 15.2 mg kg^{-1} (K-3.3), with a mean concentration of 12 mg kg^{-1}. For core-3, the relatively higher concentrations of the studied trace elements were found in K-3.9 (40-45 cm) and lower concentrations were found in K-3.13 (60-65 cm).

3.2 Assessment of elemental contamination

Various pollution indices have been developed to assess the environmental contamination and risk of trace elements in sediments based on their total contents. Among the contamination indices, the enrichment factors (EFs) of trace elements have been commonly used to assess human-made contamination. In general, EF values of 0.5–1.5 reflect regional rock compositions, whereas EF>1.5 indicates non-crustal contributions and/or anthropogenic influences.

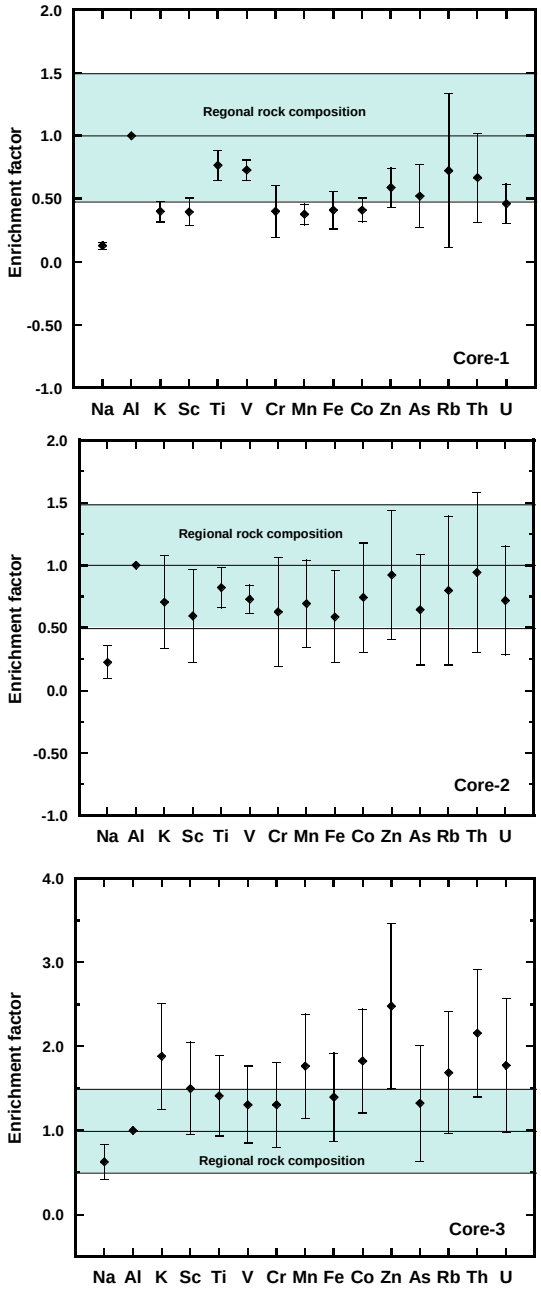

Fig. 1 The average enrichment factor values of the studied elements for sediments core-1, core-2 and core-3 of the Karnaphuli river

In this study, for core-1, the range of EF value for the studied elements are as follows: Na, 0.09–0.16; K, 0.29-0.54; Sc, 0.25-0.64; Ti, 0.55-0.93; V, 0.56-0.85; Cr, 0.22-0.88; Mn, 0.24-0.48; Fe, 0.25-0.76; Co, 0.26-0.57; Zn, 0.35-0.85; As, 0.26-1.12; Rb, 0.26-2.29; Th, 0.33-1.49 and U, 0.23-0.77. The average EF values along with standard deviations of the studied elements for core-1, core-2 and core-3 of the Karnaphuli river are shown in Fig. 1. The average and standard deviation values were calculated for core-1, n=12 and for core-2 and core-3, n=14. For core-1, the average EF values of all elements are below 1.5 indicates no pollution by these elements.

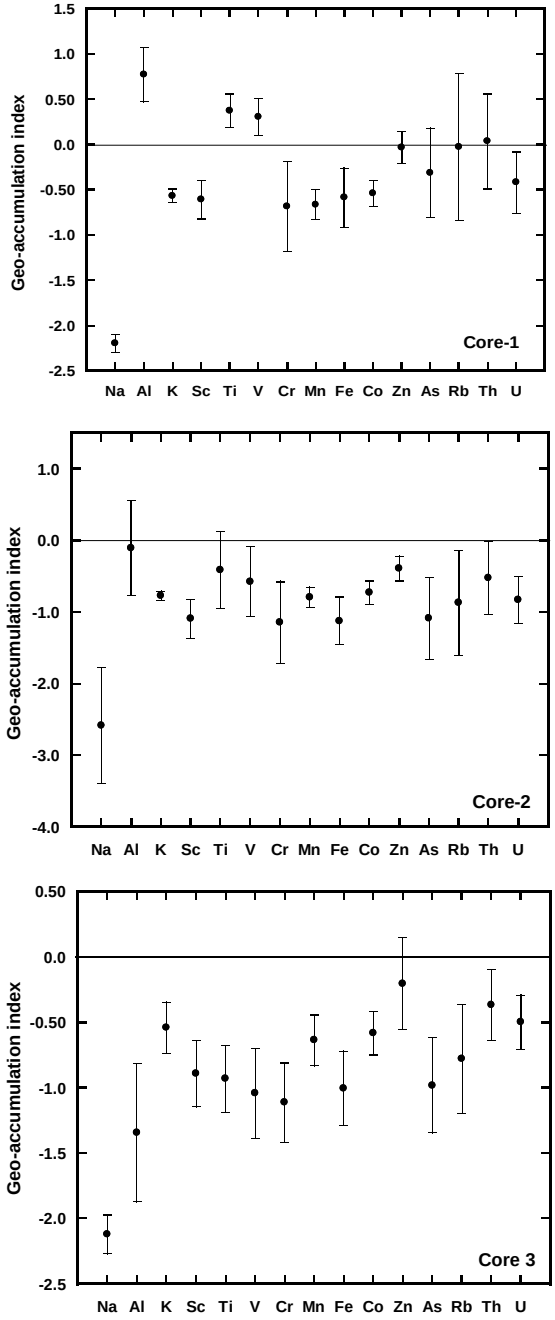

Fig. 2 Theaverage geo-accumulation index values of the studied elements forsediments core-1, core-2 and core-3 of the Karnaphuli river

For core-2, the range of EF value for the studied elements are as follows: Na, 0.01–0.51; K, 0.32-1.65; Sc, 0.19-1.53;

Ti, 0.66-1.18; V, 0.57-0.95; Cr, 0.14-1.58; Mn, 0.27-1.55; Fe, 0.18-1.50; Co, 0.28-1.91; Zn, 0.41-2.21; As, 0.17-1.45; Rb, 0.16-2.17; Th, 0.27-2.41 and U, 0.24-1.77. From EF values, it is observed that Co, Zn, Rb, Th and U at some layers, especially at K-2.13 layer, are minorly enriched.

For core-3, the range of EF value for the studied elements are as follows: Na, 0.22–1.04; K, 0.58-2.95; Sc, 0.46-2.12; Ti, 0.69-2.22; V, 0.69-2.27; Cr, 0.4-1.91; Mn, 0.65-2.73; Fe, 0.44-2.00; Co, 0.68-2.63; Zn, 0.59-3.95; As, 0.0-2.17; Rb, 0.45-2.50; Th, 0.69-2.98 and U, 0.0-2.80. For core-3, at most of the layers K, Sc, Mn, Co, Zn, Rb, Th and U are above 1.5 which indicates contamination of the sediments at this area of the Karnaphuli river by these elements. The depth-wise trace elemental distribution at core-3 indicates that this area is contaminated by these elements from previous time to still now. This study also indicates that rest of the elements Na, Ti, V, Cr, Fe, As are not a major concern for the contamination of the sediments of the river at this area. From Fig.1, it is also observed that the EF values of Na is significantly lower than unity, which indicate elemental mobilization of this element in sediments of this river. The highest EF value is observed for Zn (EF = 3.95) and ranges from 0.59 to 3.95. The high contents of Zn in the sediments of the Karnaphuli river may be due to the precipitation of Zn in the river system from effluents of battery, paints and different chemical industries like fertilizer and tannery [19]. The higher level of Th and U in the sediments may be due to the contamination of these elements from chemical fertilizer used in the agricultural fields of that area [20]. The degree of contamination with studied elements as indicated by EF was: Zn>Th> K>Co> U>Mn>Rb>Sc>Ti>Fe>As>V>Cr>Al>Na (high to low).

The calculated average geo-accumulation index (I_{geo}) values along with standard deviation of each core for the studied elements are shown in Fig. 2. According to I_{geo} classification, the average I_{geo}values ($0<I_{geo}<1.0$)of core-1 indicate that sediments of the core-1 are uncontaminated to moderately contaminated by Al, Ti, V and Th. For core-2 and core-3 sediments are practically uncontaminated.

PLI values at all layers of core-1 are ≥1.0, ranging from 1.00 to 1.52 withaverage PLI = 1.20. The highest PLI value is observed in the sampling point K-1.1 (PLI = 1.5). PLI values in all layers of core-2 are<1.0, except at K-2.8 (PLI = 1.03), ranging from 0.65 to 1.03 with average PLI = 0.84. PLI values at all layers for core-3 are <1.0. According to the classification adopted by Tomlinson et al. (1980) [21], PLI> 1.0 indicates deterioration of the sediment quality. From this study, estimated PLI values indicate the deterioration of the sediment quality at all layers of the core-1 (Table 3). For core-2 and core-3, there is no pollution in the sediment layers (except at K-2.8). The range of calculated modified degree of contamination (mC_d) for core-1, 1.1 to 1.8 with mean 1.3; for core-2, 0.73 to 1.12 with mean 0.91 and for core-3, 0.67 to 1.05 with mean 0.87. According to the gradation of mC_d, sediments at top three layers (K-1.1=1.81, K-1.2=1.63 and K-1.3=1.51) of core-1 represent low degree of contamination, whereas other deeper layers of this core represent nil to very low degree of contamination. For core-2 and core-3, all layers of sediments represent nil to very low degree of contamination. In this study, the PLI and mC_d values indicate that contamination of surface sediments at core-1 and core-3 is relatively higher than the deeper layers indicating that recent pollution level of the sediments is higher than the past in the Karnaphuli river.

4. Conclusion

In this study, 15 major and trace elements are determined in core sediments of the Karnaphuli river by NAA. It is observed that mean concentrations of Al, Ti, V, Zn, Rb and Th (core-1), mean concentration of Al, Ti, V, Zn and Th (core-2), mean concentration of K, Co, Zn and Th (core-3) show elevated values with respect to UCC. Among the studied 15 elements, the highest EF value is observed for the Zn (EF = 3.95) and ranges from 0.59 to 3.95 (core-3). The degree of contamination with studiedtrace elements as indicated by EF was: Zn>Th> K>Co > U>Mn>Rb>Sc> Ti>Fe>As>V>Cr>Al>Na (high to low). The calculated PLI and mC_d values indicate that sediments at core-1 are deteriorated. This study recommends that continuous monitoring of trace elements in sediment and other aquatic biota of Karnaphuli river should be directed to assess the risk of these elements to safe ecology of this river.

Acknowledgement

The authors thank personnel of the Center for Research Reactor (CRR) of Bangladesh Atomic Energy Commission for sample irradiation to perform NAA. The technical personnel of NAA, RNPD are gratefully acknowledged for their kind help during sample preparation and analysis for this study.

References

1. J. Casas, H. Rosas, M. Solé and C. Lao, Heavy metals and metalloids in sediments from the Llobregat basin, Spain,Environ. Geol., **44**, 325-332 (2003).
2. M. S. Rahman, M. B.Hossain, S. O. F. Babu, M. Rahman, A. S. Ahmed, Y. N. Jolly, T. R. Choudhury, B. A. Begum, J. Kabir and S.Akter, Source of metal contamination in sediment, their ecological risk, and phytoremediation ability of the studied mangrove plants in ship breaking area, Bangladesh,Mar. Pollut. Bull., **141**, 137-146 (2019).
3. J**.** Mwamburi, Variations in trace elements in bottom sediments of major rivers in Lake Victoria's basin, Kenya, Lakes Reservoirs**:** Research & Management, **8**, 5-13 **(**2003**).**
4. E**.** Siddiqui and J**.** Pandey, Assessment of heavy metal pollution in water and surface sediment and evaluation of ecological risks associated with sediment contamination in the Ganga River**:** a basin-scale study, Environ**.** Sci**.** Pollut**.** Res**.**, **26**, 10926-10940 **(**2019**).**
5. U**.** Tamim, R**.** Khan, Y**.** N**.** Jolly, K**.** Fatema, S**.** Das, K**.** Naher, M**.** A**.** Islam, S**.** M**.** A**.** Islam and S**.** M**.** Hossain, Elemental distribution of elements in urban river sediments near an industrial effluent source, Chemosphere, **155**, 509-518 **(**2016**).**

6. H. Zhang and B. Shan, Historical records of trace element accumulation in sediments and the relationship with agricultural intensification in the Yangtze-Huaihe region, China, Sci. Total Environ., **399**,113-120 (2008).
7. 7. R. Khan, M. S. Parvez, Y. N. Jolly, M. A. Haydar, M. F. Alam, M. A. Khatun, M. M. R. Sarker, M. A. Habib, U. Tamim, S. Das, S. Sultana and M. A. Islam, K. Naher, D. Paul, S. Akter, M. H. R. Khan, F. Nahid, R. Huque, M. Rajib and S. M. Hossain, Elemental abundances, natural radioactivity and physicochemical records of a southern part of Bangladesh: Implication for assessing the environmental geochemistry. Environ. Nanotech. Monitoring & Manag., **12**, 100225 (2019).
8. M. A. Islam and M. Ebihara, Elemental characterization of Japanese green tea leaves and tea infusion residue by neutron-induced prompt and delayed gamma-ray analysis, Arabian J. Chem., **10**, S677–S682 (2017).
9. M. A. Islam, A. Al-mamun, F. Hossain, S. B. Quraish, K. Naher, R. Khan, S. Das, U. Tamim, S. M. Hossain and F. Nahid, Contamination and ecological risk assessment of trace elements in sediments of the rivers of Sundarban mangrove forest, Bangladesh, Mar. Pollut. Bull., **124**, 356-366 (2017).
10. S. A. Latif, D. Afroj, S. M. Hossain, M. S. Uddin, M. A. Islam, K. Begum, Y. Oura, M. Ebihara and M. Katada, Determination of toxic trace elements in foodstuffs, soils and sediments of Bangladesh using instrumental neutron activation analysis, Bull Environ Contam Toxicol., **82**, 384–388 (2009).
11. R. R. Greenberg, P. Bode and E. A. D. N. Fernandes, Neutron activation analysis: a primary method of measurement, Spectrochimica Acta Part B: Atomic Spectroscopy, **66**, 193–241 (2011).
12. M. M. Ali, M. L. Ali, M. S. Islam and M. Z. Rahman, Preliminary assessment of heavy metals in water and sediment of Karnaphuli River, Bangladesh, Environmental Nanotechnology, Monitoring & Management, **5**, 27–35 (2016).
13. M. M. Islam, M. R. Karim, X. Zheng and X. Li, Heavy metal and metalloid pollution of soil, water and foods in Bangladesh: A Critical Review, Int. J. Environ. Res. Public Health, **15**, 2825 (2018).
14. G. M. S. Abrahim and R. J. Parker, Assessment of trace element enrichment factors and the degree of contamination in marine sediments from Tamaki Estuary, Auckland, New Zealand, Environ. Monit. Assess., **136**, 227–238 (2008).
15. R. L. Rudnick and S. Gao, Composition of the continental crust. In: Treatise on Geochemistry, second ed., (Chapter 4), 1–64 (2014).
16. L. Hakanson, An ecological risk index for aquatic pollution control. A sedimentological approach, Water Res., **14**, 975-1001 (1980).
17. D. K. Datta and V. Subramanian, Distribution and fractionation of heavy metals in the surface sediments of the Ganges-Brahmaputra-Meghna river system in the Bengal basin. Environ Geol., **36**, 93-101(1998).
18. M. S. Islam, M. K, Ahmed, M. Raknuzzaman, M. H. Al-Mamun and M. K. Islam, Heavy metal pollution in surface water and sediment: a preliminary assessment of an urban river in a developing country, Ecol. Indic., **48**, 282-291 (2015).
19. F. R. Siegel, Environmental Geochemistry of Potentially Toxic Elements. Springer-Verlag Berlin Heidelberg GmbH, New York, 30 (2002).
20. R. Ramesh, A. Ramanathan, S. Ramesh, R. Purvaja and V. Subramanian, Distribution of rare earth elements and heavy metals in the surficial sediments of the Himalayan river system. Geochem J., **34**, 295-319 (2000).
21. D. C. Tomlinson, J. G. Wilson, C. R. Harris and D. W. Jeffery, Problems in the assessment of trace elements levels in estuaries and the formation of a pollution index, Helgoländer Meeresun., **33**, 566–575 (1980).
22. NNDC (National Nuclear Data Center), Brookhaven National Laboratory, USA (2019).

NUCLEAR SCIENCE AND APPLICATIONS

GENERAL INFORMATION AND INSTRUCTIONS TO AUTHOR(S)

Scope of the Journal

"Nuclear Science and Applications" is an indexed journal (ISSN 1016-197X). It provides scope for publication of original scientific research work of high standards in the form of full research articles, reviews and short communications. Preference is given to the works that are related to applications of nuclear science and technology.

Original papers should describe a complete investigation and short communications may represent important data, methods etc that are yet to be concluded or the original full paper manuscripts that are not justified for publication as original papers and recommended to be published as short communications by the designated reviewers. Review works of considerable scientific interests are also welcome. Efforts are made to publish the journal regularly in June and December every year.

Manuscript Submission

Manuscript should be submitted to the Chief Editor at any time of the year. Receipt of the manuscript will be acknowledged. Unpublished manuscript will not be returned to the author. Short communication should not exceed two published pages. Review articles may have an extended length but it must be approved by the editorial board.

Manuscript Preparation

In order to maintain uniformity and standard, the intending authors are requested to prepare their manuscripts by considering the following general requirements:

1. Two copies of the manuscript should be submitted and authors are advised to retain a third copy with them for reference.
2. The manuscript should be typed in double spacing on one side of A4 size paper and computer composed with 12 pt. New Times Roman Font. Adequate margin (2.54 cm on all sides) should be kept.
3. Each paper must contain a reasonable number of keywords in order to indicate the main topics discussed in the paper and to provide basic terms for indexing.
4. The manuscript should be arranged in the following order: Title of the paper, Author(s) name and affiliations, Abstract (not exceeding 150 words), Keywords, Introduction, Materials and Method/Experimental, Results and Discussion, Conclusion(s), Acknowledgement (if any) and Reference(s).
5. The Number of Tables and Figures should be kept as minimum as possible. Same data should not be reproduced both in table & figure.
6. Tables and Figures should be numbered in Arabic numerals. Figures should be eligibly drawn either with laser printer or Indian black ink. Tables and Figures should be placed in the same order in which they appear in the text.
7. S. I. units should be used to express scientific quantities.
8. For references inside the text the following style should be followed at the appropriate places: e.g. [1] or [1,3] or [5-8] etc. The references of author's name(s) in the text should appear in the following form: e.g., Chowdhury [1], Rahman and Khan [3], Hasan et al [5] etc.

   The references arranged at the end of the paper should be written in the following order:

   (a) Reference to a journal publication: author's name, title of the paper, abbreviated name of the journal (internationally approved form, sources: http://www.nlm.nih.gov/tsd/serials/lji.html), volume number in bold face, page number (range) and year of publication in first braket: e.g.: 1. S.Z. Sarker, A. Karim and M.M. Rahman, Complex Permeability Spectra of Polycrystalline Li-Cd Ferrites, Nucl. Sci. and Appl., **22(2)**, 10-17 (2010).

   (b) Reference to a book: author's name, book's title, edition, publisher's name and place, page numbers and year of publication in braket: e.g.: 5. C.S. Piper, Soil and Plant Analysis, 2nd ed. (USA: John Wiley) 580-600 (2002).

   (c) Reference to Proceedings: author's name, title of the paper, Symposium/Conference name, paper number, date and place.

   Corresponding author should be identified in the footnote of the first page with E-mail address.
9. Authors are advised to strickly follow the structure of the paper published recently in NSA in order to speed up the review and editing processes.

Contact Details

All Communications should be addressed to the Executive Editor, Editorial Board, Nuclear Science and Applications, Scientific Information Division, Bangladesh Atomic Energy Commission, Paramanu Bhaban, E-12/A, Agargaon, Sher-e-Bangla Nagar, Dhaka-1207. E-mail: sidbaec@yahoo.com, Phone: 880 2 8181815, Fax: 880 2 8181842, 880 2 8181845.

Subscription Information

The subscription rate for each volume is Tk.150.00 for domestic or US $15.00 for foreign subscribers. Interested subscribers may contact the Executive Editor, Editorial Board, Nuclear Science and Applications, Scientific Information Division, Bangladesh Atomic Energy Commission for collection of the publication or of the reprints.

CONTENTS

NUCLEAR SCIENCE AND APPLICATIONS VOLUME 27 NUMBER 1 & 2 June, December 2018

Price Tk. 150.00 (For Bangladeshi), US$ 15.00 (For Foreigner)

Published by: Bangladesh Atomic Energy Commission, E-12/A, Agargaon, Sher-e-Bangla Nagar Dhaka-1207, Bangladesh